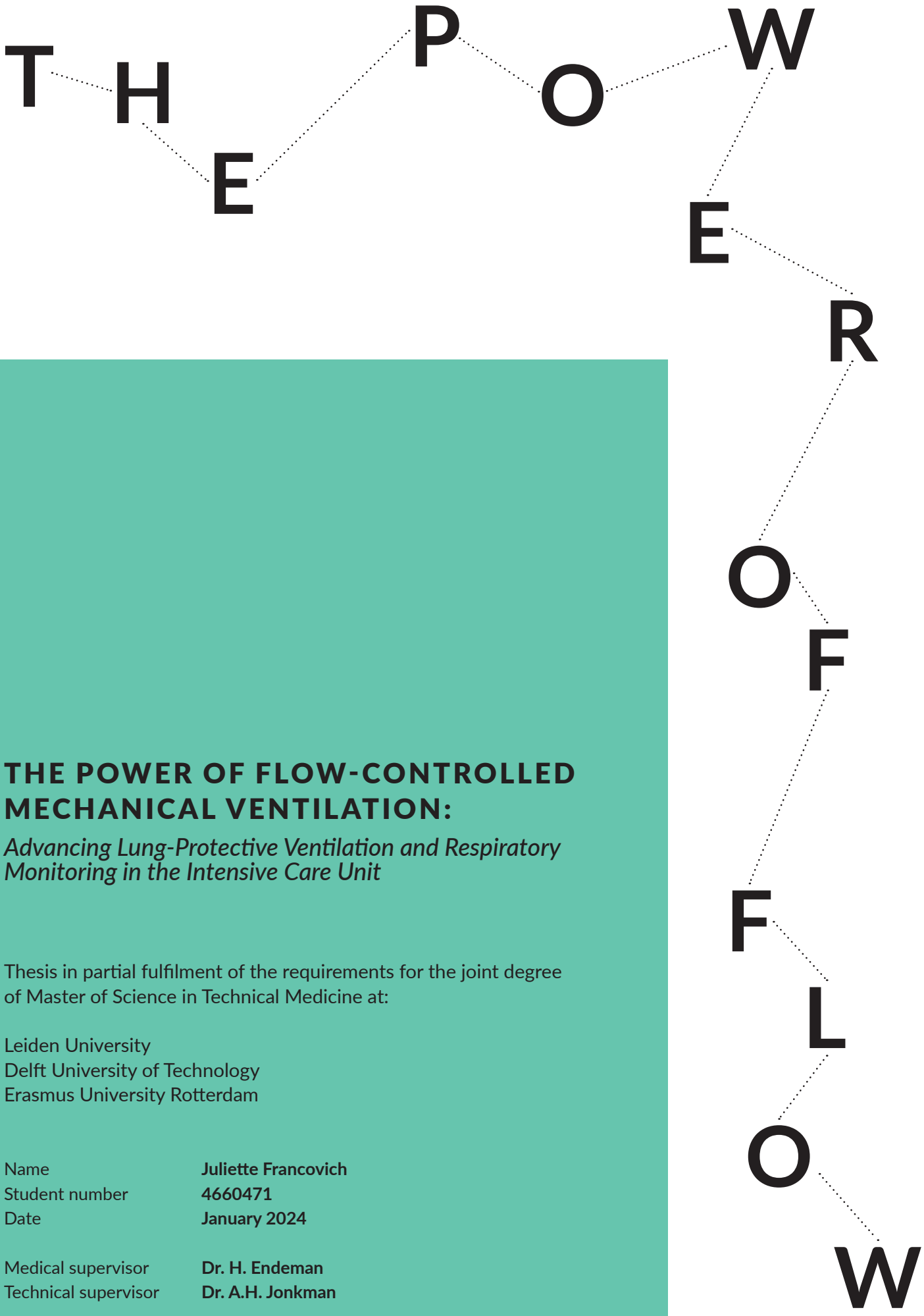

THE POWER OF FLOW-CONTROLLED MECHANICAL VENTILATION:

Advancing Lung-Protective Ventilation and Respiratory Monitoring in the Intensive Care Unit

Thesis in partial fulfilment of the requirements for the joint degree of Master of Science in Technical Medicine at:

Leiden University
Delft University of Technology
Erasmus University Rotterdam

Name	**Juliette Francovich**
Student number	**4660471**
Date	**January 2024**
Medical supervisor	**Dr. H. Endeman**
Technical supervisor	**Dr. A.H. Jonkman**

THE POWER OF FLOW-CONTROLLED MECHANICAL VENTILATION:

Advancing Lung-Protective Ventilation and Respiratory Monitoring in the Intensive Care Unit

Juliette Francovich
Student number: 4660471
January 2024

Thesis in partial fulfilment of the requirements for the joint degree of Master of Science in Technical Medicine
Leiden University; Delft University of Technology; Erasmus University Rotterdam

Master thesis project (TM30004; 35 ECTS)
Dept. of Biomechanical Engineering, TU DELFT
June 2023 – January 2024

Supervisors:
Dr. H. Endeman
Dr. A.H. Jonkman

Thesis committee members:
Dr. H. Endeman, Erasmus MC (chair)
Dr. A.H. Jonkman, Erasmus MC
Dr. A. Schoe, LUMC
Dr. ir. C.C. de Vos, Erasmus MC

An electronic version of this thesis is available at http://repository.tudelft.nl/.

PREFACE

This thesis marks the end of my journey as a student in Technical Medicine. I am still as excited about my study choice as I was six and a half years ago. These years have been a blend of learning, challenges, and the discovery of an emerging field on the edge of medicine and technology. Above all, these years have been an opportunity to discover what I find interesting and what brings me joy.

During my thesis internship at the intensive care unit of the Erasmus Medical Center, I had the opportunity to experience innovative research with a very direct impact on clinical practice. I thoroughly enjoyed the opportunity to contribute to different projects, ranging from helping with a clinical study to developing open-source research software. Along the way, I gained hands-on clinical and research experience.

My gratitude goes out to my supervisors, Annemijn and Rik. Annemijn, you serve as an excellent role model for what a Technical Physician can contribute to the medical world. I enjoyed exchanging thoughts with you and your never-ending enthusiasm for new projects. Rik, your enthusiasm for intensive care medicine is infectious ;). Thank you for providing your clinical insights and taking me in tow during your ICU shifts. I am very excited to continue to work with you both in the coming years as I start my research career in the ICU.

I would also like to thank all the colleagues working at the intensive care unit for showing me the ropes, the interesting discussions during our research meetings, and the relaxing walks during our lunch breaks. Specifically, Peter, thank you for your endless patience with my programming questions. I am proud to look back at how my programming skills have evolved over the past months. I would also like to thank Dr. Abraham Schoe and Dr. ir. Cecile de Vos for investing the time to be a part of my thesis committee.

Lastly, to my family and friends, thank you for all the support, fun moments of distraction, and study sessions (or breaks) over the years. A special thanks to my sisters for providing me with design tips and helping me put together the layout of this thesis.

As my time as a student comes to a close, my learning is far from over. I'm eager to further develop the skills and knowledge acquired, and I’m excited about the opportunities that lie ahead.

First, I hope that you will enjoy reading this thesis. I surely enjoyed working on it.

Juliette Francovich

TABLE OF CONTENTS

Preface 4
Abbreviations 8
Rationale 10

PART 1: FLOW-CONTROLLED VENTILATION IN ICU PATIENTS

Chapter 1: Introduction to flow-controlled ventilation: concept and current evidence 15

Chapter 2: Flow-controlled ventilation in postoperative ICU patients

1. Introduction 21
2. Methods 22
3. Results 32
4. Discussion 34
5. Conclusion 37

References 38

Chapter 3: Flow-controlled ventilation in ICU patients with ARDS: preliminary results

1. Introduction 41
2. Methods 41
3. Results 46
4. Discussion 50
5. Conclusion 53

References 54

PART 2: ADDITIONAL RESEARCH

Chapter 4: Physiological definition for region of interest selection in electrical impedance tomography data: description and validation of a novel method

1. Introduction 59
2. Methods 60
3. Results 63

4. Discussion 68
5. Conclusion 71
References 72

Chapter 5: Advanced lung image processing for personalized mechanical ventilation (ALIVE project)

1. Introduction to ALIVE 75
2. Contributions to ALIVE 75
References 78

Chapter 6: Development of a clinical trial protocol: expiratory muscle stimulation for lung-protective ventilation

1. Introduction 81
2. Objectives 83
3. Study design and population 83
4. Study procedures 84
5. Outcome parameters 88
6. Analysis methods 90
7. Medical ethical approval 91
References 92

Chapter 7: General discussion and future work 95

SUPPLEMENTS

Supplement Chapter 2
Supplemental Analysis 99
Supplemental Tables 104
Supplemental Figures 105

Supplement Chapter 3
Supplemental Tables 109
Supplemental Figures 111

Supplement Chapter 4
Supplemental Figures 116

ABBREVIATIONS

AHRF: Acute hypoxemic respiratory failure

ANOVA: Analysis of variance

ARDS: Acute respiratory distress syndrome

CCMO: Dutch Central Committee on Research Involving Human Subjects

CCW: Chest wall compliance

CMV: Controlled mechanical ventilation

CO: Cardiac output

CoV: Center of ventilation

CSA: Cross sectional area

EELI: End-expiratory lung impedance

EELV: End-expiratory lung volume

EFL: Expiratory flow limitation

EIT: Electrical impedance tomography

EMC: Erasmus Medical Center

EMD: Empirical mode decomposition

$EtCO_2$: End-tidal CO_2

FCV: Flow-controlled ventilation

FES: Functional electrical stimulation

FiO_2: Fraction of inspired oxygen

GI: Global inhomogeneity index

HR: Heart rate

IBW: Ideal body weight

ICU: Intensive care unit

I:E ratio: Inspiratory to expiratory ratio

IQR: Interquartile range

MDN: Multiple digital notch

MDR: Medical Device Regulation

MP: Mechanical power

$PaCO_2$: Arterial partial carbon dioxide pressure

PaO_2: Arterial partial oxygen pressure

PBW: Predicted body weight

PEEP: Positive end-expiratory pressure

PEEPi: Intrinsic PEEP

P_{aw} = Airway pressure

P_{es} = Esophageal pressure

P_{ga}: Gastric pressure

Ppeak: Peak pressure

P_L: Transpulmonary pressure

PV-loop: Pressure-volume loop

RASS: Richmond Agitation-Sedation Scale

ROI: Region of interest

RR: Respiratory rate

RVD: Regional ventilation delay

RVDI: Regional ventilation delay inhomogeneity

$ScvO_2$: Central venous oxygen saturation

SV: Stroke volume

TIV / ΔZ: Tidal impedance variation

TV: Tidal volume

VCV: Volume-controlled ventilation

VILI: Ventilator-induced lung injury

VTI: Velocity Time Integral

RATIONALE

Many patients in the intensive care unit (ICU) depend on mechanical ventilation due to conditions such as severe lung disease, traumatic brain injury, or postoperative coma. While mechanical ventilation is a potentially life-saving intervention, it also has harmful side effects.[1] Especially in patients with lung disease, such as the acute respiratory distress syndrome (ARDS), the lungs can have significantly different physiological and inflammatory characteristics, which differ across different lung regions. Inappropriate ventilator settings can result in cyclic opening and closing of collapsed alveoli and/or pulmonary overdistension,[2] which in turn promotes secondary lung injury and inflammation, also referred to as ventilator-induced lung injury (VILI).[3,4] Therefore, it is important to be able to adjust the ventilator settings to specific patient physiology and needs.[5] Lung-protective ventilation strategies aim to mitigate VILI and involve small tidal volumes, low driving pressures and respiratory rates resulting in low mechanical power, and adequate end-expiratory pressure while maintaining effective gas exchange.[3,4]

The research group, within which this thesis project was conducted, has a focus on investigating novel methods and technologies and implementing advanced respiratory monitoring to improve and facilitate lung-protective ventilation. The primary focus of this thesis involves two physiological studies comparing the effects of a new flow-controlled ventilation (FCV) mode with pressure-controlled ventilation (PCV) in ICU patients. FCV, characterized by constant flow during both inspiration and expiration, holds promise for its potential lung-protective effects.[4] The goal is to evaluate the effect of FCV versus conventional PCV on lung physiology in two patient groups in the ICU by using several advanced respiratory monitoring techniques, such as electrical impedance tomography (EIT) and esophageal manometry. EIT is a non-invasive radiation free imaging modality that enables bedside monitoring of regional lung aeration dynamics.[6] Esophageal manometry is a minimally invasive monitoring method to estimate pleural pressure, facilitating the calculation of transpulmonary pressure.[7]

In Part 1, two clinical studies into the physiological effects of FCV are described. Chapter 1 introduces the concept of flow-controlled ventilation and discusses current evidence for

this novel ventilation mode. Chapter 2 centers on ICU patients who required postoperative mechanical ventilation following cardiothoracic surgery, a group characterized by relatively 'healthy' lungs. Chapter 3 discusses an ongoing study in ICU patients requiring mechanical ventilation for respiratory failure due to moderate to severe ARDS. Preliminary results for this study will be presented.

In Part 2, additional research related to advanced respiratory monitoring and novel concepts for lung-protective ventilation is described. Chapter 4 outlines the rationale and validation of the choice of regions of interest for the EIT analyses that were employed in Chapters 2 and 3. The goal is to contribute to standardization of EIT analyses within the field of respiratory research. Chapter 5 highlights contributions to the ALIVE project, an open-source software development initiative for standardized, reusable EIT data analysis. Chapter 6 elaborates on the development of a clinical study protocol, testing a medical device for expiratory muscle stimulation with potential implications within a lung-protective ventilation strategy. Finally, Chapter 7 provides a general discussion and future developments in the field of respiratory monitoring and improving outcomes of patients on mechanical ventilation.

References

1. Brochard L, Slutsky A, Pesenti A. Mechanical Ventilation to Minimize Progression of Lung Injury in Acute Respiratory Failure. Am J Respir Crit Care Med. 2017;195(4):438-442.
2. Hinz J, Gehoff A, Moerer O, et al. Regional filling characteristics of the lungs in mechanically ventilated patients with acute lung injury. Eur J Anaesthesiol. 2007;24(5):414-424.
3. Costa ELV, Slutsky AS, Brochard LJ, et al. Ventilatory Variables and Mechanical Power in Patients with Acute Respiratory Distress Syndrome. Am J Respir Crit Care Med. 2021;204(3):303-311.
4. Schmidt J, Wenzel C, Mahn M, et al. Improved lung recruitment and oxygenation during mandatory ventilation with a new expiratory ventilation assistance device: A controlled interventional trial in healthy pigs. Eur J Anaesthesiol. 2018;35(10):736-744.
5. Karagiannidis C, Waldmann AD, Róka PL, et al. Regional expiratory time constants in severe respiratory failure estimated by electrical impedance tomography: a feasibility study. Crit Care. 2018;22(1):221.
6. Tomicic V, Cornejo R. Lung monitoring with electrical impedance tomography: technical considerations and clinical applications. J Thorac Dis. 2019; 11(7):3122-3135.
7. Yoshida T, Amato MBP, Grieco DL, et al. Esophageal Manometry and Regional Transpulmonary Pressure in Lung Injury. Am J Respir Crit Care Med. 2018; 197(8):1018-1026.

FLOW-CONTROLLED VENTILATION IN ICU PATIENTS

CHAPTER 1

INTRODUCTION TO FLOW-CONTROLLED VENTILATION: CONCEPT AND CURRENT EVIDENCE

INTRODUCTION TO FLOW-CONTROLLED VENTILATION: CONCEPT AND CURRENT EVIDENCE

Lung-protective strategies for mechanical ventilation aim to prevent secondary lung injury.[1,2] Different phenomena have been described to contribute to ventilator-induced lung injury (VILI), such as high plateau pressures causing barotrauma, large tidal volumes causing volutrauma, and cyclic collapse and reinflation of alveoli causing atelectrauma.[3] Mechanical power is a theoretical explanation that unifies all these factors related to VILI into a measure of the energy transferred from the ventilator to the respiratory system.[1] When this energy is applied to the lungs, it can be stored and (partially) recovered, for instance due to elastic recoil during expiration.[4] Energy that is not recovered during expiration is dissipated in the airways and lung tissue.[4] This dissipated energy can potentially cause injury.[4] In cases of alveolar heterogeneity, such as in the acute respiratory distress syndrome (ARDS), the effects of mechanical power are exacerbated due to an abnormal distribution of lung stress and strain.[3,5] In fact, mechanical power is independently associated with intensive care unit (ICU) mortality during controlled mechanical ventilation in patients with ARDS.[1]

FCV concept

During conventional controlled mechanical ventilation (CMV), the inspiration is controlled by a set driving pressure (pressure-controlled ventilation; PCV) or a set tidal volume (volume-controlled ventilation; VCV). The expiration is not controlled by the ventilator and depends mainly on the passive elastic recoil of the respiratory system.[2] In contrast, flow-controlled ventilation is a ventilation mode that controls the flow to be constant, continuous, and equal during inspiration and expiration (see Figure 1).[3,4] The flow-controlled mechanical ventilator (Evone, Ventinova Medical B.V.) uses an ejector pump, based on Bernoulli's principle, to generate negative pressure and actively draw air from the lungs during expiration.[6,7]

By controlling the expiration, it is theoretically possible to minimize the energy dissipation during expiration, lowering the mechanical power and thereby reducing the risk of lung damage.[3,4] Ventilation efficiency with FCV can be optimized by increasing the tidal volume within safe lung-mechanical limits based on changes in lung compliance.[8] By optimizing the tidal volume based on the dynamic compliance, the risk of atelectasis and/or overdistension can be reduced.[9]

Furthermore, the linearized pressure drop during expiration can facilitate recruitment by stabilizing recruited lung areas during expiration.[10,11] In this way, the proportion of dead space ventilation can be minimized.[8] Thus, lower respiratory rate and minute volume can be applied to achieve efficient gas exchange, resulting in a lower mechanical power and dissipated energy.[8] Therefore, FCV is of interest as a novel method for lung-protective ventilation in critically ill patients in the ICU.

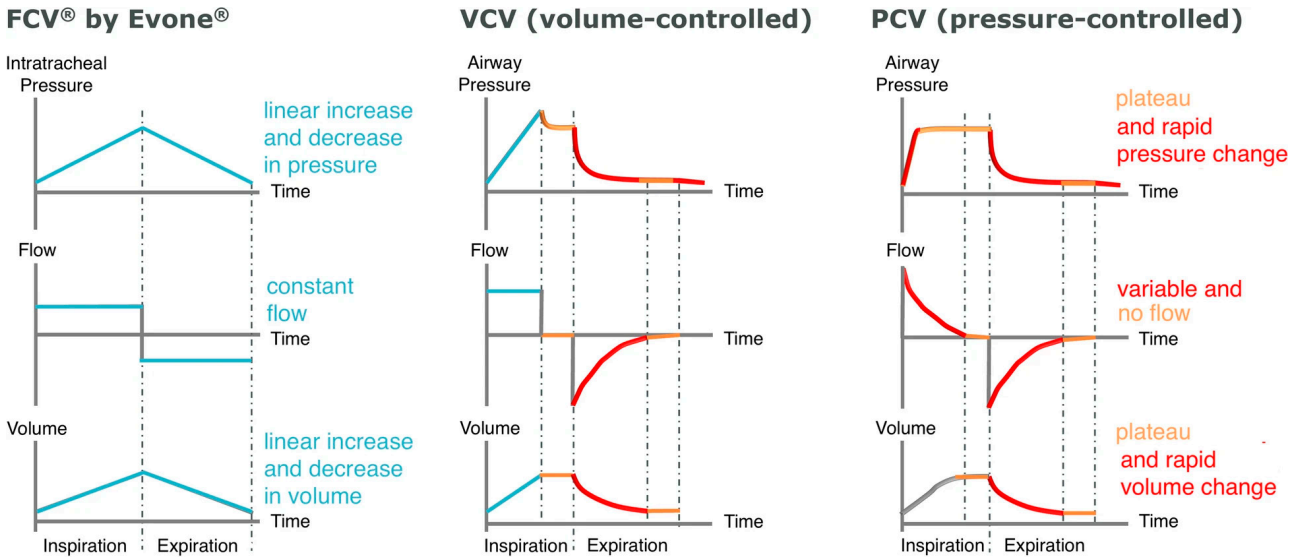

Figure 1. Figure from Grassetto et al.[12]. Flow-controlled ventilation uses a controlled inspiratory and expiratory flow. The flow is generated from a set positive end-expiratory pressure (PEEP) to a set peak pressure during inspiration and from the peak pressure to PEEP during expiration. The ventilator uses intratracheally measured airway pressure to aim for linear increases and decreases in pressure and constant flows during inspiration and expiration. An important difference between FCV and conventional ventilation modes is that there are no sudden pressure drops at the beginning of expiration and no frequent phases without flow.[12]

Current evidence

In healthy and ARDS porcine models, FCV was shown to increase ventilation efficiency and increase alveolar aeration, especially in the dependent lung region.[2,13] In a healthy porcine study, FCV was shown to generate an elevated mean tracheal pressure, without affecting the minimal and maximal pressure of the ventilation cycle.[2] The elevated mean tracheal pressure resulted in increased alveolar aeration and more efficient gas exchange.[2] Similar results were found in a porcine model of ARDS, where FCV was shown to enhance lung aeration in the dependent lung region and increase ventilation efficiency.[13] These findings suggest that FCV could be especially beneficial in critically ill patients requiring prolonged mechanical ventilation.

Moreover, some pilot work with FCV in ARDS patients has been published recently. In a pilot study in 10 patients with COVID-19-related ARDS, FCV resulted in increased ventilation efficiency and decreased mechanical power because of lower inspiratory flow rates and respiratory rates in comparison to conventional CMV.[14] However, the results on mechanical power cannot be interpreted reliably since for power calculations during CMV the pressure at the proximal end of the endotracheal tube was used, whereas in FCV the intratracheal pressure was used.[14] This affects the mechanical power calculation due to the energy dissipated by the resistance of the endotracheal tube.[3,15] Another study in 11 COVID-19-related ARDS patients showed the feasibility of maintaining oxygenation with FCV during 30 minutes.[16] However, in this study airway pressures were also measured at different locations in CMV versus FCV modes, affecting reliability of results.[16]

Therefore, in the following chapters two physiological pilot studies are described to reliably compare the physiological effects of FCV to conventional PCV in postoperative ICU patients and ICU patients with ARDS.

References

1. Costa ELV, Slutsky AS, Brochard LJ, et al. Ventilatory Variables and Mechanical Power in Patients with Acute Respiratory Distress Syndrome. Am J Respir Crit Care Med. 2021;204(3):303-311.

2. Schmidt J, Wenzel C, Mahn M, et al. Improved lung recruitment and oxygenation during mandatory ventilation with a new expiratory ventilation assistance device: A controlled interventional trial in healthy pigs. Eur J Anaesthesiol. 2018;35(10):736-744.

3. Barnes T, van Asseldonk D, Enk D. Minimisation of dissipated energy in the airways during mechanical ventilation by using constant inspiratory and expiratory flows – Flow-controlled ventilation (FCV). Medical Hypotheses. 2018;121:167-176.

4. Barnes T, Enk D. Ventilation for low dissipated energy achieved using flow control during both inspiration and expiration. Trends in Anaesthesia and Critical Care. 2019;24:5-12.

5. Kollisch-Singule M, Emr B, Smith B, et al. Airway pressure release ventilation reduces conducting airway micro-strain in lung injury. J Am Coll Surg. 2014;219(5):968-976.

6. Filauro M, Mora F, Vallin A, et al. Evone® Flow controlled ventilation: a new device for laryngotracheal surgery. Acta Otorhinolaryngologica Italica. 2022;42(2):189.

7. Hamaekers AEW, Götz T, Borg PAJ, Enk D. Achieving an adequate minute volume through a 2 mm transtracheal catheter in simulated upper airway obstruction using a modified industrial ejector. British Journal of Anaesthesia. 2010;104(3):382-386.

8. Spraider P, Martini J, Abram J, et al. Individualised flow-controlled ventilation versus pressure-controlled ventilation in a porcine model of thoracic surgery requiring one-lung ventilation: A laboratory study. Eur J Anaesthesiol. 2022;39(11):885-894.

9. Spraider P, Martini J, Abram J, et al. Individualized flow-controlled ventilation compared to best clinical practice pressure-controlled ventilation: a prospective randomized porcine study. Critical Care. 2020;24(1):662.

10. Goebel U, Haberstroh J, Foerster K, et al. Flow-controlled expiration: a novel ventilation mode to attenuate experimental porcine lung injury. Br J Anaesth. 2014; 113(3):474-483.

11. Wirth S, Springer S, Spaeth J, Borgmann S, Goebel U, Schumann S. Application of the Novel Ventilation Mode FLow-Controlled EXpiration (FLEX): A Crossover Proof-of-Principle Study in Lung-Healthy Patients. Anesth Analg. 2017;125(4):1246-1252.

12. Grassetto A, Pettenuzzo T, Badii F, et al. A new perspective during laryngo-tracheal surgery: the use of an ultra-thin endotracheal tube (Tritube®) and flow-controlled ventilation—a retrospective case series and a review of the literature. Journal of Anesthesia, Analgesia and Critical Care. 2022;2.

13. Schmidt J, Wenzel C, Spassov S, et al. Flow-Controlled Ventilation Attenuates Lung Injury in a Porcine Model of Acute Respiratory Distress Syndrome: A Preclinical Randomized Controlled Study. Crit Care Med. 2020;48(3):e241-e248.

14. Grassetto A, Pettenuzzo T, Badii F, Carlon R, Sella N, Navalesi P. Flow-controlled ventilation may reduce mechanical power and increase ventilatory efficiency in severe coronavirus disease-19 acute respiratory distress syndrome. Pulmonology. 2023;29(2):154-156.

15. Bolder P, Healy T, Bolder A, Beatty P, Kay B. The extra work of breathing through adult endotracheal tubes. Anesthesia & Analgesia. 1986;65(8):853-859.

16. Van Dessel ED, De Meyer GR, Morrison SG, Jorens PG, Schepens T. Flow-controlled ventilation in moderate acute respiratory distress syndrome due to COVID-19: an open-label repeated-measures controlled trial. Intensive Care Medicine Experimental. 2022;10(1):19.

CHAPTER 2

FLOW-CONTROLLED VENTILATION IN POSTOPERATIVE ICU PATIENTS

The full paper of the study described in this chapter was recently submitted as 'Flow-controlled ventilation decreases mechanical power in postoperative ICU patients.' with authors:

Julien P. Van Oosten, Juliette E. Francovich, Peter Somhorst, Philip van der Zee, Henrik Endeman, Diederik A.M.P.J. Gommers and Annemijn H. Jonkman

1. INTRODUCTION

In patients with the acute respiratory distress syndrome (ARDS), flow-controlled ventilation (FCV) was shown to increase ventilation efficiency and decrease mechanical power in comparison to conventional controlled mechanical ventilation (CMV).[1] However, the pressure measurements used for the mechanical power calculations were done at different locations in the respiratory system, making the comparison unreliable.[1-3] Moreover, the physiological mechanisms of FCV resulting in increased ventilation efficiency are not entirely clear but are hypothesized to be related to improved distribution of ventilation across different lung regions.[1]

Therefore, a physiological pilot study was initiated to improve our understanding of the physiological effects of FCV. To eliminate the effects of alveolar inhomogeneity associated with ARDS, this study was performed in postoperative cardiothoracic surgery patients requiring mechanical ventilation at the intensive care unit (ICU). These patients have relatively healthy lungs. The objective was to assess the difference in mechanical power, dissipated energy, and distribution and homogeneity of ventilation between FCV and pressure-controlled ventilation (PCV).

This chapter focuses primarily on the methods and results regarding the effects of FCV on lung aeration and ventilation distribution as secondary endpoints of the submitted paper 'Flow-controlled ventilation decreases mechanical power in postoperative ICU patients.' We hypothesize that FCV results in increased lung aeration and more homogenized ventilation as compared to PCV.

2. METHODS

2.1 Study protocol

This prospective interventional study was conducted at the department of Intensive Care of the Erasmus Medical Center (EMC), Rotterdam, The Netherlands between February 2022 and May 2023. The study was approved by the EMC Medical Ethics Committee and registered on ClinicalTrials.gov (NCT05644418). Adults scheduled for cardiothoracic surgery requiring post-op mechanical ventilation in the ICU were screened and informed consent was obtained before surgery. Eligibility was confirmed upon ICU admission based on the following criteria: 1) endotracheal tube ventilation, 2) FiO_2 ≤50%, 3) positive end-expiratory pressure (PEEP) ≤10 cmH_2O. Exclusion criteria were: 1) excessive bronchial suctioning needs, 2) severe respiratory insufficiency, 3) untreated pneumothorax, 4) hemodynamic instability, 5) contraindications to EIT monitoring, 6) intracranial pressure >15mmHg, and 7) inner tube diameter ≤6mm.

Figure 1 illustrates the study steps described below. All measurements were taken with sedated (RASS ≤-3) patients in supine position. Arterial blood gases, central venous blood gases, SpO_2, hemodynamics, and respiratory mechanics were assessed at each step. EIT monitoring was performed during all study steps with the Dräger PulmoVista 500 with an electrode belt placed at the 4th-5th intercostal space. Moreover, continuous recordings of flow and airway pressure (measured intratracheally) were acquired using a dedicated signal acquisition system (MP160, BIOPAC Systems Inc., USA).

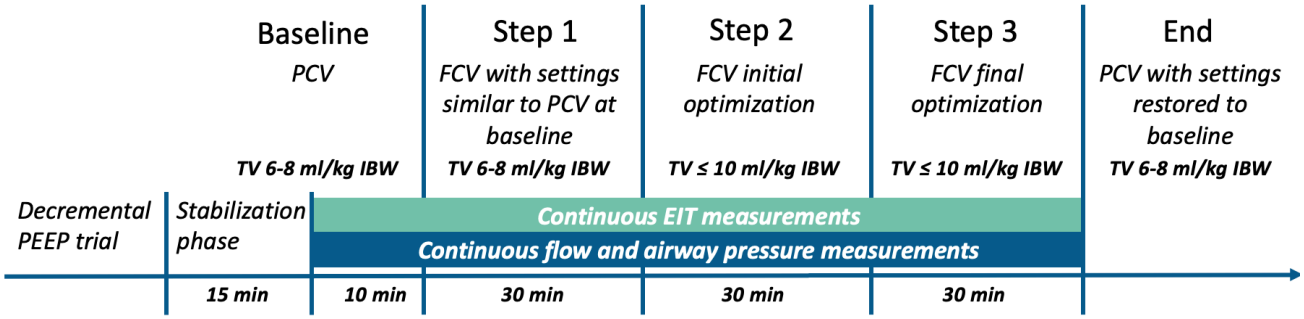

Figure 1. Depiction of study protocol and duration of steps. Abbreviations: PCV = Pressure-controlled ventilation; FCV = Flow-controlled ventilation; TV = Tidal volume; EIT = Electrical impedance tomography; IBW = Ideal body weight; PEEP = Positive end-expiratory pressure.

Baseline
PCV settings were optimized for 15 minutes, followed by 10 minutes of baseline recordings. Optimization included a decremental PEEP trial for PEEP setting at the highest dynamic compliance, FiO_2 to reach an SpO_2 of 95 – 100% and PaO_2 < 15 kPa, peak pressure (Ppeak) aiming for lung-protective tidal volumes of 6-8 mL/kg ideal body weight (IBW), respiratory rate aiming for a minute ventilation with an end-tidal CO_2 ($EtCO_2$) and $PaCO_2$ between 4.5-6.5 kPa, and an inspiratory to expiratory (I:E) ratio aiming for a brief zero flow phase at the end of inspiration and expiration.

Step 1
Switch to FCV with the same PEEP and FiO_2 as baseline. Ppeak was titrated to reach the same tidal volume as with PCV. The flow was titrated to maintain a stable $EtCO_2$. I:E ratio during FCV is 1:1 to achieve the lowest energy dissipation in the airways as possible.[3] The respiratory rate cannot be set but is rather a direct result of the combination between the set flow, pressure difference between the PEEP and Ppeak and the resistance and compliance of the patient's respiratory system. FCV settings were held for 30 minutes.

Step 2
Initial optimization of FCV was performed. Flow and FiO_2 were adapted, if necessary, based on $PaCO_2$ and PaO_2 and target values that were used at baseline. Flow was adjusted to maintain $PaCO_2$ within baseline target values. Ppeak was titrated in steps of 1 cmH_2O to reach the highest dynamic compliance or until the safety limit for tidal volume of 10 mL/kg IBW was reached. Settings were held for 30 minutes.

Step 3
Final optimization of FCV was performed. Flow and FiO_2 were adapted, if necessary, based on $PaCO_2$ and PaO_2 and target values that were used at baseline. Settings were held for 30 minutes.

End of study
After completion of the study protocol, patient management resumed according to local protocols with PCV settings similar to baseline.

2.2 Data analysis

The collected EIT data was converted for offline analysis using dedicated software (PV500 Data Analysis SW130) and pixel-level data were then processed using a custom software developed in Python. The collected flow and airway pressures, gas exchange and hemodynamic parameters were also analyzed but the focus for this chapter of my thesis is on the analysis of EIT data. For a description of the methods and results of the flow and airway pressures, gas exchange and hemodynamics, see Supplement Chapter 2, Supplemental analysis.

Signal selection

Per patient and using the global impedance signal, a stable period of at least 10 breaths was manually selected at the end of each step (baseline, step 1, step 3). A peak detection algorithm was applied to select the start (nadir) and end (peak) of each inspiration. Then, for the global impedance signal and for each individual pixel in the EIT image (totaling 32x32=1024 pixels), an average inspiratory impedance signal was calculated over these 10 breaths. Figure 2 shows an example of such stable period for the global impedance signal (figure 2a) and the resulting average inspiratory signal of these breaths (figure 2b).

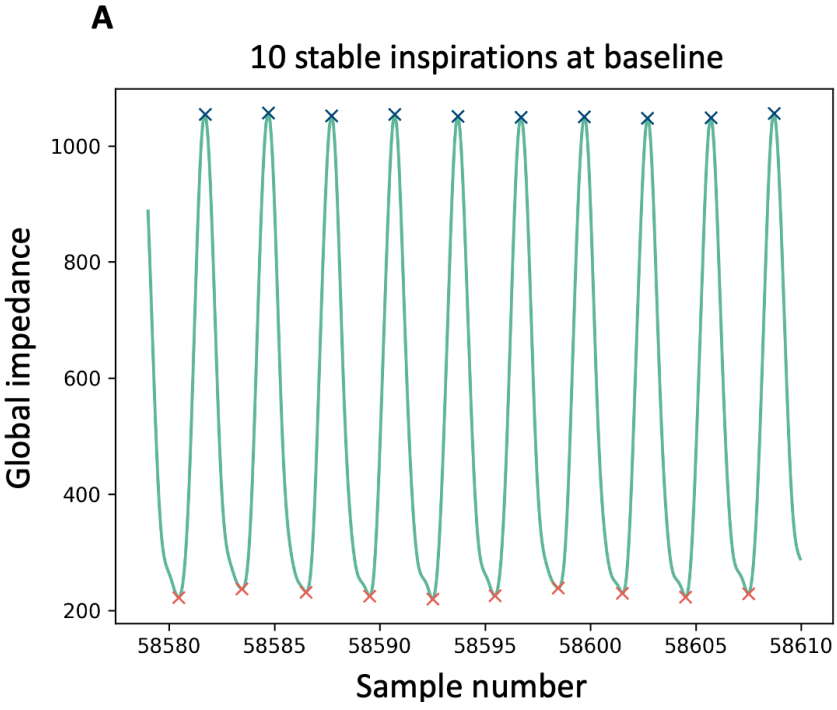

Figure 2a. Example of 10 stable inspirations at baseline pressure-controlled ventilation (PCV).

For this average breath, signal baseline correction was performed, and inspiratory times were normalized to allow comparisons within and between patients, since the respiratory rate varied between the different breaths/steps.

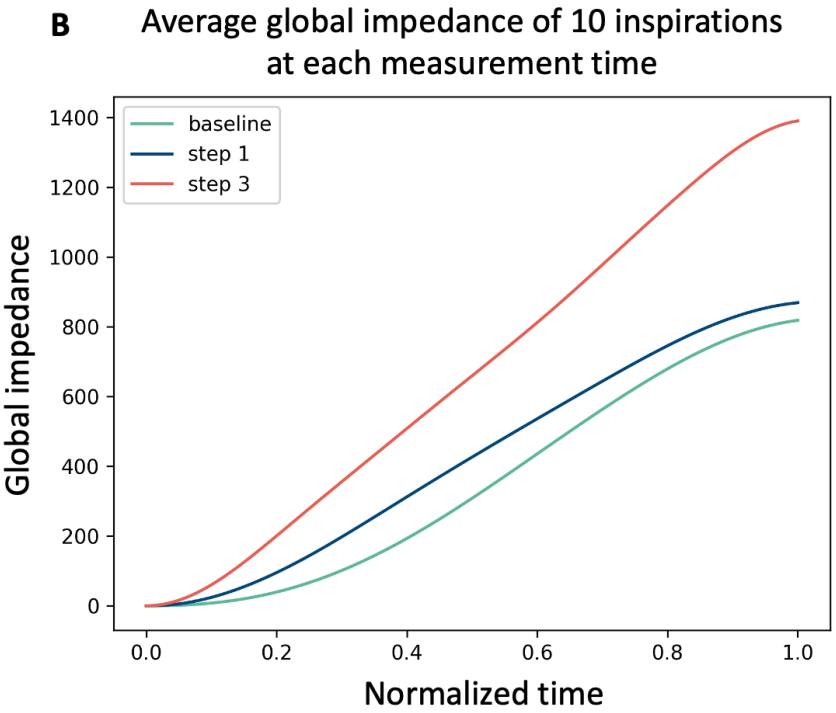

Figure 2b. Example of average global impedance over 10 selected inspirations normalized over time at each step (baseline, step 1, step 3).

Note that the average global impedance for flow-controlled ventilation (step 1 and step 3) has a more linear shape as compared to baseline PCV, inherent to the working principle of FCV.

Determination of ventilated lung space

No signal filtering was performed to avoid information loss, as this could especially influence temporal ventilation distribution analysis (see below); however, only pixels with a tidal impedance variation (ΔZ) of at least 15% of maximum pixel ΔZ were included in the further analysis (Figure 3), assuming a significant contribution to the ventilated lung space and to minimize influence of cardiac-related artefacts. If applying this threshold resulted in separate clusters of pixels (i.e., remaining artefacts), only the largest cluster of adjacent pixels was assumed to represent the functional lung area and included in the analysis (Figure 3). This 15% threshold was chosen in line with Heines et al.[4] and was also visually considered the best cut-off to lower influence of artefacts while minimizing information loss.

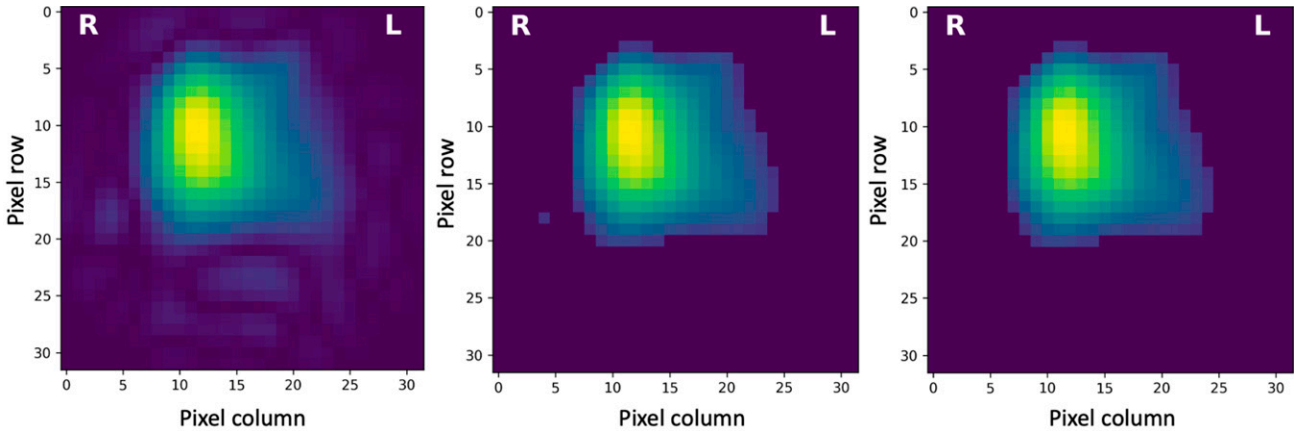

Figure 3. Left: example of a pixel tidal impedance variation (ΔZ) map at baseline, before determining the functional lung space. Middle: pixels with a ΔZ <15% of maximum pixel ΔZ were excluded. Right: pixel tidal impedance map representing the ventilated lung space, after automatically removing pixels that were not adjacent to the largest cluster. In this example, only 1 pixel (middle figure: row 18, column 4) was additionally removed.

Defining regions of interest

Defining robust regions of interest (ROIs) is crucial for analyzing subtle changes in regional ventilation distribution across ventilator modes. Simply dividing the EIT image into 2 or 4 horizontal slices based on the ventrodorsal diameter (e.g., 2 ROIs of 16x32 pixels, or 4 ROIs of 8x32 pixels) does not allow for detecting subtle changes in ventilation heterogeneity, since the functional lung area often covers only part of the total EIT field. For a more physiological definition, we defined 4 ROIs (ventral, mid-ventral, mid-dorsal and dorsal) based on the pixels' contribution to the functional lung area instead of simply dividing the functional lung area into 4 equal-sized regions. ROIs were determined using an average pixel impedance map of three study steps, with each ROI representing 25% of total impedance variation in this average map (Figure 4). In detail:

1. We first computed an average impedance map of all three study steps (baseline, step 1, and step 3). Hence, all pixels that contributed to ventilation in any step were included in the definition of the ROI (Figure 4).
2. The ROIs were then defined, each representing precisely 25% of the total tidal variation in lung impedance (ΔZ) from the average pixel impedance map. However, this introduces complexity, as a 25% division often falls within a pixel row (i.e., it is rare that a full pixel row adds up to exactly 25% of the total ΔZ) (Figure 5). Consequently, a pixel row could contribute to two ROIs. In such cases, we applied a

correction; for example, if the division between the ventral and mid-ventral region was at 40% of a given row, 40% of the ΔZ of this row was added to the ventral ROI, and the remaining 60% to the mid-ventral ROI. This approach also ensured that differences between the left and right lung did not influence the ROI definition.

3. This ROI division was then applied to the original impedance map of each step, to allow within-patient comparisons and quantification of subtle regional changes in tidal impedance variation (Figure 4).

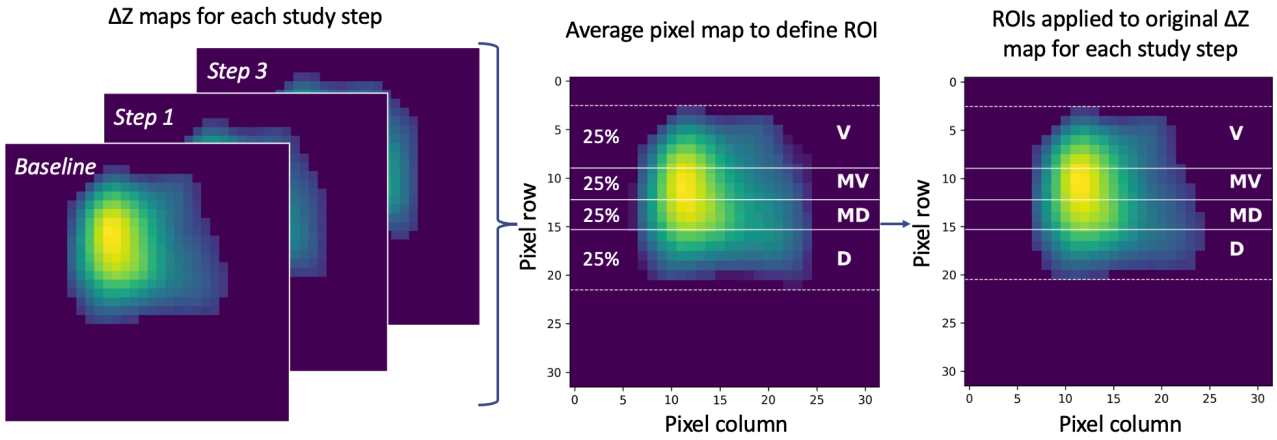

Figure 4. Example of an average pixel impedance map created with the impedance maps at baseline, step 1, and step 3. The regions of interest (ROI; ventral (V), mid-ventral (MV), mid-dorsal (MD) and dorsal (D)) each represent exactly 25% of the total tidal impedance variation of this average pixel impedance map. Note that the division line separating two ROIs could lie within one pixel row (Figure 5), which was accounted for (see text for details). This ROI division was then applied to the original impedance maps of each step for further computation of parameters.

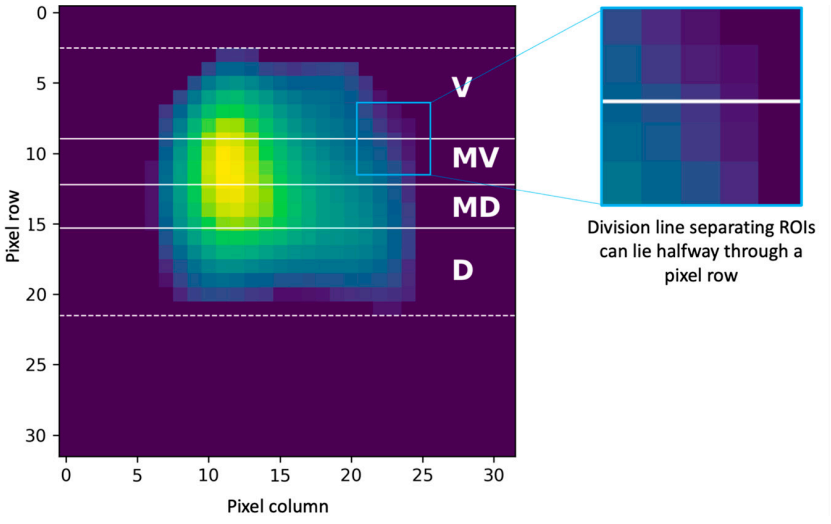

Figure 5. Example to illustrate that ROI division (ventral (V), mid-ventral (MV), mid-dorsal (MD) and dorsal (D)) can lie in between a pixel row. Dotted lines reflect the boundary of the functional lung space (i.e., ventilated pixels).

Computation of EIT parameters

The following parameters were computed for each study step, using the average breath from each stable period (as in Figure 2b):

- Tidal impedance variation (ΔZ): the global ΔZ and regional ΔZ (per ROI) were calculated as the amplitude of the respective global and regional impedance signal during inspiration (peak minus nadir). ΔZ is a reflection of tidal volume.
- Static compliance: the global and regional (per ROI) static compliance were calculated as ΔZ/driving pressure, with driving pressure being the difference between plateau pressure and total PEEP derived from the intratracheal pressure tracings at each step.
- Global end-expiratory lung impedance (EELI): computed as the baseline of the global impedance signal.

Furthermore, we computed the following parameters to visualize and quantify the overall, spatial, and temporal homogeneity of lung ventilation:

- Global inhomogeneity index (GI): as a measure for overall homogeneity of ventilation and as per Zhao et al.[5]:

$$GI = \frac{\sum_{x,y \in lung} |\Delta Z_{xy} - Median(\Delta Z_{lung})|}{\sum_{x,y \in lung} \Delta Z_{xy}} * 100$$

  ΔZ_{xy} represents the impedance change of a ventilated pixel (x,y), and ΔZ_{lung} the impedance change of the total ventilated lung area. A lower GI thus reflects a more homogeneous ventilation distribution.
- Spatial homogeneity: spatial homogeneity was evaluated in two ways:
  - First, to provide a visualisation of the continuous inspiratory volume distribution over all ROIs, the impedance waveforms per ROI were normalized over time and visualized as a percentage of the global ΔZ (Figure 6).
  - Second, the regional intra-tidal impedance distribution was visualized by dividing the global inspiration into five parts of equal ΔZ and plotting the impedance changes for each ROI (Figure 7), in line with Lowhagen et al.[6].

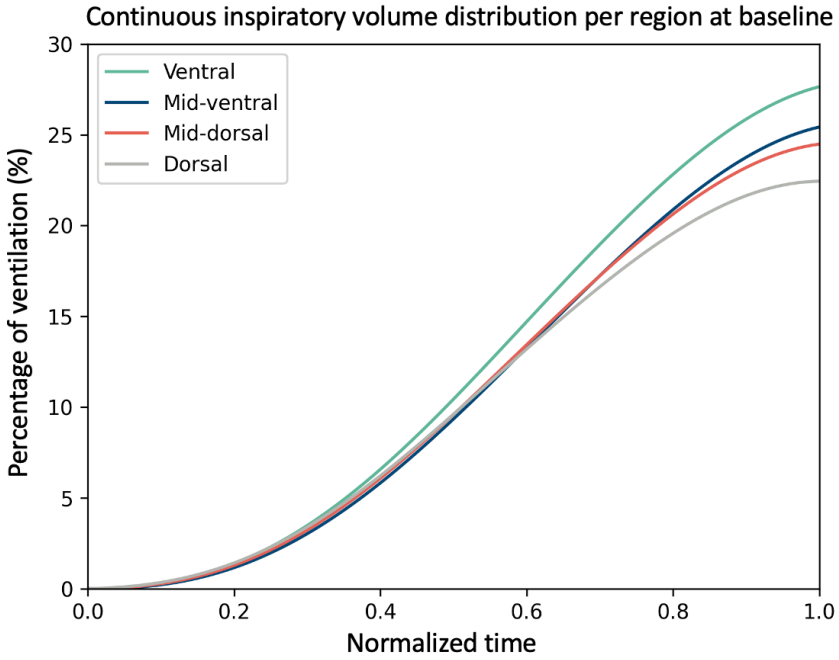

Figure 6. Example of a continuous regional volume distribution (per region of interest) in an average inspiration at baseline PCV.

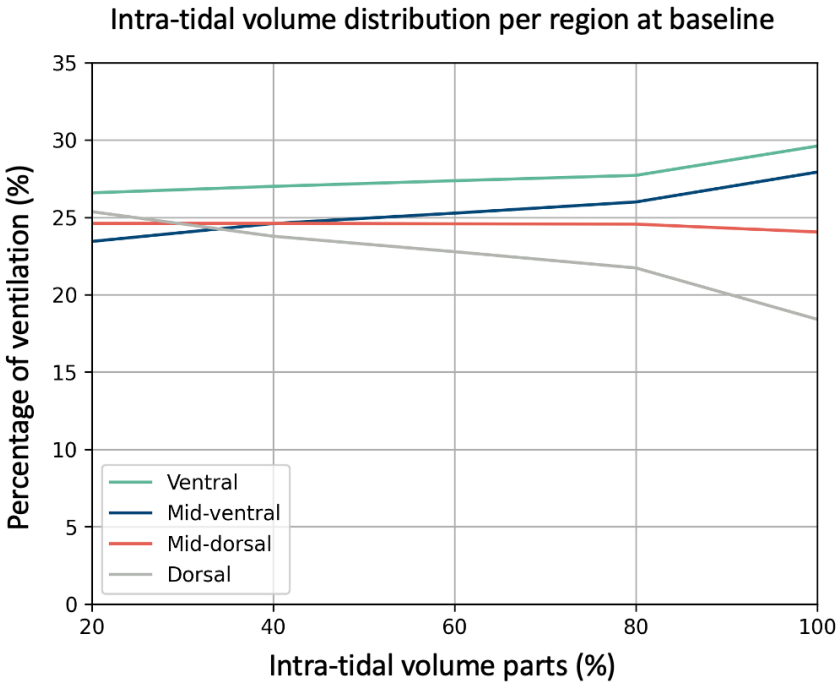

Figure 7. Example of regional intra-tidal volume distribution per region of interest in an average inspiration at baseline PCV. The inspiration was divided into five equal parts of ΔZ (intra-tidal volume parts, each representing 20% of total ΔZ). Note that throughout the inspiratory phase, ventilation is distributed more to the ventral regions in this example.

- Temporal homogeneity: The regional ventilation delay inhomogeneity (RVDI) was used as a measure of temporal homogeneity of lung inflation, as described previously.[7] Regional ventilation delay (RVD) was first computed for each pixel of the ventilated lung space as:

$$RVD = \frac{\Delta t_{RVD}}{\Delta t_{\max - min}}$$

Δt_{RVD} is the time between start of inspiration (as per the global ΔZ) until pixel ΔZ reached 40% of the maximal ΔZ and is normalized to global inspiration time ($\Delta t_{max-min}$) (see Figure 8). RVD is expressed as percentage. RVDI was then calculated as the standard deviation of all pixel RVDs. A lower RVDI thus reflects a more homogeneous lung inflation.

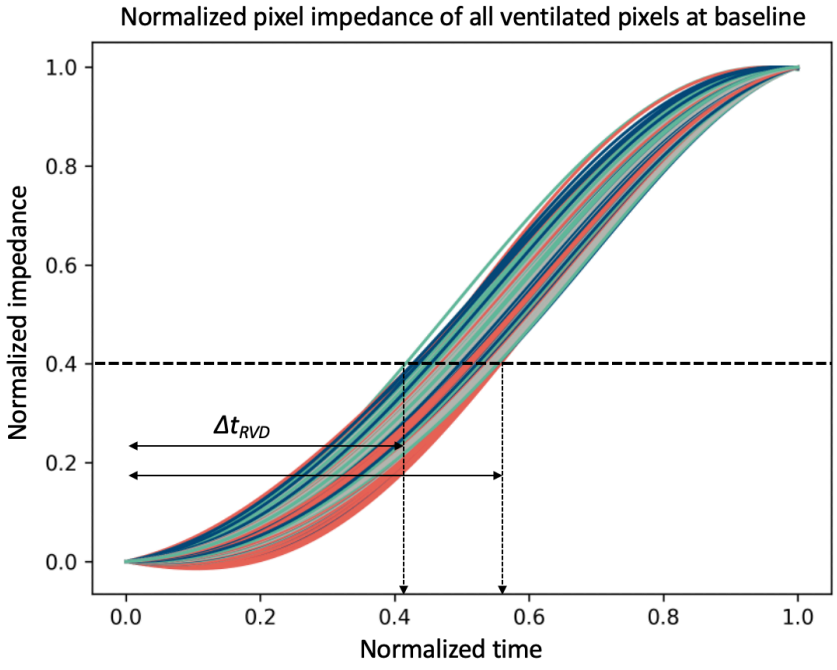

Figure 8. Example of the tidal impedance of all separate pixels involved in the ventilated lung space at baseline PCV, normalized for time and impedance. Δt_{RVD} is the time between start of inspiration (as per the global ΔZ) until pixel ΔZ reached 40% of the maximal ΔZ (dotted horizontal line at 0.4). The dotted vertical lines indicate the first and last pixel that reach the threshold of 0.4 (smallest and largest Δt_{RVD}). The regional ventilation delay inhomogeneity (RVDI) is computed as the standard deviation of the Δt_{RVD} of all pixels in the ventilated lung space.

2.3 Statistical analysis

Statistical analysis was performed using SPSS (IBM, Armonk, USA). Data were presented as median (interquartile range) and tested for normality using the Shapiro-Wilk test. Changes in ΔZ and static compliance are expressed as a percentage change between steps, as both are measured in arbitrary units, which makes direct comparisons between patients unreliable. Values were compared between steps using the repeated measures ANOVA test or the Kruskal-Wallis test, depending on the distribution, with Bonferroni correction for multiple comparisons. A p-value <0.05 was considered statistically significant. To address our study aim, we primarily focused on the difference between PCV (baseline) and step 3 (fully optimized FCV), since optimizing the tidal volume is needed to fulfill the potential of the FCV mode (i.e., tidal recruitment followed by controlled expiration to keep the lungs open).

3. RESULTS

10 patients participated in the full study protocol. One patient was excluded from EIT analysis due to artefacts in the recordings, likely due to a small ventral pneumothorax that was missed at enrollment.

EIT results of the remaining 9 patients showed that optimization of FCV did not increase end-expiratory lung impedance (ΔEELI) (Table 1). However, there was a significant increase in contribution of the dorsal ROI to tidal ventilation during optimized FCV when compared to PCV, even exceeding ΔZ values of the ventral ROI (Table 1 & Figure 9). The increased tidal volumes during optimized FCV (step 3) did not lead to overdistension of the ventral lung regions, as indicated by the increase in static compliance when comparing optimized FCV to PCV across all four ROIs (Table 1). Overall lung homogeneity and temporal ventilation homogeneity, as reflected by GI and RVDI, did not differ between the two modes. For EIT parameters comparing PCV with FCV step 1 ('similar' PCV settings) see Supplement Chapter 2, Table 1. For comparison of ventilation homogeneity parameters of all three study steps, see Supplement Chapter 2, Figures 1 and 2. For the results of the analysis of the flow and airway pressures, gas exchange and hemodynamics, see Supplement Chapter 2, Supplemental analysis.

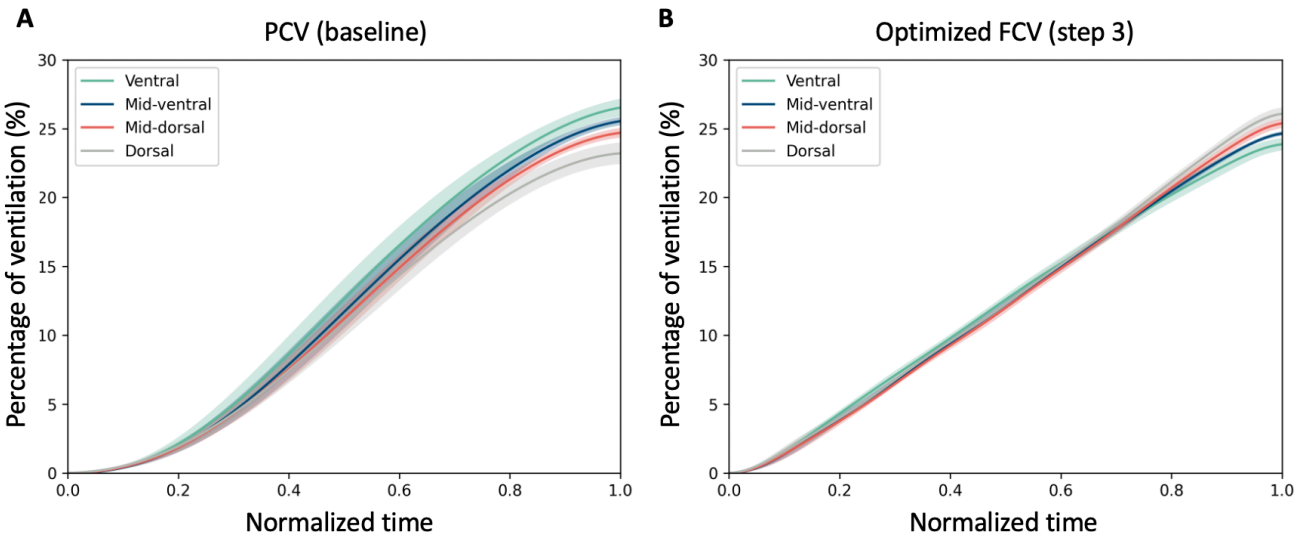

Figure 9. Continuous regional volume distribution: average normalized impedance waveforms with 95% confidence interval per ROI over time and as a percentage of the global ΔZ. A) During PCV (baseline), B) During optimized FCV (step 3).

Table 1. EIT results PCV (baseline) vs optimized FCV (step 3); values represent median (IQR)

Table 1a. Changes in EIT parameters during FCV as compared to PCV*		
	Optimized FCV	**P-value**
Global change in ΔZ (%)	59.4 (34.3-72.1)	
Regional change in ΔZ (%) ROI ventral ROI mid-ventral ROI mid-dorsal ROI dorsal	 39.7 (22.1-49.5) 50.9 (26.6-66.3) 73.6 (34.3-78.6) 81.1 (52.7-104.7)	0.030[1]
Global change in static compliance (%)	13.4 (8.0-26.7)	
Regional change in static compliance (%) ROI ventral ROI mid-ventral ROI mid-dorsal ROI dorsal	 2.4 (-7.0-19.2) 15.2 (2.7-24.2) 23.3 (7.1-32.6) 27.5 (19.9-45.2)	0.017[2]
Change in global EELI (a.u.)	53 (-17-100)	0.163

Table 1b. Absolute EIT parameters reflecting lung and ventilation homogeneity			
	PCV	**Optimized FCV**	**P-value**
GI (%)	43.8 (41.4-45.3)	43.5 (39.7-45.7)	1.000
RVDI (%)	2.75 (2.28-4.63)	4.23 (3.39-6.11)	0.717

Abbreviations: EIT = Electrical impedance tomography; FCV = Flow-controlled ventilation; PCV = Pressure-controlled ventilation; ΔZ = Tidal impedance variation; ROI = Region of interest; EELI = End-expiratory lung impedance; a.u. = arbitrary units; GI = Global inhomogeneity index; RVDI = Regional ventilation delay inhomogeneity.

* Changes in ΔZ and static compliance are expressed as percentage change between FCV step 3 and PCV at baseline, as both are expressed in arbitrary units, which makes direct comparisons between patients unreliable.

[1] p-value reflects the significant difference between PCV baseline vs. FCV step 3 regarding the distribution of ΔZ among the four ROIs, using a Kruskal-Wallis test on the percentage changes from baseline (to account for the fact that ΔZ is measured in arbitrary units).

[2] p-value reflects the significant difference between PCV baseline vs. FCV step 3 regarding the distribution of the change in static compliance among the four ROIs, using a Kruskal-Wallis test on the percentage changes from baseline (to account for the fact that ΔZ and thereby also the static compliance is measured in arbitrary units).

4. DISCUSSION

The aim of this study was to compare FCV to PCV with regards to mechanical power, dissipated energy, and distribution and homogeneity of ventilation. Our main finding related to the EIT results was that FCV mode did not provide a better overall lung homogeneity (GI and RVDI) but resulted in more homogeneous tidal inflation and relatively larger participation of the dorsal lung regions. Other findings based on the supplemental analysis were that optimized FCV provides stable gas exchange at lower minute volumes with significantly lower mechanical power and dissipated energy. This discussion will focus on the results on distribution and homogeneity of ventilation as assessed by EIT.

FCV optimization

Our study was conducted in two phases. First, we transitioned from PCV to FCV with settings similar to those in PCV, primarily adjusting the driving pressure to maintain consistent tidal volumes. This initial step aimed to evaluate the immediate impact of switching to FCV on lung aeration and to gain a better understanding of the working mechanism of FCV. In the second phase, FCV settings were optimized during steps 2 and 3, focusing on achieving the highest dynamic compliance by adjusting Ppeak.

This optimization approach maximized the benefits of FCV in several ways. The increase in tidal volume during optimized FCV (reflected by an increase in ΔZ) was accompanied by an increase in regional static compliance, indicating that the increase in tidal volume led to lung recruitment rather than overdistension. However, optimization of FCV did not increase end-expiratory lung volume (reflected by ΔEELI). The lack of significant difference in ΔEELI can be explained by the fact that the EELI was heavily influenced by changes in fluid status and patient management rather than representing actual differences in lung aeration in this postoperative ICU population (see Supplement Chapter 2, Figure 3 for an example of the effect of fluid administration on EELI).[8] Important to note is that these changes in EELI did not affect computation of other EIT parameters. Moreover, inherent to the working principle of FCV, increasing tidal volumes during optimization resulted in a lower respiratory rate (a direct effect of changes in compliance). Lowering the respiratory rate allows lung units with longer time constants to inflate adequately, supporting recruitment.[9]

Effect of FCV on lung recruitment and homogeneity

Our results showed recruitment of dorsal lung regions but no significant difference in GI and RVDI when comparing FCV to PCV. Our study population of postoperative patients with relatively healthy lungs likely had limited potential for improving alveolar inhomogeneity. This could explain the relatively low RVDI values and lack of significant difference in GI and RVDI between FCV and PCV.

Previously, Weber et al.[10] showed that ΔEELI and mean lung volume decreased less during FCV than during VCV in obese patients during elective surgery, indicating improved lung recruitment with FCV. Moreover, Weber et al.[10] also reported improved regional ventilation distribution. Our results differ from those observed by Weber et al.[10], in part because EELI was not reliable in our study due to patient fluid management, as mentioned previously.[8] Although we also report improved regional ventilation distribution, the methods and data substantiating these conclusions are very different. Thus, some key differences with Weber et al.[10] should be mentioned.

Firstly, patients in the study by Weber et al.[10] only underwent seven minutes of ventilation in each mode, limiting the ability to fully evaluate the effects of FCV on regional ventilation. It is unlikely that a 'steady state' would be reached within seven minutes. Moreover, the EIT image was divided in two equal-sized horizontal regions based on 50% of the ventrodorsal diameter.[10] This can lead to a significant difference in the number of pixels attributed to a particular ROI between different ventilation modes. Therefore, we chose to define our ROIs based on 25% of the average variation in lung impedance over the different ventilator settings. This physiological approach to computation of ROIs allowed assessment of more subtle changes in regional EIT parameters between PCV and FCV.

Furthermore, Weber et al.[10] used a specific parameter - the reduction in tidal volume per 25% decrease in expiratory impedance - to conclude that FCV enhances regional ventilation distribution.[10] However, this particular parameter does not offer insights into ventilation homogeneity. Essentially, their findings simply demonstrated that the FCV mechanism maintains a continuous airflow during both inhalation and exhalation.

The continuous outflow of air results in a linear decline in tidal volume (impedance) during expiration, in contrast to the exponential volume reduction observed with PCV. In contrast, our approach involved a comprehensive EIT analysis that examined ventilation homogeneity, encompassing overall, spatial, and temporal aspects.

Strengths and limitations

A limitation of our study is that the sequence of ventilation modes was not randomized. This could have resulted in order effects. The influence of slow recruitment of partly collapsed lungs postoperatively may have affected the results in favor of FCV. However, by performing a decremental PEEP trial before the start of the study we expect fast recruitment to have taken place before measurements started. Moreover, this was a pilot study with a relatively small number of patients. Nevertheless, the observed physiological effects of FCV on the ventilation distribution were strong, especially after optimizing FCV by titrating the tidal volume aiming for the highest dynamic compliance.

Clinical implications

Our study was performed in postoperative ICU patients with relatively healthy lungs. How these results can be translated to ICU patients with hyperinflammatory heterogeneous lungs, such as in ARDS, is yet unknown and requires further study. In addition, during optimized FCV a safety limit for tidal volume of 10 mL/kg IBW was used. This is higher than the current guidelines for patients with ARDS, where tidal volumes are limited to 4-8 ml/kg IBW.[11] Nevertheless, these guidelines were not designed with the working principles of FCV in mind. Therefore, future research should evaluate if optimizing FCV in ARDS can be considered safe outside the conventional limits of tidal volume.

5. CONCLUSION

In conclusion, optimized FCV as compared to PCV in postoperative ICU patients did not provide a better overall lung homogeneity but resulted in more homogeneous tidal inflation and relatively larger participation of the dorsal lung regions. Hence, FCV holds the potential for personalized application of the open lung concept. Further research is warranted to investigate the physiological effects of FCV in the presence of alveolar heterogeneity, such as in ARDS, to prevent ventilator-induced lung injury (VILI).

REFERENCES

1. Grassetto A, Pettenuzzo T, Badii F, Carlon R, Sella N, Navalesi P. Flow-controlled ventilation may reduce mechanical power and increase ventilatory efficiency in severe coronavirus disease-19 acute respiratory distress syndrome. Pulmonology. 2023;29(2):154-156.

2. Bolder P, Healy T, Bolder A, Beatty P, Kay B. The extra work of breathing through adult endotracheal tubes. Anesthesia & Analgesia. 1986;65(8):853-859.

3. Barnes T, van Asseldonk D, Enk D. Minimisation of dissipated energy in the airways during mechanical ventilation by using constant inspiratory and expiratory flows – Flow-controlled ventilation (FCV). Medical Hypotheses. 2018;121:167-176.

4. Heines SJH, de Jongh SAM, Strauch U, van der Horst ICC, van de Poll MCG, Bergmans D. The global inhomogeneity index assessed by electrical impedance tomography overestimates PEEP requirement in patients with ARDS: an observational study. BMC Anesthesiol. 2022;22(1):258.

5. Zhao Z, Möller K, Steinmann D, Frerichs I, Guttmann J. Evaluation of an electrical impedance tomography-based Global Inhomogeneity Index for pulmonary ventilation distribution. Intensive Care Med. 2009;35(11):1900-1906.

6. Lowhagen K, Lundin S, Stenqvist O. Regional intratidal gas distribution in acute lung injury and acute respiratory distress syndrome assessed by electric impedance tomography. Minerva Anestesiol. 2010;76(12):1024-1035.

7. Muders T, Hentze B, Simon P, et al. A Modified Method to Assess Tidal Recruitment by Electrical Impedance Tomography. J Clin Med. 2019;8(8).

8. Becher T, Wendler A, Eimer C, Weiler N, Frerichs I. Changes in Electrical Impedance Tomography Findings of ICU Patients during Rapid Infusion of a Fluid Bolus: A Prospective Observational Study. Am J Respir Crit Care Med. 2019; 199(12):1572-1575.

9. Barnes T, van Asseldonk D, Enk D. Minimisation of dissipated energy in the airways during mechanical ventilation by using constant inspiratory and expiratory flows - Flow-controlled ventilation (FCV). Med Hypotheses. 2018;121:167-176.

10. Weber J, Straka L, Borgmann S, Schmidt J, Wirth S, Schumann S. Flow-controlled ventilation (FCV) improves regional ventilation in obese patients – a randomized controlled crossover trial. BMC Anesthesiology. 2020;20(1):24.

11. Fan E, Del Sorbo L, Goligher EC, et al. An Official American Thoracic Society/ European Society of Intensive Care Medicine/Society of Critical Care Medicine Clinical Practice Guideline: Mechanical Ventilation in Adult Patients with Acute Respiratory Distress Syndrome. Am J Respir Crit Care Med. 2017;195(9):1253-1263.

CHAPTER 3

FLOW-CONTROLLED VENTILATION IN ICU PATIENTS WITH ARDS - PRELIMINARY RESULTS

1. INTRODUCTION

In the previous chapter, a study comparing flow-controlled ventilation (FCV) to pressure-controlled ventilation (PCV) was described in cardiothoracic surgery patients requiring postoperative mechanical ventilation at the intensive care unit (ICU), which are patients with relatively healthy lungs. However, patients with alveolar heterogeneity, such as in the acute respiratory distress syndrome (ARDS), are especially prone to developing ventilator-induced lung injury (VILI) and may therefore especially benefit from the working principle of FCV.[1,2] Thus, it is of interest to compare FCV to PCV in patients with ARDS in terms of ventilation homogeneity, lung aeration, mechanical power and dissipated energy.

Therefore, a physiological study was designed comparing PCV and FCV in patients with ARDS, where pressure measurements were performed intratracheally for both ventilation modes, enabling a reliable comparison between PCV and FCV. Our hypothesis is that FCV results in a lower mechanical power (J/min) and an improved regional ventilation distribution and temporal and spatial ventilation homogeneity. Thereby, FCV can potentially reduce the risk of VILI and facilitate lung-protective ventilation.

2. METHODS

2.1 Study protocol

This is an ongoing randomized crossover interventional study that is conducted at the department of Intensive Care of the Erasmus Medical Center (EMC) and Maasstad Ziekenhuis, Rotterdam, The Netherlands. Inclusions started in September 2023. The study was approved by the EMC Medical Ethics Committee and registered on ClinicalTrials.gov (NCT06051188).

Patients that were admitted to the ICU and received controlled mechanical ventilation (CMV) for a moderate to severe ARDS (including COVID-19) were screened for eligibility based on the following criteria: 1) ≥ 18 years old, 2) meeting all criteria (timing, chest imaging, origin of edema and oxygenation) of the Berlin definition of ARDS.[3] Exclusion criteria were: 1) excessive bronchial suctioning needs, 2) untreated pneumothorax, 3) hemodynamic instability, 4) contraindications for EIT monitoring, 5) contraindications for esophageal balloon for transpulmonary

pressure measurements, 6) intracranial pressure > 15mmHg or unstable (increase in sedation or osmotherapy required), 7) inner tube diameter ≤6mm, and 8) anticipating withdrawal of life support and/or shift to palliation as the goal of care.

Upon inclusion patients were randomized to a ventilation mode sequence. Figure 1 shows the study steps described below. Patients either received 90 minutes of PCV followed by 90 minutes of FCV or vice versa. Continuous EIT monitoring was performed with the Timpel Enlight with an electrode belt placed at the 4th-5th intercostal space. Moreover, continuous recordings of flow, airway pressure (measured intratracheally) and esophageal pressure were acquired using a dedicated signal acquisition system (MP160, BIOPAC Systems Inc., USA). Additionally, arterial blood gas samples were collected every 30 minutes during the study period.

Baseline

PCV was set according to standard of care and then optimized. Optimization included a decremental positive end-expiratory pressure (PEEP) trial for PEEP setting at the highest dynamic compliance, FiO_2 to reach an SpO_2 of 95 - 100% and PaO2 < 15 kPa, peak pressure (Ppeak) aiming for lung-protective tidal volumes of 6 - 8 mL/kg ideal body weight (IBW), respiratory rate aiming for a minute ventilation with an end-tidal CO_2 ($EtCO_2$) and $PaCO_2$ between 4.5 - 6.5 kPa, and an inspiratory to expiratory (I:E) ratio aiming for a brief zero flow phase at the end of inspiration and expiration.

PCV measurements

For PCV measurements PCV settings at baseline were kept or restored, depending on the order of ventilation modes. Measurements were performed for 90 minutes.

FCV measurements

Switch to FCV after baseline or after PCV measurements with the same PEEP and FiO_2 as PCV at baseline. Ppeak was titrated to reach the same tidal volume as with PCV. The flow was titrated to maintain a stable $EtCO_2$. I:E ratio during FCV is 1:1 to achieve the lowest energy dissipation in the airways as possible.[4] After 30 minutes FCV was optimized. Flow was adjusted to maintain $PaCO_2$ within target values. Ppeak was titrated in steps

of 1 cmH_2O to reach the highest dynamic compliance or until the safety limits were reached. Safety limits included a tidal volume of ≤ 8 ml/kg IBW and transpulmonary driving pressure ≤ 12 cmH_2O. FCV was continued for a total of 90 minutes.

End of study

After completion of the study protocol, patient management resumed according to local protocols with PCV settings similar to baseline.

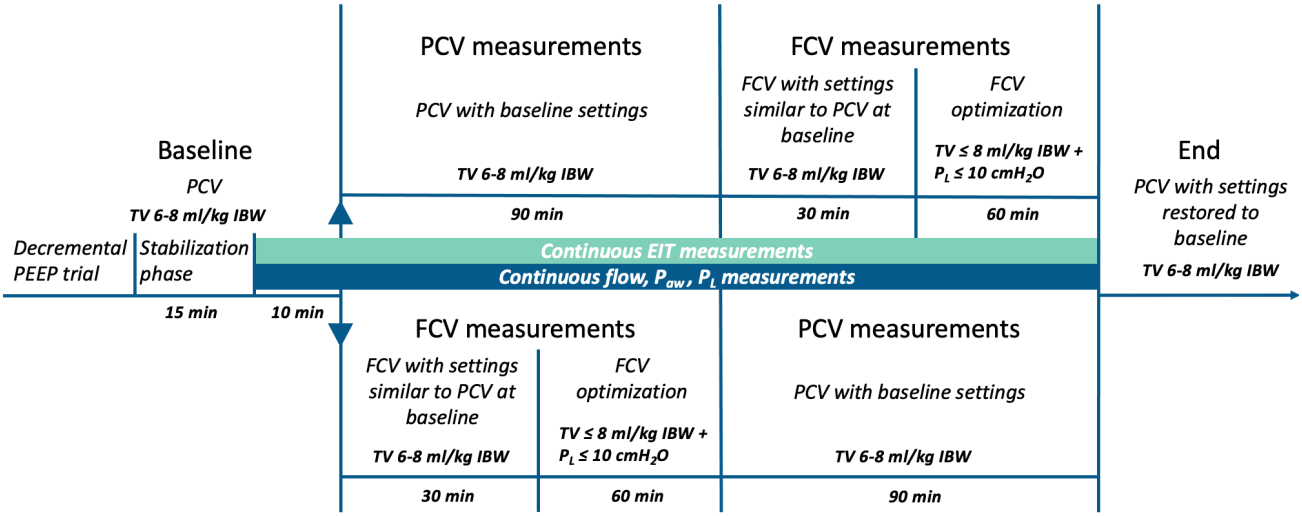

Figure 1. Depiction of study protocol and duration of steps. Patients are randomized to PCV-FCV or FCV-PCV order. Abbreviations: PCV = Pressure-controlled ventilation; FCV = Flow-controlled ventilation; EIT = Electrical impedance tomography; P_{aw} = Airway pressure, P_L = Transpulmonary pressure; TV = Tidal volume; IBW = Ideal body weight; PEEP = Positive end-expiratory pressure.

2.2 Data analysis

Computation of parameters was performed for PCV, initial FCV (FCV with settings similar to PCV) and optimized FCV.

EIT analysis

EIT data were converted for offline analysis using dedicated software (PV500 Data Analysis SW130) and processed using a custom software developed in Python. Methods for EIT analysis are similar to the methods in Chapter 2. At the end of each step (PCV, initial FCV and optimized FCV), a stable period of at least 10 breaths was manually selected for computation of parameters.

To reduce cardiac artefacts in the recordings, global and pixel impedance data were filtered using multiple digital notch (MDN) filtering. MDN filtering was first described for cardiac artefact removal in EIT data by Wisse and Somhorst et al. (results are yet to be published). MDN outperformed other filtering techniques by selectively removing cardiac frequencies and preserving respiratory information in the signal. Personalized cutoff frequencies are used for each patient by employing multiple fifth-order Butterworth notch filters. To determine the cutoff frequencies, an automatic heart rate detection algorithm was used. The first filter's stopband frequencies were set to the heart rate ± 10 beats per minute (BPM; 0.6 Hz). Subsequent notch filters were applied to the harmonics of the heart rate ± 10 BPM, until the harmonic frequency exceeded 210 BPM (3.5 Hz). These notch filters were then combined with a low-pass filter with a cutoff frequency of 210 BPM (3.5 Hz).

Signal baseline correction was performed, and inspiration time was normalized to allow comparisons within and between patients. Only pixels with a tidal impedance variation (ΔZ) of at least 15% of maximum pixel ΔZ were included in the analysis. For each stable period at each ventilation mode, the global ΔZ and regional ΔZ (i.e., per ROI) and global and regional static compliance (ΔZ/driving pressure) were calculated, as well as the change in global end-expiratory lung impedance (ΔEELI). Moreover, global inhomogeneity index (GI), regional spatial volume distribution for ventral, mid-ventral, mid-dorsal and dorsal ROIs, and regional ventilation delay inhomogeneity (RVDI) were computed. For a more detailed description of the parameter computation methods, see Chapter 2.

Flow and pressure analysis
From the flow and pressure recordings, a stable period of 10 minutes was selected at the end of each step (PCV, initial FCV and optimized FCV) and processed using a custom software developed in Python.

Breath-by-breath analysis was performed on the flow, intratracheal pressure and esophageal pressure tracings. Flow and intratracheal pressure were filtered with a second-order low-pass Butterworth filter with a cutoff frequency of 20 Hz. Even after low-pass filtering, esophageal pressure recordings

were contaminated by cardiac artefacts. Therefore, more advanced filtering was applied. Several different filtering techniques were tested. MDN filtering was chosen as it had the best visual performance in terms of preserving esophageal pressure information but removing the cardiac artefacts (Supplement Chapter 3, Figure 1). MDN filtering was performed as described above for the EIT data. To determine the cutoff frequencies, manual detection of the heart rate in the frequency spectrum was performed. After filtering, the transpulmonary pressure (P_L) signal was computed as: P_L = intratracheal pressure (P_{aw}) – esophageal pressure (P_{es}).

Median inspiratory time, respiratory rate, tidal volume (TV; time-integral of inspiratory flow) and minute volume were calculated per patient using the flow tracings. Peak pressure (Ppeak), total PEEP, and mean airway pressure were derived from the intratracheal pressure tracings. Transpulmonary peak pressure (P_L peak), end-expiratory transpulmonary pressure and mean transpulmonary pressure were derived from the transpulmonary pressure tracings. Moreover, airway and transpulmonary plateau pressure and driving pressure were determined manually during inspiratory and expiratory holds on the intratracheal and transpulmonary pressure curves. The driving pressures were used to calculate the static compliance of the total respiratory system (TV/ P_{aw} driving pressure) and the static compliance of the lungs (TV/ P_L driving pressure).

Pressure-volume (PV) loops were computed using the intratracheal pressure and the time-integral of flow tracings (Supplement Chapter 3, Figure 2). Transpulmonary pressure-volume (PV) loops were computed using the transpulmonary pressure and the time-integral of flow tracings (Supplement Chapter 3, Figure 3). From the intratracheal and transpulmonary PV-loops, the total energy per breath was determined as the integral of the PV-loop multiplied by 0.098 (conversion to Joule). The total energy per breath includes elastic dynamic and resistive components but excludes the static component, as the volume generated by PEEP is unknown. The mechanical power (Joule/min) was calculated by multiplying the total energy per breath by the respiratory rate. Dissipated energy was computed as the hysteresis area of the PV-loop per breath (in Joule/Liter).

Gas exchange and hemodynamics
PaO_2, $PaCO_2$, PaO_2/FiO_2 ratio, ventilatory ratio[5], and noradrenalin dose were obtained for each study step to compare gas exchange and hemodynamic status of the patient during PCV and FCV.

2.3 Statistical analysis
Data are presented as median (interquartile range) and were tested for normality using the Shapiro-Wilk test. Changes in ΔZ and static compliance are expressed as percentage change between steps, as both are expressed in arbitrary units, which makes direct comparisons between patients unreliable.

Statistical analysis was performed using SPSS (IBM, Armonk, USA). Values were compared between steps using the repeated measures ANOVA test, or the related-samples Friedman's test depending on the distribution with Bonferroni correction for multiple comparisons. A p-value <0.05 was considered statistically significant. As in Chapter 2, we primarily focused on the difference between PCV and optimized FCV.

3. RESULTS

So far, 1 patient has completed the full study protocol. Statistical analyses were not yet performed since no reliable comparison was possible with a single patient.

In this patient, optimized FCV resulted in a slightly lower mechanical power (11% reduction) and dissipated energy (10% reduction) of the total respiratory system when compared to PCV (Table 1). The transpulmonary mechanical power and dissipated energy were also lower (5% and 26% reduction, respectively) during optimized FCV (Table 1). The respiratory rate, minute volume and ventilatory ratio were lower during optimized FCV when compared to PCV (36%, 17% and 15% reduction, respectively). Optimized FCV also resulted in a lower airway resistance but in a higher airway and transpulmonary driving pressure (Table 1). $PaCO_2$ and hemodynamics remained stable between ventilation modes, oxygenation (PaO_2 and PaO_2/FiO_2 ratio) was slightly improved during optimized FCV (Table 1).

Similar results in terms of mechanical power and dissipated energy were found when comparing initial FCV to PCV, although reductions were slightly smaller. However, between initial FCV and PCV, minute volume and the airway driving pressure and transpulmonary driving pressures were similar. Important to note is that the goal during initial FCV was to reach the same tidal volume as with PCV. However, the results show that the tidal volume was 4.8 ml/kg during initial FCV rather than 5.2 ml/kg during PCV. For the full results of initial FCV compared to PCV, see Supplement Chapter 3, Table 1.

EIT results of this patient showed increased contribution of the dorsal ROI to tidal ventilation during optimized FCV when compared to PCV, even exceeding ΔZ values of the ventral ROI (Table 2 & Figure 2). However, the increased tidal volumes during optimized FCV may have led to overdistension of the ventral lung regions, as indicated by the decrease in static compliance when comparing optimized FCV to PCV across the ventral, mid-ventral, and mid-dorsal ROI (Table 2). Overall lung homogeneity, as reflected by GI, did not differ between the two modes. Temporal lung inhomogeneity was slightly higher in optimized FCV when compared to PCV as indicated by the RVDI.

During initial FCV, increased participation of the dorsal lung region can also be witnessed, while the participation of the other regions decreases, which can be explained by the slightly lower tidal volume during initial FCV than during PCV. For all EIT parameters comparing PCV with initial FCV ('similar' PCV settings) see Supplement Chapter 3, Table 2. For comparison of ventilation homogeneity parameters of all three study steps, see Supplement Chapter 3, Figures 4 and 5.

Table 1. Respiratory parameters PCV vs. optimized FCV

	PCV	Optimized FCV
Inspiratory TV/IBW (mL)	5.2	7.0
RR (x/min)	22	14
Minute volume (L/min)	6.5	5.4
Resistance (cmH_2O/L/s)	18.0	9.0
Total respiratory system parameters		
P_{aw} driving pressure (cmH_2O)	8.6	12.4
PEEP set (cmH_2O)	15	15
PEEP total (cmH_2O))	14.9	14.6
Ppeak set (cmH_2O)	26	29
Ppeak measured (cmH_2O))	25.1	29.6
Pplat (cmH_2O)	24.1	28.1
Pmean (cmH_2O)	18.9	22
Total compliance static (mL/cmH_2O)	34.3	32
Total Mechanical power (J/min)	13.2	11.8
Total Dissipated energy (J/L)	0.29	0.26
Transpulmonary parameters		
P_L driving pressure (cmH_2O)	6.7	9.8
P_L end-expiratory (cmH_2O)	4.2	4.1
P_L peak (cmH_2O)	12.1	16.3
P_L plat (cmH_2O)	11.4	14.8
P_L mean (cmH_2O)	7.4	10.2
Lung compliance static (mL/cmH_2O)	44	40.5
Transpulmonary Mechanical power (J/min)	5.7	5.4
Transpulmonary Dissipated energy (J/L)	0.27	0.20
Gas exchange parameters		
P/F ratio (mmHg)	246	229
PaO_2 (kPa)	11.48	13.73
$PaCO_2$ (kPa)	5.8	5.72
Ventilatory ratio	1.3	1.1
Hemodynamic parameters		
Dose noradrenalin (y)	0.36	0.38

Abbreviations: PCV = Pressure-controlled ventilation; FCV = Flow-controlled ventilation; IQR = Interquartile range; TV = Tidal volume; IBW = Ideal body weight; RR= Respiratory rate; P_{aw} = Airway pressure; PEEP = Positive end-expiratory pressure; Ppeak = Peak pressure; Pplat = Plateau pressure; Pmean = Mean airway pressure; P_L = Transpulmonary pressure. PaO_2 = Arterial partial oxygen pressure; $PaCO_2$ = Arterial partial carbon dioxide pressure; P/F ratio = PaO_2/FiO_2 ratio.

Table 2. EIT results PCV vs optimized FCV

Table 2a. Changes in EIT parameters during optimized FCV as compared to PCV			
	PCV	**Optimized FCV**	**% change**
Global ΔZ (a.u.)	12.1	15.8	30.6
Regional ΔZ			
ROI ventral	3.69	3.98	7.9
ROI mid-ventral	3.04	3.79	24.7
ROI mid-dorsal	2.83	3.88	37.1
ROI dorsal	2.52	4.19	66.2
Global static compliance (a.u.)	1.40	1.28	-8.6
Regional static compliance (a.u.)			
ROI ventral	0.43	0.32	-25.6
ROI mid-ventral	0.35	0.31	-11.4
ROI mid-dorsal	0.33	0.31	-6.1
ROI dorsal	0.29	0.34	17.2
Global EELI (a.u.)	3.26	3.51	7.7

Table 2b. Absolute EIT parameters reflecting lung and ventilation homogeneity		
	PCV	**Optimized FCV**
GI (%)	42.4	42.3
RVDI (%)	1.5	3.1

Abbreviations: EIT = Electrical impedance tomography; FCV = Flow-controlled ventilation; PCV = Pressure-controlled ventilation; ΔZ = Tidal impedance variation; a.u. = Arbitrary units; ROI = Region of interest; EELI = End-expiratory lung impedance; GI= Global inhomogeneity index; RVDI = Regional ventilation delay inhomogeneity.
The % change column shows the percentage changes in ΔZ, static compliance and EELI between optimized FCV and PCV.

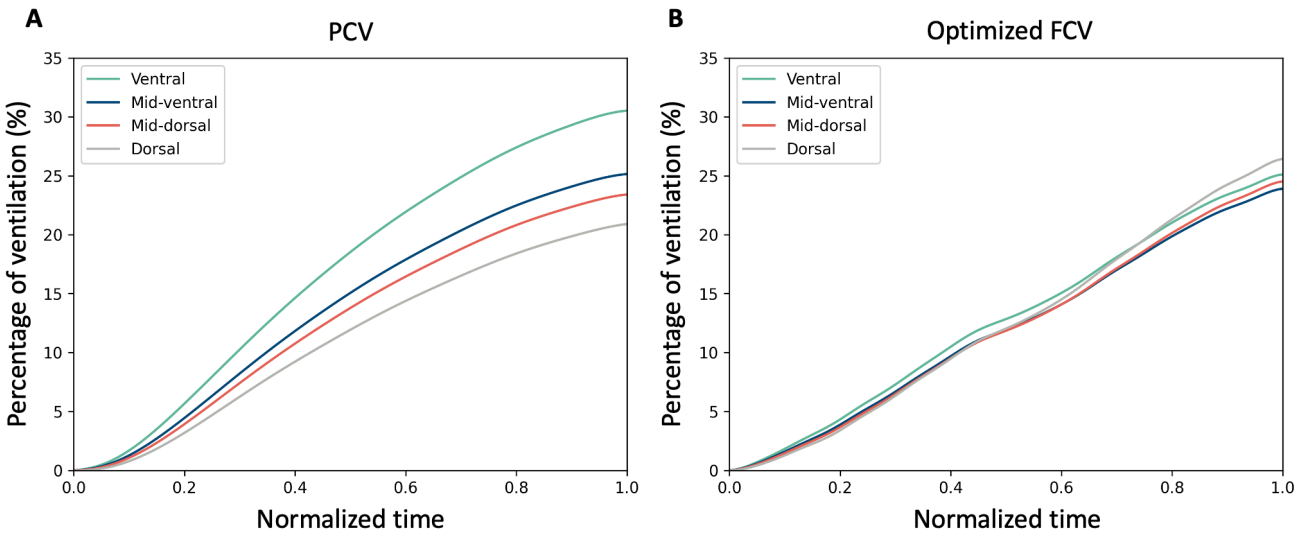

Figure 2. Continuous regional volume distribution of a single patient: normalized impedance per ROI over time and as a percentage of the global ΔZ. A) During PCV, B) During optimized FCV.

4. DISCUSSION

The aim of this study is to compare FCV to PCV in patients with ARDS in terms of ventilation homogeneity, lung aeration, mechanical power, and dissipated energy. Preliminary findings indicate that, in the case of this first ARDS patient, both the mechanical power and dissipated energy of the entire respiratory system, along with the transpulmonary mechanical power and dissipated energy, decrease during optimized FCV in comparison to PCV. Also, a stable gas exchange is achieved during FCV with lower minute volume than during PCV. Moreover, optimized FCV results in an increased contribution of the dorsal lung region to the ventilation distribution.

Effect of FCV on mechanical power

Previously, Grassetto et al.[6] demonstrated a significantly lower mechanical power during FCV than during volume-controlled ventilation (VCV) in ARDS patients. However, they measured pressure and flow proximally of the tube during VCV and distally during FCV.[6] As a result, during VCV the mechanical power could be higher due to the energy needed to overcome tube resistance, which is not incorporated in the FCV calculation. In contrast, we calculated mechanical power and dissipated energy by computing pressure-volume loops using flow and pressure determined intratracheally for both PCV and FCV.

In our previous study (Chapter 2), optimized FCV significantly lowered mechanical power and dissipated energy compared to PCV. Haudebourg et al.[7] demonstrated that employing a low driving pressure strategy increased tidal volume and reduced respiratory rate, leading to a 7% decrease in mechanical power. In patients with relatively healthy lungs, optimized FCV resulted in a substantial 30% reduction in mechanical power (Supplement Chapter 2, Supplemental analysis). This difference, compared to the 7% in the study by Haudebourg et al.[7], suggests an additional mechanism inherent to FCV that lowers mechanical power. Hypothetically, lower inspiratory flow rates result in a more even distribution of tidal volume across areas with different time constants, resulting in a more even distribution of lung stress and thus lower mechanical power.[8] In our first ARDS patient, optimized FCV yielded an 11% decrease in total respiratory system mechanical power and a 5% reduction in transpulmonary mechanical power compared to PCV. Further research is required to confirm if FCV in ARDS patients inherently reduces mechanical power of both the total respiratory system and lungs (determined by transpulmonary pressure-volume loops).

Effect of FCV on lung recruitment and homogeneity

In healthy lungs, the GI and RVDI were not significantly different between PCV and optimized FCV. However, due to the limited alveolar inhomogeneity, the potential for FCV to have an improving effect on the RVDI and GI is low. In ARDS patients, we might expect more room for improvement in this area. However, Muders et al.[9] showed that higher tidal volumes result in higher RVDI values during low flow inflation maneuvers.[9] Therefore, the higher tidal volumes during FCV might result in a lack of significant improvement in RVDI during FCV, but further results in our ARDS population are needed to draw conclusions.

Our results show an observable increase in ventilation in the dorsal lung areas when comparing optimized FCV to PCV. However, in this patient the increase in tidal volume during optimized FCV was accompanied by a decrease in regional static compliance, indicating that the increase in tidal volume led to overdistension of the ventral lung regions. This is in contrast with the results in patients with healthy lungs where the regional static compliance improved. Further results are needed to assess whether the increase in tidal volume in FCV results in increased

participation of the dorsal lung region but overdistension of the ventral lung region across the entire study population of ARDS patients.

Strengths and limitations

Until now, no physiological study has assessed the mechanical power, dissipated energy, and specific ventilation distribution between FCV and PCV in patients with ARDS using intratracheal pressure and flow sensors, and EIT monitoring. Moreover, we also used esophageal pressure to estimate transpulmonary mechanical power and dissipated energy. These transpulmonary measures provide important additional information on the lungs as compared to the total respiratory system (including the chest wall). A strength of the current study is the randomization of ventilation sequence, which is important to consider when comparing the results to the results of the study in postoperative ICU patients (Chapter 2), since ventilation modes were not randomized in that study. For now, interpretation of the results is limited by the sample size of 1 but the effects should be interpretable when the goal of 28 inclusions is reached.

Clinical implications

This study aims to clarify the role of FCV in lung-protective mechanical ventilation for patients with ARDS. FCV results in higher tidal volumes and driving pressures than during conventional PCV, which conflicts with the idea of low tidal volumes for lung-protective ventilation.[1] In fact, the driving pressure, respiratory rate and mechanical power are significant predictors of mortality in patients with ARDS on controlled mechanical ventilation.[10] However, the driving pressure and respiratory rate are also independently associated with mortality, with the impact of driving pressure being four times as large as of the respiratory rate.[10] Nevertheless, the mechanism of FCV is different than that of conventional controlled mechanical ventilation and in postoperative patients with healthy lungs, FCV resulted in a significantly lower mechanical power and dissipated energy. Further results are needed in this study in ARDS patients to determine the relevant clinical implications. If FCV proves promising, it is important to study its impact on long-term outcomes, like ventilator-free days and mortality. Moreover, there might be a role for the use of advanced respiratory monitoring to assess which patients are likely to benefit from

FCV. For instance, patients who are recruitable are more likely to benefit from the recruitment effect of FCV without causing overdistension of the more ventral lung areas.

5. CONCLUSION

In conclusion, this study holds promise to uncover the effects of FCV on mechanical power, dissipated energy, and ventilation homogeneity in patients with ARDS. More results are needed to determine these effects and to discover interindividual differences between patients. These differences might be relevant in the future to determine which patients are likely to have a beneficial response to FCV.

REFERENCES

1. Barnes T, van Asseldonk D, Enk D. Minimisation of dissipated energy in the airways during mechanical ventilation by using constant inspiratory and expiratory flows – Flow-controlled ventilation (FCV). Medical Hypotheses. 2018;121:167-176.

2. Kollisch-Singule M, Emr B, Smith B, et al. Airway pressure release ventilation reduces conducting airway micro-strain in lung injury. J Am Coll Surg. 2014;219(5):968-976.

3. Force* TADT. Acute Respiratory Distress Syndrome: The Berlin Definition. JAMA. 2012;307(23):2526-2533.

4. Barnes T, van Asseldonk D, Enk D. Minimisation of dissipated energy in the airways during mechanical ventilation by using constant inspiratory and expiratory flows - Flow-controlled ventilation (FCV). Med Hypotheses. 2018;121:167-176.

5. Sinha P, Calfee CS, Beitler JR, et al. Physiologic Analysis and Clinical Performance of the Ventilatory Ratio in Acute Respiratory Distress Syndrome. Am J Respir Crit Care Med. 2019;199(3):333-341.

6. Grassetto A, Pettenuzzo T, Badii F, Carlon R, Sella N, Navalesi P. Flow-controlled ventilation may reduce mechanical power and increase ventilatory efficiency in severe coronavirus disease-19 acute respiratory distress syndrome. Pulmonology. 2023;29(2):154-156.

7. Haudebourg A-F, Tuffet S, Perier F, et al. Driving pressure-guided ventilation decreases the mechanical power compared to predicted body weight-guided ventilation in the Acute Respiratory Distress Syndrome. Critical Care. 2022;26(1):185.

8. Marini JJ, Rocco PRM, Gattinoni L. Static and Dynamic Contributors to Ventilator-induced Lung Injury in Clinical Practice. Pressure, Energy, and Power. Am J Respir Crit Care Med. 2020;201(7):767-774.

9. Muders T, Hentze B, Simon P, et al. A Modified Method to Assess Tidal Recruitment by Electrical Impedance Tomography. J Clin Med. 2019;8(8).

10. Costa ELV, Slutsky AS, Brochard LJ, et al. Ventilatory Variables and Mechanical Power in Patients with Acute Respiratory Distress Syndrome. Am J Respir Crit Care Med. 2021;204(3):303-311.

ADDITIONAL RESEARCH

CHAPTER 4

PHYSIOLOGICAL DEFINITION FOR REGION OF INTEREST SELECTION IN ELECTRICAL IMPEDANCE TOMOGRAPHY DATA: DESCRIPTION AND VALIDATION OF A NOVEL METHOD

This chapter was recently submitted as a full paper with authors:

Juliette E. Francovich, Peter Somhorst, Diederik A.M.P.J. Gommers, Henrik Endeman and Annemijn H. Jonkman

1. INTRODUCTION

Electrical impedance tomography (EIT) is a non-invasive and real-time bedside lung imaging technique that is increasingly employed with mechanically ventilated patients, especially with conditions like the acute respiratory distress syndrome (ARDS).[1-3] It is often used to assess the gravity-related ventilation distribution and changes in this distribution upon adjustments in ventilator settings or body position.[1,4,5] For instance, the ventral-to-dorsal ratio has been used to guide positive end-expiratory pressure (PEEP) titration, with a ratio of 1 suggesting homogeneous anteroposterior distribution of ventilation.[6] Other similar descriptions that reflect the spatial inhomogeneity include the dorsal fraction of ventilation (i.e., the fraction of tidal impedance variation (TIV) to the dorsal lung (TIVdorsal/TIVglobal))[5], or the ventrodorsal Center of Ventilation (CoV)[7]. A higher ventilation distribution to the dependent lung region typically indicates excessive PEEP. However, when dividing the EIT image into two equal horizontal regions of interest (ROIs), which is often described[8-10], it is not uncommon for the dependent ROIs to exhibit much smaller ventilation changes as compared to the non-dependent lung.[7] This also implies that in case of homogeneous ventilation the ventral-to-dorsal ratio is not expected to be 1, which is especially relevant in ARDS.

Ideally, ROI selection should be based on the sensitivity to local ventilation-induced changes in electrical impedance.[11] In fact, Frerichs et al.[7] recommended using the CoV over the ventral-to-dorsal ratio as a more robust parameter to assess changes in ventrodorsal ventilation distribution. The CoV has been shown to be a useful index that is sensitive to (de) recruitment during incremental and decremental PEEP trials.[12] The CoV is a linear measure of the weighted geometrical center in an EIT image.[13] Thus, the CoV is sensitive to changes in the position of the ventilation distribution, and as the distribution shifts, the CoV changes proportionally. On the other hand, the ventral-to-dorsal ratio assesses the relative amounts of ventilation in these two specific regions. Changes in ventilation distribution may not impact both regions in a proportional manner, leading to a non-proportional change in their ratio. Moreover, many EIT parameters, including the CoV and ventral-to-dorsal ratio, are influenced by the method of lung segmentation. Lung segmentation refers to the process

of identifying the functional lung area in the global EIT image[7] and is often performed prior to calculation of EIT parameters, or prior to further ROI selection. Generally, the functional lung area is defined as those pixels with a TIV above a certain threshold percentage of the maximum pixel TIV.[7] Inherent to this segmentation, the threshold determines which pixels are included in further analyses.[14] Therefore, both accurate lung segmentation and ROI selection is crucial for EIT analyses to effectively assess changes in spatial ventilation distribution, especially when the evaluation of subtle changes is of interest.

In this paper, we propose a novel method of ROI definition, where each ROI equally contributes to the total TIV at different time points with different ventilator settings. This physiological approach for ROI selection prior to calculation of parameters such as the ventral-to-dorsal ratio should allow the assessment of subtle changes in regional impedance variation, congruent with the CoV. We describe this new method and demonstrate its implications for EIT parameter calculation. To this end, we compare the values of both the CoV and ventral-to-dorsal ratio as computed utilizing the new method, with those after different commonly used methods for ROI selection. Furthermore, we describe the impact of ROI selection on PEEP titration when using the ventral-to-dorsal ratio.

2. METHODS

Subjects and EIT acquisition

To compare the effects of different methods of ROI selection, EIT measurements from 49 pressure-controlled mechanically ventilated patients were used. Data were part of a previous study in COVID-19 ARDS[15] where decremental PEEP trials were performed within standard of care in the intensive care unit of the Erasmus Medical Centre (EMC) in Rotterdam. The EMC Medical Ethics Review Committee approved that retrospective study and permitted a waiver of informed consent.

The EIT measurements were performed using the Dräger PulmoVista® 500 with a silicone belt consisting of sixteen electrodes placed between the 5th and 6th intercostal space. The measurements were performed with the patient in supine position during a decremental PEEP trial in pressure-controlled

ventilation. During the PEEP trial, the PEEP level was decreased in the range from 30 cmH_2O to 2 cmH_2O in steps of 2 cmH_2O with intervals of 1 to 2 minutes. The exact range and number of PEEP steps varied per patient. Therefore, measurements for PEEP levels ranging from 24 to 6 cmH_2O were included in the analysis.

Data preprocessing

Raw EIT data were converted using dedicated software (EITdiag; Dräger Medical) and pixel-level data were then processed using a custom software developed in Python (version 3.10). Per patient a stable period of at least 10 breaths was selected at each PEEP step. From each stable period an average breath was computed to calculate the TIV. Signal baseline correction was performed, and inspiration time was normalized to allow further comparisons within and between patients.

ROI calculation methods

The TIV map was summed over all PEEP steps and divided into a ventral and dorsal region based on five different combinations of lung segmentation and ROI selection:

- Global lung, geometrical ROI selection: the global TIV map (no lung segmentation performed) was divided into two horizontal equal-sized regions (16 rows each).

- Functional lung area, geometrical ROI selection - 15%, 20% and 35% thresholds:
  The functional lung area was defined as those pixels with a TIV of at least 15%, 20% and 35% of maximum pixel TIV, respectively. These thresholds were chosen in line with earlier work including the EIT consensus paper.[7,16]
  To determine this functional lung area, the TIV maps were first summed over all PEEP steps to include all pixels that were ventilated at any step throughout the PEEP trial.
  The resulting functional lung area was divided into two equal-sized horizontal regions. If there was an uneven number of rows left after the lung segmentation, the ventral ROI was chosen to be larger (with one pixel row) than the dorsal ROI.

- Functional lung area, physiological ROI selection:
  The functional lung area was defined as those pixels with

a TIV of at least 20% of maximum pixel TIV. As previously described, the TIV maps were first summed over all PEEP steps to include all pixels that were ventilated in any step throughout the PEEP trial. The resulting functional lung area was divided into two ROIs with each ROI representing exactly 50% of the total TIV of this summed TIV map. Since this division at 50% rarely falls exactly at the border of two pixel rows, the pixel row that lies on the dividing line can contribute to both the ventral and dorsal ROI. Hence, we applied the following computation: if the division between the ventral and dorsal ROI was e.g., at 40% of a given pixel row, we added 40% of the TIV of that pixel row to the ventral ROI, and the remaining 60% of the TIV of that pixel row to the dorsal ROI. See Supplemental Figures 1 and 2 for a visual explanation of this ROI division method.

Next, these ROI divisions, as determined using the summed TIV map of all PEEP steps, were applied to the original TIV map (global or functional lung area) of each PEEP step (see Supplemental Figure 1).

Computation of parameters

The CoV was computed on the TIV map of each PEEP step as the weighted mean of the sum of TIV per row in the global or functional lung area, in line with the original description of Frerichs et al.[7]. Per patient, the average vertical position of the CoV over all PEEP steps was compared to the vertical position of the division line separating the ventral and dorsal ROI according to each method of ROI definition (see Supplemental Figure 3). Since our physiological ROI division lies between 50% TIV in the ventral region and 50% in the dorsal region, the division line should approximate the CoV, except for in patients with an uneven vertical distribution of the TIV over the two regions. Moreover, for each ROI selection method, the ventral-to-dorsal ratio at each PEEP step was computed for all patients.

Evaluation of methods

Computed parameters (CoV and ventral-to-dorsal ratio) after different methods of ROI definition were compared using descriptive statistics and visual representation of the differences. Data were tested for normality using the Shapiro-Wilk test. The distribution of the difference between the average

vertical position of the CoV and the vertical position of the division line between the ventral and dorsal ROI for each ROI selection method was visualized using a violin plot. The Wilcoxon signed-rank test was used to test whether the median was statistically different from zero. Moreover, the mean ventral-to-dorsal ratio over all patients was computed and plotted per PEEP step for each ROI selection approach. The PEEP level at which the ventral-to-dorsal ratio was closest to 1 for each patient was compared between ROI selection methods. A linear mixed effects model was used to estimate the interaction effect between the ROI selection method and PEEP level. Differences between ROI selection methods were evaluated with the repeated measures analysis of variance (ANOVA) or the non-parametric Friedman's test depending on the distribution and using Tukey post-hoc tests with Bonferroni correction for multiple comparisons. Statistical analyses were performed in Python (version 3.10) and a p-value < 0.05 was considered statistically significant.

3. RESULTS

Figure 1 shows the result of the different methods of ROI definition on the summed TIV map over all PEEP steps in a representative patient. In addition, the average position of the CoV (average over all PEEP steps) is shown, illustrating that the threshold chosen for the functional lung area (or the lack of a threshold in the global geometrical method) strongly influences the number of pixels included in the ROIs, but also the position of the division line separating the ventral and dorsal ROI and the CoV.

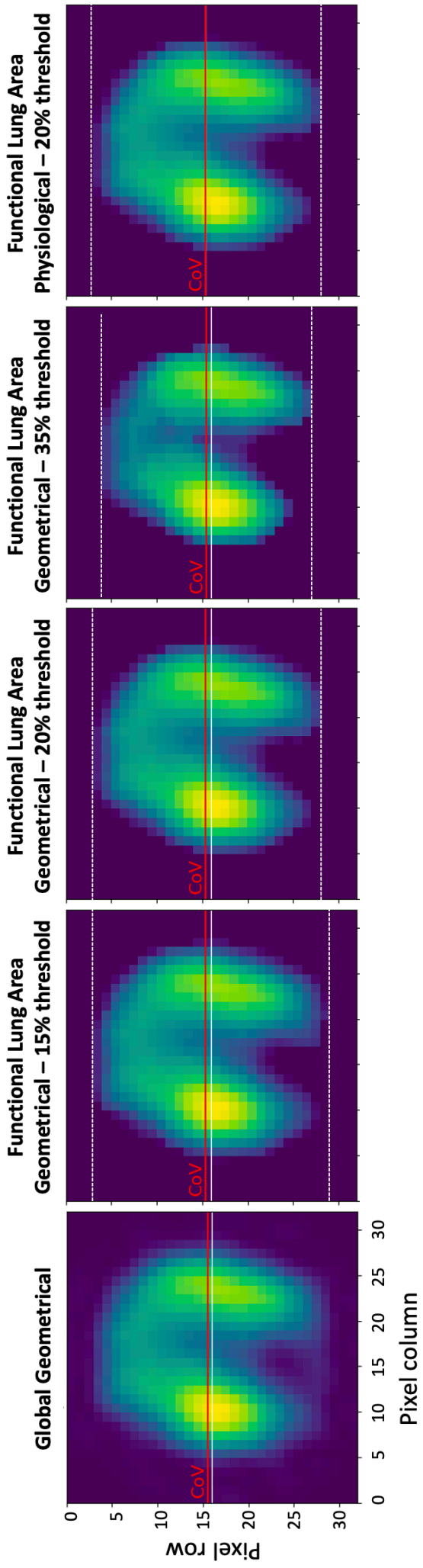

Figure 1. Example of different ROI types in a single patient. Each tile shows the average TIV map of all PEEP steps in a single patient that is divided into a ventral and dorsal region using different types of ROI definition. Global geometrical divides the global image into two regions of 16 rows each. Functional lung area geometrical divides the functional lung area into two equally sized regions. The functional lung area is defined as the area of pixels above a certain percentage of the maximal TIV. Functional lung area physiological divides the functional lung area into two areas that each comprise exactly 50% of the total TIV. The red line shows the average vertical position of the Center of Ventilation (CoV) over all PEEP steps. The CoV is plotted exactly over the physiological ROI division in the rightmost panel. The dotted lines reflect the boundary of the functional lung area.

Effect of ROI selection on CoV

The distribution of the difference between the vertical position of the ROI division line and the CoV for each ROI calculation method is shown in Figure 2. On a group level, there was no significant difference between the CoV position and ROI division line for most methods of ROI definition, except for the functional lung area geometrical ROI with a 35% threshold (p = 0.04) (Figure 2); however, the distribution of these differences indicated a large variability between patients depending on the ROI selection method, with the smallest variability found for the physiological ROI method (Figure 2). Post-hoc testing revealed that the position differences were significantly different between the different ROI methods (p = 0.006), especially between the functional geometrical ROI with a 20% threshold and with a 35% threshold (p = 0.0007).

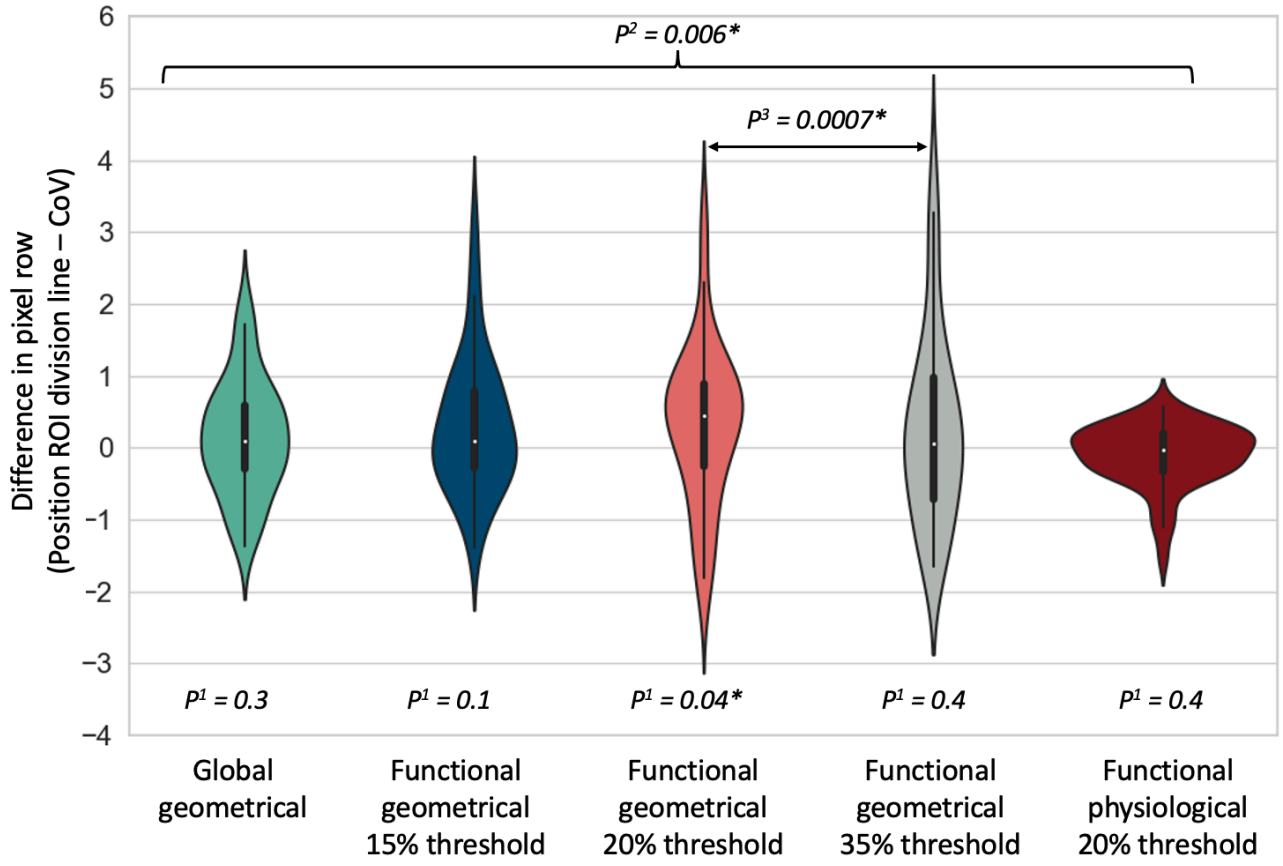

Figure 2. Violin plot of the difference in vertical position (number of rows) of the division line between the ventral and dorsal region of interest (ROI division line) and the Center of Ventilation (CoV) over all PEEP levels per patient for five methods of ROI selection.
* Indicates significant p-values < 0.05.
[1] P-values indicate whether the median is statistically different from 0.
[2] P-value indicates that there is a statistically significant difference between ROI selection methods based on the Friedman's test.
[3] P-value indicates a statistically significant difference between two specific ROI selection methods based on post-hoc testing.

Effect of ROI selection on ventral-to-dorsal ratio

Figure 3 shows, for each ROI selection method, the calculated ventral-to-dorsal ratio across the decremental PEEP trial for all patients, indicating large within- and between-subject variation in this computed parameter ($p<0.001$ for interaction term of ROI method and PEEP level). The PEEP level corresponding to a ventral-to-dorsal ratio closest to 1 was significantly different between the different ROI methods ($p = 0.01$); the within-subject range was 6.2 cmH_2O on average (min-max: 0 to 16 cmH_2O) when considering all ROI selection methods. Table 1 shows, for the different ROI methods, the within-patient difference in the PEEP level corresponding to a ventral-to-dorsal ratio closest to 1, when using the physiological ROI method as reference.

Table 1. Median (IQR), minimum and maximum difference of all patients between the PEEP level at which the ventral-to-dorsal ratio was closest to 1 (selected PEEP) for each ROI method and as compared to the physiological ROI method (PEEP ROI method – PEEP physiological ROI method).

ROI method	Difference in selected PEEP compared to physiological ROI method (cmH_2O) Median (IQR) [min-max]
Global geometrical	-2 (-6 – +2) [-10 – +12]
Functional lung area geometrical 15% threshold	-2 (-6 – +2) [-12 – +8]
Functional lung area geometrical 20% threshold	-2 (-6 – +2) [-10 – +8]
Functional lung area geometrical 35% threshold	-2 (-6 – 0) [-10 – +10]

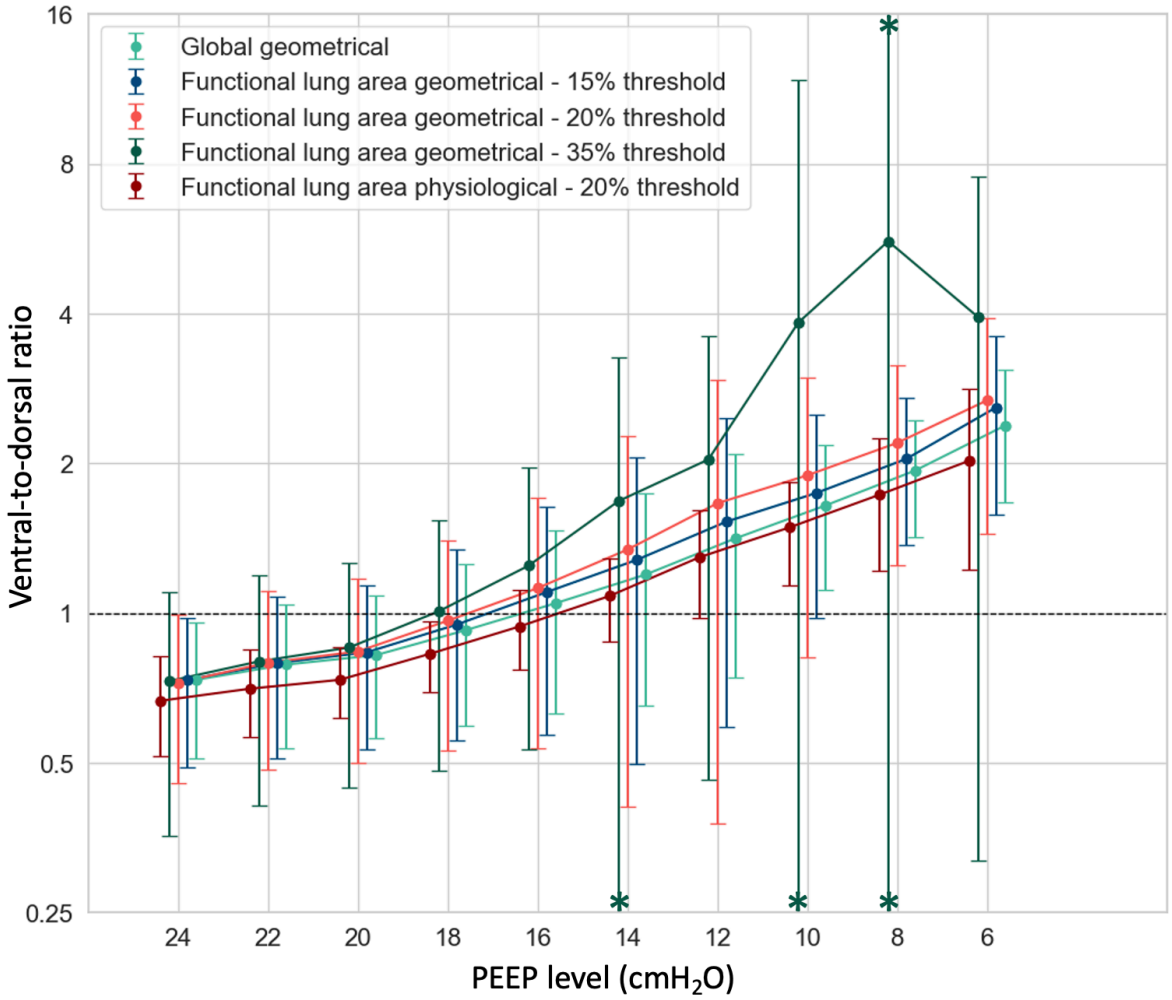

Figure 3. Mean ventral-to-dorsal ratio with 95% confidence interval of all patients per ROI type at each PEEP step. The dotted line at 1 indicates the PEEP level at which a ventral-to-dorsal ratio of 1 was reached. A ventral-to-dorsal ratio of 1 is considered a homogeneous anteroposterior ventilation. An asterisk (*) on the error-bar indicates that the boundaries of the confidence-interval were beyond the plotted y-axis limits that were chosen as a cut-off for better visualization. A logarithmic scale was used to visualize smaller differences around the ventral-to-dorsal ratio of 1.

4. DISCUSSION

We have proposed a novel method of ROI selection where each ROI represents an equal contribution to the total impedance variation summed over all steps that are included in an EIT analysis. Benefits were demonstrated by applying this method to decremental PEEP trials and computing the CoV and ventral-to-dorsal ratio. We found that our novel physiological method for ROI selection yielded the smallest variation when comparing the vertical position of the ROI division line to the vertical position of the CoV, indicating highest agreement with the sensitivity of the CoV. Moreover, the PEEP level associated with a ventral-to-dorsal ratio of 1 is strongly influenced by the chosen ROI selection method, which could have a profound impact on PEEP titration as indicated by a within-subject range of 6.2 cmH_2O depending on the chosen ROI selection.

Remarkably, the global geometrical ROI was closest to the functional physiological ROI with respect to the difference with the CoV and the ventral-to-dorsal ratio. We can offer two possible explanations. First, the ROIs were determined on the sum of impedance maps at each PEEP step. This implies that across a decremental PEEP trial, low PEEP levels with typically less ventilation in the dependent lung areas are balanced by higher PEEP levels with increased ventilation in these areas. This is especially relevant in our cohort of patients with mostly recruitable lungs.[15] If we were to compute the differences between the global geometrical ROI and the functional physiological ROI within a single PEEP level, we would likely observe more discrepancies. Moreover, when functional geometrical ROIs are computed, the ventral region will be larger than the dorsal region if the functional lung area has an uneven number of rows. This may explain why larger differences could arise between the physiological ROI definition and the functional geometrical ROI definition in terms of CoV.

We demonstrated large inter- and intraindividual differences of parameters calculated after various methods of ROI definition. We could argue that a threshold of 35% for the functional lung area (the maximum threshold recommended by Frerichs et al.[7]) is too high, considering the large number of pixels that is removed from further analyses. This could limit adequate interpretation of the ventral-to-dorsal ratio, especially at lower PEEP steps with a small dependent lung area. Hence, small

impedance changes in this region could have a large influence on the ventral-to-dorsal ratio. Nevertheless, even when removing the functional lung area with a 35% threshold from the analysis, the ventral-to-dorsal ratio closest to 1 was significantly different between the different ROI methods ($p = 0.005$) and the within-subject PEEP range was 5.4 cmH_2O on average (min-max: 0 to 16 cmH_2O).

Development of a physiological method for ROI selection

We have developed a physiological approach for computation of ROIs that allows to assess subtle regional impedance changes between different data segments. Inherent to the computation of our physiological ROI division method (representing 50% of the average ventilation), the line that divides the ventral and dorsal ROI is on average similar to the CoV. Only in patients with an uneven vertical distribution of the TIV over the two regions, small differences arise between the CoV and the physiological ROI 50% division line. Moreover, the ventral-to-dorsal ratio is not always a reliable measure for homogeneity of ventrodorsal ventilation distribution.[6,7] For instance, the ventral-to-dorsal ratio can become arbitrarily large if the dorsal region has low TIV, which is especially relevant in ARDS patients.[6,7] However, when using the physiological ROI division across different ventilator settings, a ventral-to-dorsal ratio of 1 does imply a homogenous ventrodorsal ventilation distribution.

Moreover, in addition to impedance changes from lung aeration, pulmonary perfusion also introduces slight fluctuations (about 3%) in thoracic impedance between heartbeats.[17] Maintaining uniform relative impedance across various ROIs mitigates the influence of cardiac artifacts, as a 3% fluctuation can have a more pronounced impact in areas with initially low impedance. Therefore, another advantage of our new method of ROI definition is the mitigation of cardiac artifacts in regional impedance analysis.

Another method for mitigation of cardiac artefacts is adequate thresholding for the functional lung area. We argue that a threshold of 35% is too high, removing relevant ventilatory information. However, a threshold that is too low might introduce too much noise and cardiac artefacts. We chose to compute the physiological ROI on a functional lung area with a

20% threshold. Nevertheless, a sensitivity analysis with a 15% threshold did not alter the results.

Finally, if the functional lung area has an uneven number of rows, attributing the extra row to the ventral region rather than the dorsal region is an arbitrary choice. Our new physiological method for ROI definition does not involve such arbitrary choices since EIT rows will be exactly equally divided across the two regions.

Strengths and limitations

Previous work has been performed to determine the effects of threshold selection for lung segmentation.[11,14] However, this is the first study to date to systematically compare the effects of region selection in this segmented lung, which is essential when calculating regional parameters such as the ventral-to-dorsal ratio. Moreover, we have introduced a novel method that we have validated by comparing it to a varied range of different ROI selection methods in a large dataset of 49 patients using commonly used EIT parameters (i.e. CoV and ventral-to-dorsal ratio).

Some limitations should be acknowledged. First, our new method has only been performed on two regions. If more than two regions are defined (i.e., four layers), the differences between ROI methods will likely increase due to limited ventilation in the most dependent lung region with geometrical ROIs. For readability of this paper, we chose to use only two regions, but our methods can easily be extended to an application with more regions (e.g. four ROIs with 25% of total TIV each). Furthermore, the analysis was performed for only three lung segmentation thresholds, 15%, 20% and 35% respectively. We did not aim to validate the different threshold levels but to compare geometrical ROIs to our physiological approach; results were robust when altering the threshold to 15% for the physiological ROI. Third, we used data from decremental PEEP trials to illustrate the impact of ROI selection. Differences between ROI selection methods will change according to the clinical setting. As we included a wide range of PEEP steps (24 to 6 cmH_2O), it is expected that most of the variation in terms of ventilated lung area was captured. It should be noted, however, that the ROI division depends on

the maximum and minimum PEEP level applied. Adding more steps at higher PEEP levels will increase the total TIV in the then recruited dependent area, while adding more steps at the lower PEEP range will increase the total TIV in the then well-ventilated non-dependent area. As a sensitivity analysis, we added PEEP steps of 26 to 30 cmH_2O to the analysis when available, but this did not alter the results.

Clinical importance

We have demonstrated that the method for ROI selection has a strong influence on the consecutively computed EIT parameters, both between and within patients. Our new method offers an ROI definition that is sensitive to subtle impedance changes, like the CoV. Therefore, we urge clinicians and researchers to carefully consider the ROI method chosen for a specific application. For instance, when titrating PEEP according to the ventral-to-dorsal ratio we found an average within-subject range of 6.2 cmH_2O for the selected PEEP depending on the ROI selection method, which has important clinical implications. Even though the ventral-to-dorsal ratio might not be commonly used to titrate PEEP, it serves as an important reminder to be aware of the effects of ROI selection when using regional EIT parameters to guide clinical decisions. These results also underscore the importance of standardization of EIT analyses and motivation for the choices made in specific analyses. Our team is currently developing open-source software to contribute to such standardized EIT analyses.[18]

5. CONCLUSION

Our novel method for ROI definition based on equal impedance variation per region is a useful method for defining ROIs that are sensitive to (de)recruitment during mechanical ventilation, similar to the CoV. In this way, regional EIT analyses can be performed with ROIs that are sensitive to subtle ventilation-induced changes in regional impedance.

REFERENCES

1. Yang L, Dai M, Cao X, et al. Regional ventilation distribution in healthy lungs: can reference values be established for electrical impedance tomography parameters? Ann Transl Med. 2021;9(9):789.

2. Jonkman AH, Alcala GC, Pavlovsky B, et al. Lung RecruitmEnt assessed by eleCtRical Impedance Tomography (RECRUIT): a multicenter study of COVID-19 ARDS. American Journal of Respiratory and Critical Care Medicine. 2023(ja).

3. Blankman P, Hasan D, Erik GJ, Gommers D. Detection of 'best'positive end-expiratory pressure derived from electrical impedance tomography parameters during a decremental positive end-expiratory pressure trial. Critical care. 2014;18:1-10.

4. Lehmann S, Leonhardt S, Ngo C, et al. Electrical impedance tomography as possible guidance for individual positioning of patients with multiple lung injury. Clin Respir J. 2018;12(1):68-75.

5. Yoshida T, Piraino T, Lima CAS, Kavanagh BP, Amato MBP, Brochard L. Regional Ventilation Displayed by Electrical Impedance Tomography as an Incentive to Decrease Positive End-Expiratory Pressure. Am J Respir Crit Care Med. 2019;200(7):933-937.

6. Hochhausen N, Biener I, Rossaint R, et al. Optimizing PEEP by Electrical Impedance Tomography in a Porcine Animal Model of ARDS. Respiratory Care. 2017;62(3):340-349.

7. Frerichs I, Amato MB, van Kaam AH, et al. Chest electrical impedance tomography examination, data analysis, terminology, clinical use and recommendations: consensus statement of the TRanslational EIT developmeNt stuDy group. Thorax. 2017;72(1):83-93.

8. de Souza Rossi F, Yagui ACZ, Haddad LB, Deutsch ADA, Rebello CM. Electrical impedance tomography to evaluate air distribution prior to extubation in very-low-birth-weight infants: a feasibility study. Clinics. 2013;68(3):345-350.

9. Schramel J, Nagel C, Auer U, Palm F, Aurich C, Moens Y. Distribution of ventilation in pregnant Shetland ponies measured by Electrical Impedance Tomography. Respiratory Physiology & Neurobiology. 2012;180(2):258-262.

10. Radke Oliver C, Schneider T, Heller Axel R, Koch T. Spontaneous Breathing during General Anesthesia Prevents the Ventral Redistribution of Ventilation as Detected by Electrical Impedance Tomography: A Randomized Trial. Anesthesiology. 2012;116(6):1227-1234.

11. Pulletz S, van Genderingen HR, Schmitz G, et al. Comparison of different methods to define regions of interest for evaluation of regional lung ventilation by EIT. Physiol Meas. 2006;27(5):S115-127.

12. Luepschen H, Meier T, Grossherr M, Leibecke T, Karsten J, Leonhardt S. Protective ventilation using electrical impedance tomography. Physiol Meas. 2007;28(7):S247-260.

13. Frerichs I, Hahn G, Golisch W, Kurpitz M, Burchardi H, Hellige G. Monitoring perioperative changes in distribution of pulmonary ventilation by functional electrical impedance tomography. Acta Anaesthesiol Scand. 1998;42(6):721-726.

14. Becher T, Vogt B, Kott M, Schädler D, Weiler N, Frerichs I. Functional Regions of Interest in Electrical Impedance Tomography: A Secondary Analysis of Two Clinical Studies. PLoS One. 2016;11(3):e0152267.

15. Somhorst P, van der Zee P, Endeman H, Gommers D. PEEP-FiO(2) table versus EIT to titrate PEEP in mechanically ventilated patients with COVID-19-related ARDS. Crit Care. 2022;26(1):272.

16. Heines SJH, de Jongh SAM, Strauch U, van der Horst ICC, van de Poll MCG, Bergmans D. The global inhomogeneity index assessed by electrical impedance tomography overestimates PEEP requirement in patients with ARDS: an observational study. BMC Anesthesiol. 2022;22(1):258.

17. Tomicic V, Cornejo R. Lung monitoring with electrical impedance tomography: technical considerations and clinical applications. J Thorac Dis. 2019;11(7):3122-3135.

18. ALIVE: Advanced Lung Image processing for personalized mechanical VEntilation. Research Software Directory. https://research-software-directory.org/projects/alive. Accessed 2023.

CHAPTER 5

ADVANCED LUNG IMAGE PROCESSING FOR PERSONALIZED MECHANICAL VENTILATION (ALIVE PROJECT)

1. INTRODUCTION TO ALIVE

Mechanical ventilation, while life-saving for patients with acute respiratory failure, can also exacerbate lung injury and inflammation.[1,2] Therefore, there is a crucial need for simple and dependable bedside techniques to deliver personalized, lung-protective ventilation.[3,4] One highly promising technology is electrical impedance tomography (EIT), which enables bedside monitoring of regional lung aeration dynamics in mechanically ventilated patients.[5]

Nevertheless, the integration of EIT data into clinical practice lags, primarily due to technological challenges in processing this data. Existing built-in software tools from EIT manufacturers allow only relatively simple parameter calculation at selected time points. However, the potential exists for far more valuable information to be derived from EIT data, for instance on pixel level, by selecting specific regions of interest or by performing a breath-by-breath analysis.

The ALIVE project is the development of an open source Python workflow for standardized EIT analysis. It will also allow for synchronization with simultaneously recorded ventilator waveforms and functional respiratory signals (e.g., transpulmonary pressures and respiratory muscle activity). Automated integration of these signals with EIT data enables a more comprehensive interpretation of EIT information within the framework of personalized lung-protective mechanical ventilation. This open source software will allow for standardized, reusable, and sustainable analyses of EIT data for a wide range of applications. It will enhance clinical use of EIT data and streamline the processing of research data.

2. CONTRIBUTIONS TO ALIVE

The envisioned ALIVE workflow that is currently being developed within the research team and together with research software engineers from the Netherlands eScience Center encompasses all stages from data loading and preprocessing to analysis. Figure 1 shows a simplified version of the ALIVE workflow with examples of each step. ALIVE software can handle input data in various formats, depending on the EIT machine vendor (e.g., Dräger, Timpel, Sentec) and includes ventilator waveforms and functional respiratory signals, such as

transpulmonary pressure. These different input signals can be synchronized, which is particularly useful for tasks like detecting the start and end of breaths in EIT data based on ventilator flow recordings.

Subsequently, users can manually select data segments for further processing or use built-in algorithms to perform stable period or positive end-expiratory pressure (PEEP) step detection automatically. For example, automated PEEP step detection can aid in comparing EIT parameters at different PEEP levels during a decremental PEEP trial. The selected data segments can then be tailored to the user's requirements through filtering and are ready for analysis.

The possibilities for EIT analysis and parameter computation are extensive. In my thesis project, I developed several methods for parameter calculation and defining regions of interest. Chapters 2 and 3 outline the EIT parameters I computed to assess the effects of flow-controlled ventilation, such as tidal impedance variation, the global inhomogeneity index, regional ventilation delay inhomogeneity, and end-expiratory and end-inspiratory lung impedance. These are well-established EIT parameters that I implemented in a processing pipeline using Python programming. Additionally, I introduced a novel method to define regions of interest based on equal contributions to the total impedance variation and used these regions of interest to calculate and plot the continuous regional inspiratory impedance distribution. In Chapter 4, I discussed and compared other methods for defining regions of interest and presented a method for calculating the center of ventilation. By incorporating all these methods into ALIVE, we can standardize the process, eliminating the need for each user to reinvent the wheel. To maintain flexibility while using these methods, I translated each one into a standardized Python format known as a 'Class'. Each Class serves as a recipe for computing different parameters and operates with standard inputs, a selected data segment, and standard outputs, the resulting parameter.

Finally, it is essential to consolidate all the calculated parameters and figures into a comprehensive overview that the user can use for generating reports or conducting further statistical analysis. To facilitate user-friendliness, all these steps will be integrated

into a user interface, granting users the flexibility to select and execute specific operations.

Throughout bi-weekly ALIVE meetings, I actively contributed to shaping how the results should be presented to the user and the choices that should be made available within the user interface. This ongoing software development project will continue to progress in the coming months, and can be followed at https://research-software-directory.org/projects/alive and https://github.com/EIT-ALIVE.

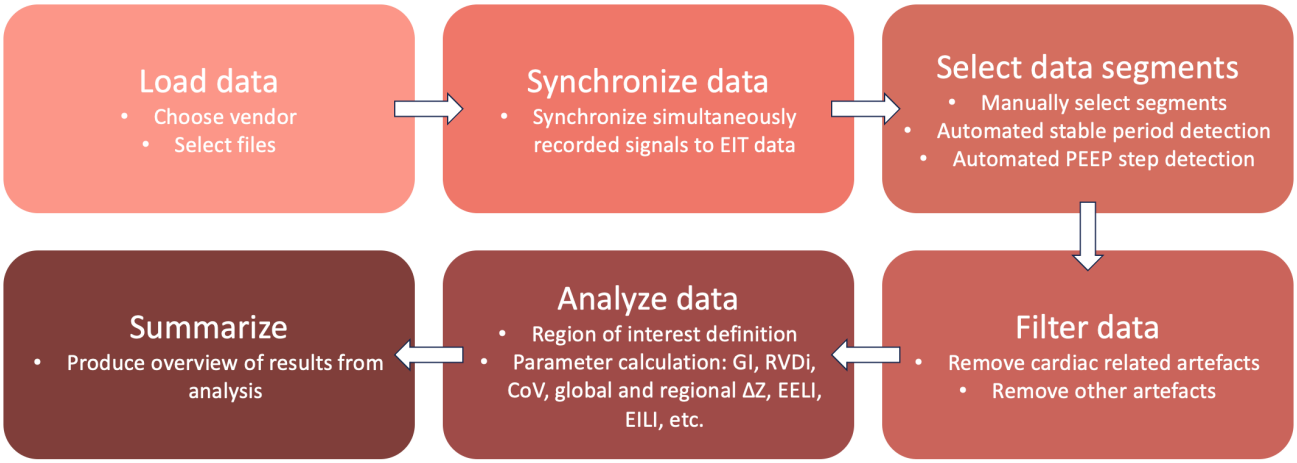

Figure 1. Simplified overview of the ALIVE workflow. All steps will be incorporated into a user interface so that a user can determine which operations to perform. In each step, examples of possible operations are shown.

Abbreviations: PEEP = Positive end-expiratory pressure; GI = Global inhomogeneity; RVDI = Regional ventilation delay inhomogeneity; CoV = Center of Ventilation; ΔZ = Tidal impedance variation; EELI = End-expiratory lung impedance; EILI = End-inspiratory lung impedance.

REFERENCES

1. Slutsky AS, Ranieri VM. Ventilator-induced lung injury. N Engl J Med. 2013;369(22):2126-2136

2. Amato MB, Meade MO, Slutsky AS, et al. Driving pressure and survival in the acute respiratory distress syndrome. N Engl J Med. 2015;372(8):747-755.

3. Goligher EC, Jonkman AH, Dianti J, et al. Clinical strategies for implementing lung and diaphragm-protective ventilation: avoiding insufficient and excessive effort. Intensive Care Med. 2020;46(12):2314-2326.

4. Goligher EC, Dres M, Patel BK, et al. Lung- and Diaphragm-Protective Ventilation. Am J Respir Crit Care Med. 2020;202(7):950-961.

5. Frerichs I, Amato MB, van Kaam AH, et al. Chest electrical impedance tomography examination, data analysis, terminology, clinical use and recommendations: consensus statement of the TRanslational EIT developmeNt stuDy group. Thorax. 2017;72(1):83-93.

CHAPTER 6

DEVELOPMENT OF A CLINICAL TRIAL PROTOCOL: EXPIRATORY MUSCLE STIMULATION FOR LUNG-PROTECTIVE VENTILATION (EXPROVE)

NOTE

Originally, the primary objective of my thesis internship was to initiate a study on expiratory muscle stimulation during mechanical ventilation as described in this chapter. However, the initiation was delayed due to compliance to the medical device regulation (MDR). Therefore, my primary focus shifted to the FCV project described in chapters 1-3. Nevertheless, I will demonstrate the considerations that were made to develop this protocol.

1. INTRODUCTION

In physiological breathing, contraction of the inspiratory muscles, especially the diaphragm, generates negative intrathoracic pressure, allowing air to flow into the lungs. During expiration, muscle relaxation and the elastic recoil pressure of the respiratory system increases intrathoracic pressure, allowing air to flow out of the lungs. The expiratory muscles are actively used when a disbalance occurs between the inspiratory muscle capacity and the demand for alveolar ventilation.[1] The main muscles for expiration are the transversus abdominis muscle, internal oblique muscle and external oblique muscle.[2-7]

During mechanical ventilation, some patients recruit their expiratory muscles, for instance due to an increase in relative load on the respiratory system (e.g., due to exertion, to achieve higher minute volume or in case of diaphragm weakness).[1] Activation of the expiratory muscles during expiration results in a higher abdominal pressure and pleural pressure and places the diaphragm to a more cranial position.[1] This increases expiratory flow out of the lungs and therefore results in a lower end-expiratory lung volume.[1] This could decrease hyperinflation and thus lung strain during positive pressure ventilation.[1,8] This could be a beneficial effect, since during the next inspiration, larger tidal volumes could be obtained without increasing the end-inspiratory transpulmonary pressure.[1] However, increasing pleural pressure during expiration by abdominal muscle activity also may result in negative transpulmonary pressure during expiration leading to alveolar collapse.[8] Furthermore, an increase in abdominal and intrathoracic pressure could also affect venous return, left ventricular afterload and pulmonary vascular resistance.[1,9-11]

Functional electrical stimulation (FES) is a non-invasive technique using surface electrodes that can safely elicit contractions of the expiratory muscles in a controlled setting. Therefore, in this study, FES will be used to investigate the physiological effects of expiratory muscle stimulation during mechanical ventilation.[12] The hypothesis is that by activating the expiratory muscles using FES, larger tidal volumes can be obtained without an increase in the end-inspiratory transpulmonary pressure (or similar tidal volumes can be obtained with a lower end-inspiratory transpulmonary pressure) (Figure 1).[1] If this hypothesis proves to be true, expiratory muscle FES could be a novel application within a lung-protective ventilation strategy.

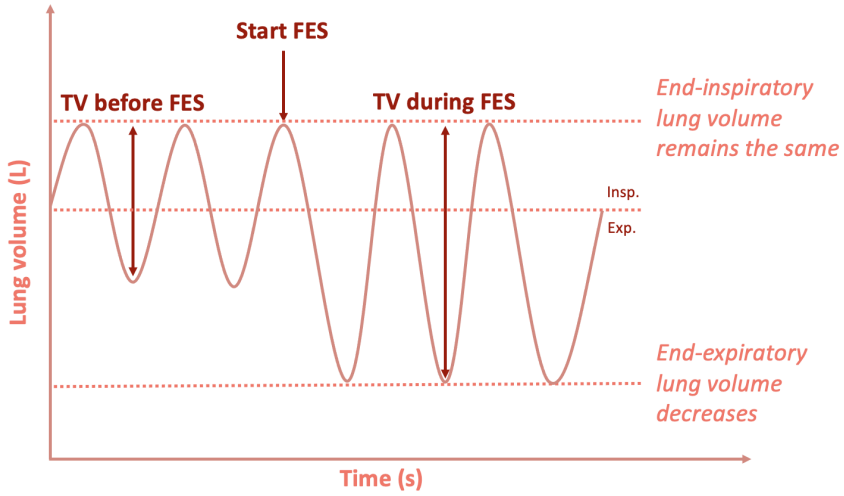

Figure 1. By activating the abdominal muscles during expiration using functional electrical stimulation (FES), the expiratory flow of air out of the lungs is increased, resulting in a lower end-expiratory lung volume. Furthermore, pleural pressure increases during expiration, which results in a lower transpulmonary driving pressure and a higher expiratory driving pressure. Hypothetically, during the next inspiration, larger tidal volumes could therefore be obtained without increasing the end-inspiratory transpulmonary pressure. Abbreviations: Insp. = Inspiration; Exp. = Expiration; TV = Tidal volume.

2. OBJECTIVES

The primary objective of this study is to investigate the effects of expiratory muscle FES on end-inspiratory transpulmonary pressure (a key determinant of ventilator-induced lung injury (VILI)[13]).

The secondary objectives of this study are:

1. To investigate the effects of expiratory muscle FES on lung volume distribution.
2. To evaluate the correlation between changes in end-expiratory transpulmonary pressure and regional lung ventilation (reflecting collapse/overdistension) due to expiratory muscle FES.
3. To investigate the effects of expiratory muscle FES on gas exchange and hemodynamics.

3. STUDY DESIGN AND POPULATION

The study was set up as a single-center prospective physiological study to be conducted in the Intensive Care Unit (ICU) of the Erasmus Medical Center, in Rotterdam, the Netherlands.

The study population consists of adult patients on controlled mechanical ventilation in the ICU. The reason for mechanical ventilation must be acute hypoxemic respiratory failure (AHRF) with a PaO_2/FiO_2-ratio of 100-300 mmHg. This patient group was chosen as patients with alveolar heterogeneity are especially prone to developing VILI and therefore especially benefit from lung-protective ventilation strategies.[14,15] Moreover, patients must be sedated with a Richmond Agitation-Sedation Scale (RASS) score of -4 or -5.

Exclusion criteria are:

- (Congenital) myopathies or neuropathies at ICU admission
- Muscle paralysis
- Patients with expiratory flow limitation (EFL; type COPD/asthma) as reason for mechanical ventilation. EFL may result in increased rather than decreased end-expiratory lung volume and the development of intrinsic PEEP (PEEPi).[8] Patients with EFL not due to COPD or asthma will be identified and excluded during an eligibility test (see study procedures).

- Pneumothorax
- Contraindications to expiratory muscle FES (e.g., cardiac pacemaker, refractory epilepsy, recent (<4 weeks) abdominal surgery, body mass index > 35 mg/m^2, and known pregnancy).
- Contraindications to esophageal balloon catheter (e.g., history of gastric bypass surgery, gastro-esophageal junction surgery, esophageal stricture, recent upper gastrointestinal hemorrhage, or known/suspected varices). Esophageal balloon will be used for measuring transpulmonary pressures.
- Contraindications to electrical impedance tomography (EIT) monitoring (e.g., burns, pacemaker, thoracic wounds limiting electrode placement). EIT monitoring will be used to monitor lung volume distribution.

Eligible patients will be screened upon admission to the ICU and informed consent will be obtained. After obtaining informed consent, an expiratory muscle FES eligibility test will be performed. A participant will be excluded from further participation if no contraction of the abdominal wall muscles can be elicited in response to abdominal expiratory muscle FES (see study procedures).

4. STUDY PROCEDURES

The experimental study protocol is summarized in Figure 2 and detailed below. From a practical perspective and to increase reliability of study endpoints, the main respiratory and hemodynamic effects of expiratory muscle FES will be assessed in two different steps, since cardiac ultrasound measurements interfere with reliable EIT monitoring.

Expiratory muscle FES will be performed with a commercially available CE-marked device (VentFree, Liberate Medical LLC, USA), which applies electrical stimulation (pulses at 30 Hz, 350 µs) to the expiratory muscles via surface electrodes placed on the abdominal wall, and in synchrony with the expiratory phase of the ventilator. FES elicits muscle contractions through the delivery of small electrical pulses to the motor nerve endings that supply a muscle. When FES is applied to the abdominal wall muscles in synchrony with exhalation, the effect on ventilation

is similar to a physiological contraction of the abdominal wall muscles.

Expiratory muscle FES eligibility test

Before the study measurements, an eligibility test will be performed to test whether the patient's expiratory abdominal wall muscles contract effectively in response to abdominal expiratory muscle FES, in line with a previous study by Jonkman et al.[8]. The FES electrodes will be applied to the posterolateral abdominal wall and single stimulations with incremental intensities will be administered to determine the stimulation threshold for tetanic muscle contraction. This contraction in response to stimulation will be verified with ultrasound assessment of the abdominal wall muscles. A patient will be excluded from further participation if stimulation at a maximum intensity of 100 mA does not result in a visible contraction of the expiratory abdominal wall muscles. A patient will also be excluded if the intensity needed to achieve a tetanic contraction, results in patient discomfort based on clinical judgement. To confirm and quantitate the effectiveness of muscle contraction, the increment in airway pressure induced by expiratory muscle FES during an inspiratory hold will be recorded. An increase in airway pressure of >2 cmH_2O is considered an effective contraction.[8] Patients with EFL are also identified and excluded based on this eligibility test as EFL will prevent the peak expiratory flow from effectively increasing by abdominal muscle stimulation.

Preparations for continuous monitoring of endpoints

If not already in place for clinical purposes, a nasogastric double balloon catheter will be inserted to measure esophageal pressure and gastric pressure using a dedicated catheter (Nutrivent, Sidam). Pressure data will be recorded for subsequent offline analysis with a specialized measurement setup. Continuous EIT monitoring (using the Draeger EIT Pulmovista® or Timpel® device) will be initiated via a dedicated belt positioned at the 4th-5th intercostal space, following clinical protocols. Additional monitoring will be performed using routine bedside monitoring systems, including ventilator waveforms and hemodynamic monitoring.

Step 1: Baseline

With the patient on volume-controlled ventilation with a pre-set tidal volume (TV) of 6 ml/kg predicted body weight (PBW), standard of care mechanical ventilation settings (positive end-expiratory pressure (PEEP) setting to reach end-expiratory transpulmonary pressure of 0 cmH_2O, FiO_2 aimed at an oxygen saturation between 94-98%) will be verified such that baseline situation is comparable between patients. Study recordings (pressures, ventilator waveforms, EIT) at this baseline step will be acquired for at least 10 minutes. At the end of this step, respiratory mechanics measurements (end-inspiratory and end-expiratory occlusions) and blood gas from indwelling arterial and venous catheters will be obtained as per standard protocols.

Step 2: Expiratory muscle FES to assess respiratory effects

For 10-15 minutes, the expiratory abdominal wall muscles will be stimulated with the titrated intensity obtained from the expiratory muscle FES eligibility test, with ventilator settings as baseline. The change in ventilator pressure plateau pressure and end-inspiratory transpulmonary pressure (which is expected to decrease due to the working mechanism of expiratory muscle FES) will be recorded. After 10-15 minutes, a set of respiratory mechanics measurements and arterial and venous blood gas will be obtained.

Wash-out period

EIT and pressure tracings will be recorded for 10-15 minutes post-FES and with ventilator settings as baseline. At the end of this step, a set of respiratory mechanics measurements and arterial and venous blood gas will be obtained, and the EIT belt will be removed. Afterwards, a baseline transthoracic cardiac ultrasound for the measurement of stroke volume will be conducted.

Step 3: Expiratory muscle FES to assess hemodynamic effects

FES will be applied for 10-15 minutes with the same settings as step 2. At the end of this step, transthoracic cardiac ultrasound for the measurement of the stroke volume will be performed, and an arterial and venous blood gas and set of respiratory mechanics measurements (also to evaluate if FES effect was similar in step 2 and step 3) will be obtained.

End of study

After the experimental protocol is finished, the patient will be treated again according to the local clinical protocol. Study recordings will be stored for further offline calculation and analysis of study endpoints using dedicated research software.

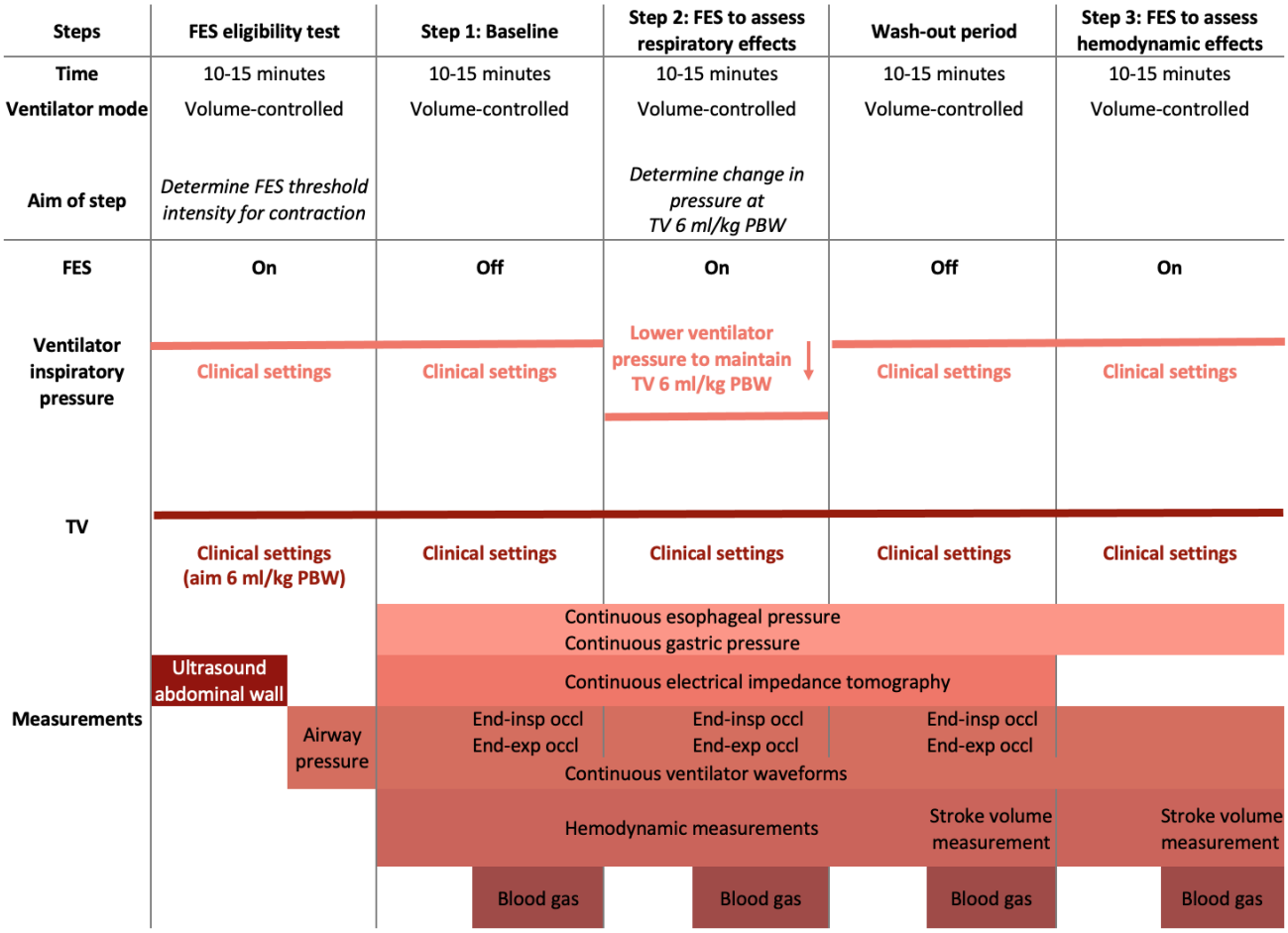

Figure 2. Study procedures. FES= Functional electrical stimulation; TV = Tidal volume; PBW = Predicted body weight; End-insp occl = End-inspiratory occlusion; End-exp occl = End-expiratory occlusion.

5. OUTCOME PARAMETERS

5.1 Primary outcome

The primary endpoint of this study will be the change in end-inspiratory transpulmonary pressure between step 1 and step 2 (baseline without stimulation versus expiratory muscle FES) of the study procedures.

5.2 Secondary outcomes

To fulfill the secondary objectives of the study the following outcome measures will be used:

EIT parameters

The continuous EIT recordings will be used to determine:

- Difference in end-expiratory lung impedance (EELI) between study steps, reflecting changes in end-expiratory lung volume (EELV), to verify whether expiratory muscle FES decreases end-expiratory lung volume compared to baseline.
- Change in static regional lung compliance (reflecting collapse/overdistension) between study steps to investigate whether expiratory muscle FES has a positive effect by reducing overinflation or rather a negative by introducing collapse.
- Distribution of ventilation and homogeneity of lung inflation/deflation to investigate the effects of expiratory muscles FES on spatial and temporal ventilation homogeneity. Spatial and temporal ventilation homogeneity can be quantified using the global inhomogeneity index and regional ventilation delay inhomogeneity (see Chapter 2).

Airway pressure/volume parameters

The continuous recordings of the ventilator curves will be used to determine:

- Tidal volume (TV) to check that the TV was constant throughout all study steps as expected with volume-controlled ventilation.
- Plateau pressure (Pplat) and peak pressure (Ppeak) to investigate the effects of airway resistance during FES.
- Intrinsic positive end-expiratory pressure (PEEPi) to determine whether FES influences PEEPi by causing air trapping.
- Static and dynamic compliance to compare lung mechanics between study steps.
- Mechanical power as a measure to compare the energy

transferred to the respiratory system between study steps.
- End-tidal CO_2 ($EtCO_2$) and saturation to determine the effects of expiratory muscle FES on ventilation and oxygenation.

Esophageal manometry (double-balloon catheter) parameters

The continuous esophageal pressure recordings will be used to determine:

- Gastric pressure (P_{ga}) amplitude during inspiration and expiration and pressure-time product during expiratory muscle FES to evaluate the effects of expiratory muscle FES on gastric pressure.
- End-expiratory transpulmonary pressure, transpulmonary driving pressure, and partitioned compliances (chest wall (C_{CW}), and lung (C_{lung})) to quantify differences in lung and chest wall mechanics between study steps and compare effects between patients.

Gas exchange and hemodynamics

- Arterial and venous blood gas (PaO_2, $PaCO_2$, SvO_2, PvO_2, $PvCO_2$, pH) to determine the effects of expiratory muscle FES on ventilation, oxygenation, and hemodynamics.
- Hemodynamic parameters (heart rate, (arterial) mean pressure, central venous pressure, stroke volume measurement using ultrasound (Velocity Time Integral (VTI), cross sectional area (CSA) aorta)). The stroke volume (SV) can be calculated as: $SV = VTI \times CSA_{aorta}$. The stroke volume can then be used to calculate the cardiac output (CO) as: $CO = SV \times HR$. The cardiac output can provide insight into the net cardiovascular effects of expiratory muscle stimulation.

Other study parameters

Other endpoints include baseline clinical characteristics (demographics, severity of hypoxemic failure, reason(s) for intubation, comorbidities) and ventilator settings.

6. ANALYSIS METHODS

All EIT, airway pressure/volume and esophageal pressure parameters will be calculated offline using a custom developed software that has in part already been developed for the ALIVE project (see Chapter 5).

Repeated measures analysis of variance (ANOVA) or linear mixed-effects models (in case of missing values) will be applied to analyze the change (expiratory muscle FES vs. no stimulation) in parameters over the different study steps. Post-hoc analysis with Bonferroni correction will be applied to test the difference in end-inspiratory transpulmonary pressure between each step. Correlations between the primary and secondary parameters will be evaluated using Spearman's correlation coefficient. Descriptive statistics to describe the characteristics of the study population (including demographics, severity of hypoxemic failure, reason(s) for intubation and comorbidities) and ventilator settings will be conducted. The association between the primary endpoint and these other endpoints will be evaluated using descriptive statistics and simple regression analysis.

7. MEDICAL ETHICAL APPROVAL

The study protocol as described in this chapter has been submitted to the Dutch Central Committee on Research Involving Human Subjects (CCMO). The CCMO ruled that, since a medical device (VentFree) is used to investigate the effects of ventilator-synchronized expiratory muscle activation, this study falls under article 82 of the Medical Device Regulation (MDR). Given the study's patient population, specifically sedated individuals on mechanical ventilation, we are working with a cohort of patients who are temporarily incapacitated and therefore unable to grant informed consent independently. Thus, the conditions for research involving incapacitated individuals from Article 64 MDR must be met. Specifically, there must be scientific reasons to anticipate that participation in the clinical study will provide a direct benefit to the incapacitated subject that outweighs the risks and burdens (Article 64, paragraph 1, sub-section g MDR). This means that the new MDR does not allow for the execution of non-therapeutic research using a medical device with incapacitated subjects. Due to the explorative and physiological nature of this study and the short timeframe in which patients are stimulated (2 x 10-15 minutes) it is unrealistic to expect a therapeutic effect of the expiratory muscle stimulation.

Therefore, the execution of this study in its current form is not possible due to legal frameworks. However, a large international study is now being initiated to assess whether abdominal muscle stimulation could improve ventilator weaning by enhancing expiratory muscle strength (Clinicaltrials.gov NCT05759013). In this study the expiratory muscle stimulation is applied repeatedly over several days and is expected to have a therapeutic effect on expiratory muscle strength. The measurements proposed in our study to uncover the physiological effects of expiratory muscle stimulation may be implemented during one of the stimulation sessions of this larger trial. In this way, we aim to address the regulatory challenges and ethical considerations surrounding incapacitated patient populations and contribute to advancements in understanding the (patho)physiology of abdominal muscles in mechanically ventilated patients.

REFERENCES

1. Shi ZH, Jonkman A, de Vries H, et al. Expiratory muscle dysfunction in critically ill patients: towards improved understanding. Intensive Care Med. 2019;45(8):1061-1071.

2. De Troyer A, Boriek AM. Mechanics of the respiratory muscles. Compr Physiol. 2011;1(3):1273-1300.

3. De Troyer A, Estenne M, Ninane V, Van Gansbeke D, Gorini M. Transversus abdominis muscle function in humans. J Appl Physiol (1985). 1990;68(3):1010-1016.

4. De Troyer A, Kirkwood PA, Wilson TA. Respiratory action of the intercostal muscles. Physiol Rev. 2005;85(2):717-756.

5. De Troyer A, Legrand A, Gevenois PA, Wilson TA. Mechanical advantage of the human parasternal intercostal and triangularis sterni muscles. J Physiol. 1998;513 (Pt 3)(Pt 3):915-925.

6. De Troyer A, Ninane V, Gilmartin JJ, Lemerre C, Estenne M. Triangularis sterni muscle use in supine humans. J Appl Physiol (1985). 1987;62(3):919-925.

7. Wilson TA, Legrand A, Gevenois PA, De Troyer A. Respiratory effects of the external and internal intercostal muscles in humans. J Physiol. 2001;530(Pt 2):319-330.

8. Ioannidis G, Lazaridis G, Baka S, et al. Barotrauma and pneumothorax. J Thorac Dis. 2015;7(Suppl 1):S38-43.

9. Corp A, Thomas C, Adlam M. The cardiovascular effects of positive pressure ventilation. BJA Education. 2021;21(6):202-209.

10. Sieck GC, Ferreira LF, Reid MB, Mantilla CB. Mechanical properties of respiratory muscles. Compr Physiol. 2013;3(4):1553-1567.

11. De Troyer A, Boriek AM. Mechanics of the respiratory muscles. Comprehensive Physiology. 2011;1(3):1273-1300.

12. Jonkman AH, Frenzel T, McCaughey EJ, et al. Breath-synchronized electrical stimulation of the expiratory muscles in mechanically ventilated patients: a randomized controlled feasibility study and pooled analysis. Crit Care. 2020;24(1):628.

13. Gattinoni L, Giosa L, Bonifazi M, et al. Targeting transpulmonary pressure to prevent ventilator-induced lung injury. Expert Rev Respir Med. 2019;13(8):737-746.

14. Barnes T, van Asseldonk D, Enk D. Minimisation of dissipated energy in the airways during mechanical ventilation by using constant inspiratory and expiratory flows – Flow-controlled ventilation (FCV). Medical Hypotheses. 2018;121:167-176.

15. Kollisch-Singule M, Emr B, Smith B, et al. Airway pressure release ventilation reduces conducting airway micro-strain in lung injury. J Am Coll Surg. 2014;219(5):968-976.

CHAPTER 7

GENERAL DISCUSSION AND FUTURE WORK

GENERAL DISCUSSION AND FUTURE WORK

The common denominator of all the chapters in this thesis is their contribution to advancing lung-protective ventilation and respiratory monitoring in the intensive care unit (ICU).

In Chapters 1 and 2, I described two physiological studies into the effects of flow-controlled ventilation (FCV) on mechanical power and ventilation distribution in postoperative ICU patients and patients with the acute respiratory distress syndrome (ARDS). In postoperative ICU patients, FCV reduced mechanical power and dissipated energy, while maintaining stable gas exchange at lower minute volumes. Moreover, FCV increased spatial homogeneity of ventilation with increased ventilation distribution to the dorsal lung regions. In ARDS patients, no conclusions can be drawn yet as further results are awaited. However, in the first patient, FCV seemed to increase ventilation in the dorsal lung regions at the expense of overdistension of the ventral lung regions as indicated by a decreased static compliance. Therefore, relevant information might be obtained from future results on the recruitment effect of FCV in patients with ARDS. Herein lies an important role for the use of advanced respiratory monitoring in clinical practice to be able to determine which patients are likely to benefit from FCV.

In Chapter 4, I described the development of a new method for ROI selection in EIT data, which was used for the analyses in Chapters 2 and 3. I demonstrated that the ROI selection, where each region contributes equally to the total tidal impedance variation over selected EIT data segments, is sensitive to subtle ventilation-induced changes in regional impedance. This chapter also demonstrates the effects of ROI selection when using regional EIT parameters to guide clinical decisions and thus highlights the importance of substantiating the choices made in research analyses.

Chapter 5 brings together the analyses performed in Chapters 2-4 as the analysis pipelines were converted to standardized formats to be used for open-source software developed for the ALIVE project. By incorporating complex EIT processing and analysis methods, such as ROI definition based on a percentage of the total tidal impedance variation rather than simply dividing the EIT image into equal parts, analyses can be made using the most suitable rather than the most convenient method.

Thereby, the goal is to enhance clinical use of EIT data and streamline the processing of research data.

Chapter 6 approaches lung-protective ventilation from a different angle and describes a proposed study protocol to investigate a novel hypothesis. If this hypothesis proves true, stimulating expiratory muscle function during mechanical ventilation might contribute to a lung-protective mechanical ventilation strategy by limiting end-inspiratory transpulmonary pressure.

Many patients experience physical impairments after ICU admission, which are often related to immobilization, sedation, and mechanical ventilation.[1] Therefore, continuous work should be done to improve respiratory monitoring techniques for clinical use and research. For instance, the ALIVE project serves as a basis to generate consensus on standardized EIT analyses and foster collaboration between experts globally. Moreover, novel techniques for lung-protective mechanical ventilation, such as FCV and respiratory muscle support, should be investigated. In this thesis, steps were taken to enhance our understanding of the mechanisms and potential behind these techniques. In conclusion, future efforts should be directed towards improving patient outcomes by personalizing mechanical ventilation treatments to patient-specific lung physiology and pathology.

References

1. Ohtake PJ, Lee AC, Scott JC, et al. Physical Impairments Associated With Post-Intensive Care Syndrome: Systematic Review Based on the World Health Organization's International Classification of Functioning, Disability and Health Framework. Phys Ther. 2018;98(8):631-645.

SUPPLEMENTS

SUPPLEMENT CHAPTER 2

SUPPLEMENTAL ANALYSIS

Supplemental methods

Breath-by-breath analysis of flow and intratracheal pressure was performed (MATLAB 2021a, MathWorks, USA) for a stable period of 8-10 minutes at the end of each step (baseline, step 1, step 3). From the flow tracings, inspiratory time, respiratory rate, tidal volume (time-integral of inspiratory flow) and minute volume were calculated. Peak pressure (Ppeak), total positive end-expiratory pressure (PEEP), and mean airway pressure were derived from the intratracheal pressure tracings.

Pressure-volume (PV) loops were computed using the intratracheal pressure and the time-integral of flow tracings. From the PV-loops, the total energy per breath was determined as the integral of the PV-loop multiplied by 0.098 (conversion to Joule). The total energy per breath includes elastic dynamic and resistive components but excludes the static component, as the volume generated by PEEP is unknown. The mechanical power (Joule/min) was calculated by multiplying the total energy per breath by the respiratory rate. Dissipated energy was computed as the hysteresis area of the PV loop per breath (in Joule/Liter).

Moreover, PaO_2, $PaCO_2$, PaO_2/FiO_2 ratio, central venous oxygen saturation ($ScvO_2$), arterial-venous CO_2 gap, ventilatory ratio[1], and noradrenalin dose were obtained per step to assess gas exchange and basic hemodynamic parameters.

Statistical analysis was performed using SPSS (IBM, Armonk, USA). Values are presented as median (interquartile range) and were tested for normality using the Shapiro-Wilk test. Steps were compared using the repeated measures ANOVA or the related-samples Friedman's test depending on the distribution, and with Bonferroni correction for multiple comparisons. A p-value <0.05 was considered statistically significant.

Supplemental results

10 patients were included in the flow and pressure analysis. During FCV with settings similar to PCV (step 1) the mechanical power was not different from PCV (9.4 (8.0-11.1) vs. 11.0 (8.5-12.8) J/min, p=0.286). However, the dissipated energy was lower than during PCV (0.22 (0.17-0.26) vs. 0.34 (0.21-0.43) J/L, p<0.05). For all results comparing FCV step 1 and PCV, see Table A.

FCV was then optimized to utilize the full potential of FCV mode for tidal recruitment followed by controlled expiration to keep the lungs open. The mechanical power, dissipated energy, minute volume and ventilatory ratio were all lower during optimized FCV than during PCV (Table B and Figure A). FCV also resulted in a significantly lower respiratory rate, lower airway resistance and higher mean airway pressure. Despite changes in ventilation, oxygenation (PaO_2 and PaO_2/FiO_2), $PaCO_2$ and hemodynamics remained stable (Table B).

Table A. Results PCV (baseline) vs. FCV with PCV settings (step 1)

	PCV baseline Median (IQR)	FCV step 1 Median (IQR)	P-value
Respiratory parameters			
Inspiratory TV/IBW (mL)	6.0 (5.5-7.1)	6.3 (5.5-7.1)	1.000
Driving pressure (cmH_2O)	9.2 (7.7-11.7)	9.6 (8.0-12.5)	1.000
PEEP set (cmH_2O)	7.5 (6.4-8.0)	8.0 (6.8-8.0)	1.000
PEEP total (cmH_2O)	8.3 (7.5-9.2)	8.8 (8.1-9.6)	0.027
Ppeak set (cmH_2O)	20.0 (18.8-22.0)	19.0 (18.0-20.5)	1.000
Ppeak measured (cmH_2O)	18.6 (16.8-21.5)	19.8 (17.4-21.8)	0.669
Pplat (cmH_2O)	17.5 (16.2-20.5)	18.6 (17.3-21.0)	0.534
Pmean (cmH_2O)	12.6 (11.0-13.4)	13.6 (12.5-14.7)	0.031
Static compliance (mL/cmH_2O)	44.5 (36.1-52.7)	41.9 (35.7-52.8)	1.000
Resistance ($cmH_2O/L/s$)	13.8 (12.4-14.9)	7.9 (7.4-8.9)	0.004
RR (x/min)	18 (17.5-20.0)	15.6 (14.3-18.7)	0.221
Minute volume (L/min)	8.0 (6.5-8.4)	6.7 (6.0-7.5)	0.438
Mechanical power (J/min)	11.0 (8.5-12.8)	9.4 (8.0-11.1)	0.286
Dissipated energy (J/L)	0.34 (0.21-0.43)	0.22 (0.17-0.26)	0.008
Gas exchange parameters			
P/F ratio	324 (241-365)	316 (255-363)	1.000
PaO_2 (kPa)	14.3 (12.9-17.7)	14.2 (13.4-14.9)	0.987
$PaCO_2$ (kPa)	5.4 (5.1-6.2)	5.3 (5.0-5.9)	1.000
Ventilatory ratio	1.20 (1.11-1.31)	1.07 (0.92-1.30)	0.791
Hemodynamic parameters			
Arterial-venous delta CO_2 (kPa)	1.06 (0.86-1.13)	0.83 (0.61-1.09)	1.000
$ScvO_2$ (%)	71.2 (64.7-75.8)	69.0 (65.6-76.6)	1.000
Dose noradrenalin (y)	0.11 (0.05-0.16)	0.10 (0.04-0.15)	0.456

Abbreviations: FCV = Flow-controlled ventilation; PCV = Pressure-controlled ventilation; IBW = Ideal body weight; IQR = Interquartile range; Ppeak = Peak pressure; PEEP = Positive end-expiratory pressure; Pmean = Mean airway pressure; Pplat = Plateau pressure; PaO_2 = Arterial partial oxygen pressure; $PaCO_2$ = Arterial partial carbon dioxide pressure; P/F ratio = PaO_2/FiO_2 ratio; RR = Respiratory rate; $ScvO_2$ = Central venous oxygen saturation; TV = Tidal volume.

Table B. Results PCV (baseline) vs. optimized FCV (step 3)

	PCV baseline Median (IQR)	FCV step 3 Median (IQR)	P-value
Respiratory parameters			
Inspiratory TV/IBW (mL)	6.0 (5.5-7.1)	8.4 (7.9-8.7)	0.004
Driving pressure (cmH_2O)	9.2 (7.7-11.7)	11.9 (9.8-14.0)	0.031
PEEP set (cmH_2O)	7.5 (6.4-8.0)	8.0 (5.8-8.0)	1.000
PEEP total (cmH_2O)	8.3 (7.5-9.2)	8.4 (7.5-10.1)	1.000
Ppeak set (cmH_2O)	20.0 (18.8-22.0)	20.5 (19.8-24.3)	0.281
Ppeak measured (cmH_2O)	18.6 (16.8-21.5)	21.1 (20.2-24.9)	0.012
Pplat (cmH_2O)	17.5 (16.2-20.5)	20.0 (19.0-24.0)	0.011
Pmean (cmH_2O)	12.6 (11.0-13.4)	14.7 (13.0-16.9)	<0.001
Static compliance (mL/cmH_2O)	44.5 (36.1-52.7)	47.0 (39.7-51.8)	1.000
Resistance ($cmH_2O/L/s$)	13.8 (12.4-14.9)	8.2 (6.8-9.1)	0.002
RR (x/min)	18 (17.5-20.0)	8.5 (7.6-13.1)	<0.001
Minute volume (L/min)	8.0 (6.5-8.4)	4.8 (4.4-7.3)	0.001
Mechanical power (J/min)	11.0 (8.5-12.8)	7.7 (5.7-11.4)	0.004
Dissipated energy (J/L)	0.34 (0.21-0.43)	0.20 (0.16-0.27)	0.009
Gas exchange parameters			
P/F ratio	324 (241-365)	300 (273-369)	1.000
PaO_2 (kPa)	14.3 (12.9-17.7)	13.1 (12.0-13.9)	0.212
$PaCO_2$ (kPa)	5.4 (5.1-6.2)	5.3 (5.1-5.9)	0.791
Ventilatory ratio	1.20 (1.11-1.31)	0.75 (0.67-1.15)	0.001
Hemodynamic parameters			
Arterial-venous delta CO_2 (kPa)	1.06 (0.86-1.13)	0.82 (0.77-1.09)	1.000
$ScvO_2$ (%)	71.2 (64.7-75.8)	69.1 (64.1-76.0)	1.000
Dose noradrenalin (y)	0.11 (0.05-0.16)	0.13 (0.04-0.16)	1.000

Abbreviations: FCV = Flow-controlled ventilation; PCV = Pressure-controlled ventilation; IBW = Ideal body weight; IQR = Interquartile range; Ppeak = Peak pressure; PEEP = Positive end-expiratory pressure; Pmean = Mean airway pressure; Pplat = Plateau pressure; PaO_2 = Arterial partial oxygen pressure; $PaCO_2$ = Arterial partial carbon dioxide pressure; P/F ratio = PaO_2/FiO_2 ratio; RR = Respiratory rate; $ScvO_2$ = Central venous oxygen saturation; TV = Tidal volume.

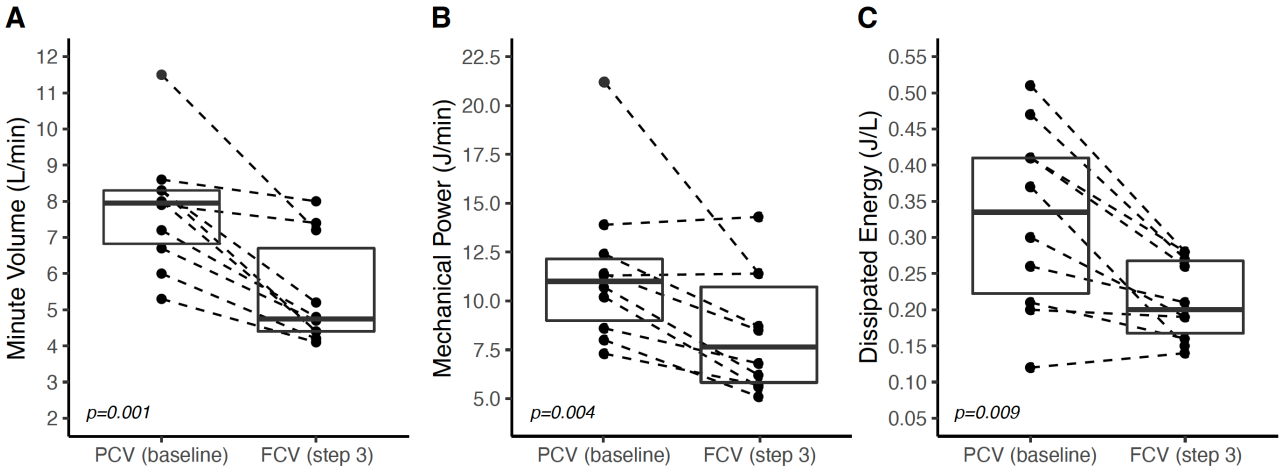

Figure A. Minute volume, mechanical power and dissipated energy decrease during flow-controlled ventilation (FCV) vs. pressure-controlled ventilation (PCV).

Supplemental discussion

The results of this supplemental analysis are discussed in comparison to the results of Chapter 3 in the discussion of that chapter.

References

1. Sinha P, Calfee CS, Beitler JR, et al. Physiologic Analysis and Clinical Performance of the Ventilatory Ratio in Acute Respiratory Distress Syndrome. Am J Respir Crit Care Med. 2019;199(3):333-341.

SUPPLEMENTAL TABLES

Supplemental Table 1. EIT results PCV (baseline) vs FCV with PCV settings (step 1); values represent median (IQR)

Supplemental Table 1a. Changes in EIT parameters during FCV as compared to PCV*		
	FCV step 1	**P-value**
Global change in ΔZ (%)	5.0 (-3.4-11.2)	
Regional change in ΔZ (%) ROI ventral ROI mid-ventral ROI mid-dorsal ROI dorsal	 -3.6 (-8.5-4.6) 3.7 (-7.1-7.1) 7.0 (-4.6-10.1) 20.8 (-1.0-24.4)	0.091[1]
Global change in static compliance (%)	-4.0 (-9.0-4.9)	
Regional change in static compliance (%) ROI ventral ROI mid-ventral ROI mid-dorsal ROI dorsal	 -12.2 (-14.8-6.7) -6.0 (-10.7-3.9) -2.8 (-8.7-1.9) 6.4 (0.2-9.8)	0.050[2]
Change in global EELI (a.u.)	29 (-38-64)	1.000

Supplemental Table 1b. Absolute EIT parameters reflecting lung and ventilation homogeneity			
	PCV	**FCV step 1**	**P-value**
GI (%)	43.8 (41.4-45.3)	43.8 (40.6-45.9)	1.000
RVDI (%)	2.75 (2.28-4.63)	3.94 (3.60-5.80)	0.264

Abbreviations: EIT = Electrical impedance tomography; FCV = Flow-controlled ventilation; PCV = Pressure-controlled ventilation; ΔZ = Tidal impedance variation; ROI = Region of interest; a.u. = Arbitrary units; EELI = End-expiratory lung impedance; RVDI = Regional ventilation delay inhomogeneity; GI = Global inhomogeneity index.

* Changes in ΔZ and static compliance are expressed as percentage change between FCV step 1 and PCV at baseline, as both are expressed in arbitrary units, which makes direct comparisons between patients unreliable.

[1] p-value reflects the non-significant difference between PCV baseline vs. FCV step 1 regarding the distribution of ΔZ among the four ROIs, using a Kruskal-Wallis test on the percentage changes from baseline (to account for the fact that ΔZ is measured in arbitrary units).

[2] p-value reflects the non-significant difference between PCV baseline vs. FCV step 1 regarding the distribution of the change in static compliance among the four ROIs, using a Kruskal-Wallis test on the percentage changes from baseline (to account for the fact that ΔZ and thereby also the static compliance is measured in arbitrary units).

SUPPLEMENTAL FIGURES

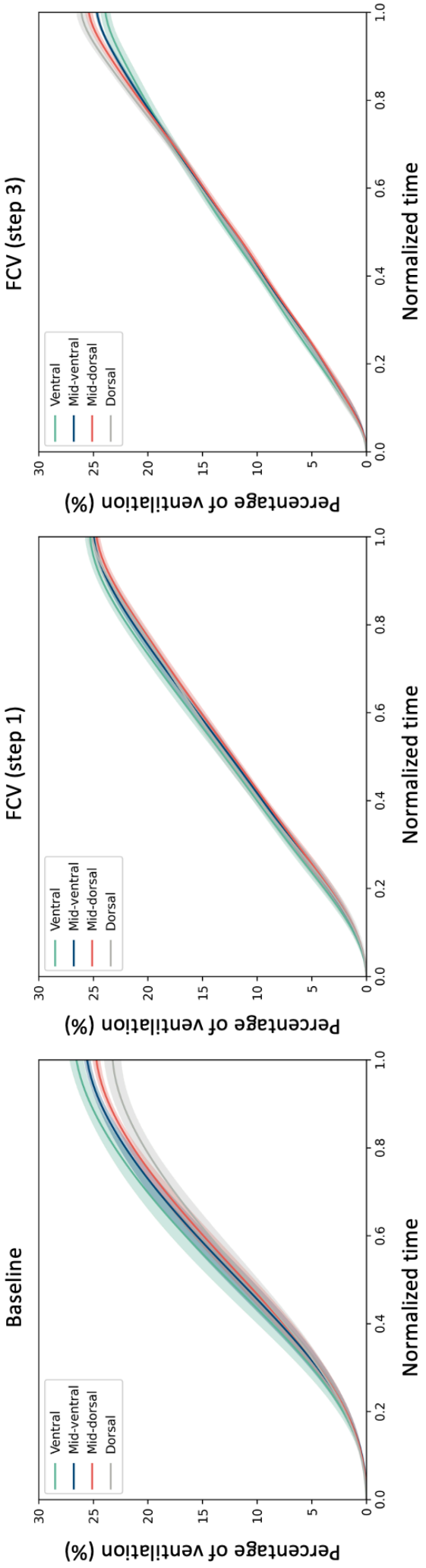

Supplemental Figure 1. Continuous regional impedance distribution averaged over all patients and per region of interest, in an average inspiration at baseline, step 1, and step 3 (left to right). Shaded areas represent 95% confidence intervals.

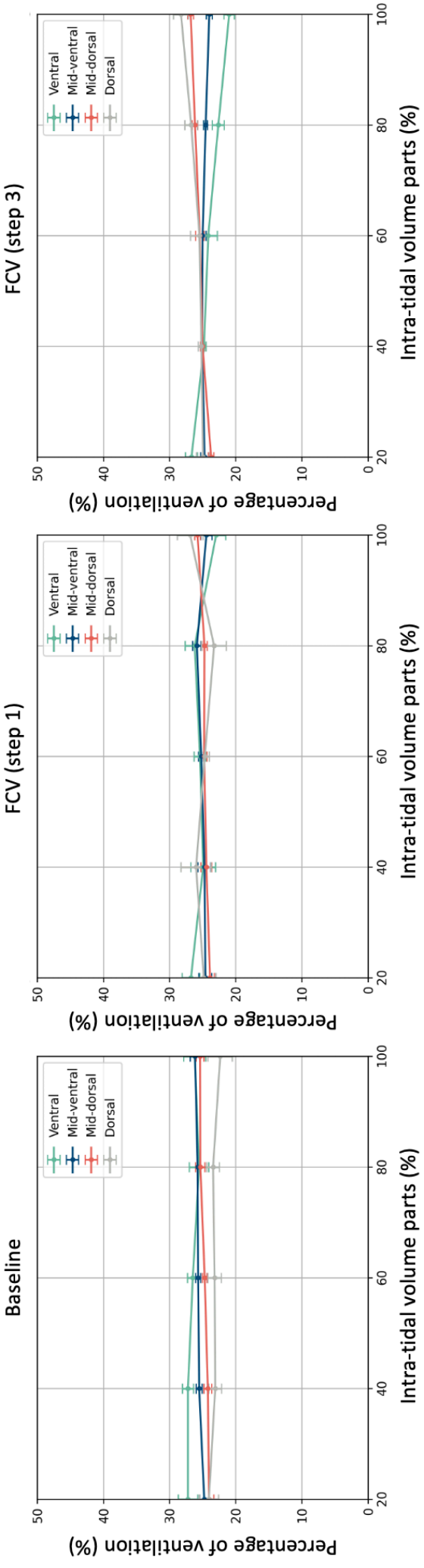

Supplemental Figure 2. Regional intra-tidal impedance distribution averaged over all patients per region of interest in an average inspiration at baseline, step 1, and step 3 (left to right). The inspiration was divided into five equal parts of ΔZ. Error bars represent 95% confidence intervals.

Supplemental Figure 3. Example of the influence of a fluid bolus on the end-expiratory lung impedance (EELI) in a postoperative cardiothoracic patient on PCV. The patient received 850ml of cellsaver blood postoperatively, which decreased the EELI value with 0.75 points without any change in positive end-expiratory pressure, tidal volume, or gas exchange. Therefore, the EELI as a parameter of lung aeration was inappropriate in our study population.

SUPPLEMENT CHAPTER 3

SUPPLEMENTAL TABLES

Supplemental Table 1.
Results PCV vs. initial FCV

	PCV	Initial FCV
Inspiratory TV/IBW (mL)	5.2	4.8
RR (x/min)	22	22.9
Minute volume (L/min)	6.5	6.2
Resistance (cmH_2O/L/s)	18.0	8.6
Total respiratory system parameters		
Paw driving pressure (cmH_2O)	8.6	8.9
PEEP set (cmH_2O)	15	15
PEEP total (cmH_2O)	14.9	14.5
Ppeak set (cmH_2O)	26	26
Ppeak measured (cmH_2O)	25.1	26.7
Pplat (cmH_2O)	24.1	24.6
Pmean (cmH_2O)	18.9	20.4
Total compliance static (mL/cmH_2O)	34.3	30.7
Total Mechanical power (J/min)	13.2	12.6
Total Dissipated energy (J/L)	0.29	0.25
Transpulmonary parameters		
P_L driving pressure (cmH_2O)	6.7	7
P_L end-expiratory (cmH_2O)	4.2	3.1
P_L peak (cmH_2O)	12.1	13.9
P_L plat (cmH_2O)	11.4	11.5
P_L mean (cmH_2O)	7.4	8.4
Lung compliance static (mL/cmH_2O)	44	39
Transpulmonary Mechanical power (J/min)	5.7	5.2
Transpulmonary Dissipated energy (J/L)	0.27	0.22
Gas exchange parameters		
P/F ratio	246	212
PaO_2 (kPa)	11.48	14.13
$PaCO_2$ (kPa)	5.8	6.4
Ventilatory ratio	1.3	1.4
Hemodynamic parameters		
Dose noradrenalin (y)	0.36	0.40

Abbreviations: PCV = Pressure-controlled ventilation; FCV = Flow-controlled ventilation; IQR = Interquartile range; TV = Tidal volume; IBW = Ideal body weight; RR = Respiratory rate; P_{aw} = Airway pressure; PEEP = Positive end-expiratory pressure; Ppeak = Peak pressure; Pplat = Plateau pressure; Pmean = Mean airway pressure; P_L = Transpulmonary pressure. PaO_2 = Arterial partial oxygen pressure; $PaCO_2$ = Arterial partial carbon dioxide pressure; P/F ratio = PaO_2/FiO_2 ratio.

Supplemental Table 2. EIT results PCV vs initial FCV

Supplemental Table 2a. Changes in EIT parameters during initial FCV as compared to PCV			
	PCV	**Initial FCV**	**% change**
Global ΔZ (a.u.)	12.1	9.83	-18.8
Regional ΔZ			
ROI ventral	3.69	2.09	-43.4
ROI mid-ventral	3.04	2.31	-24.0
ROI mid-dorsal	2.83	2.51	-11.3
ROI dorsal	2.52	2.92	15.9
Global static compliance (a.u.)	1.40	1.10	-21.4
Regional static compliance (a.u.)			
ROI ventral	0.43	0.23	-46.5
ROI mid-ventral	0.35	0.26	-25.7
ROI mid-dorsal	0.33	0.28	-15.2
ROI dorsal	0.29	0.33	13.8
Global EELI (a.u.)	3.26	3.27	0.3

Supplemental Table 2b. Absolute EIT parameters reflecting lung and ventilation homogeneity		
	PCV	**Initial FCV**
GI (%)	42.4	40.3
RVDI (%)	1.5	2.3

Abbreviations EIT = Electrical impedance tomography; FCV = Flow-controlled ventilation; PCV = Pressure-controlled ventilation; ΔZ = Tidal impedance variation; ROI = Region of interest; a.u. = Arbitrary units; EELI = End-expiratory lung impedance; RVDI = Regional ventilation delay inhomogeneity; GI = Global inhomogeneity index.
The % change column shows the percentage changes in ΔZ, static compliance and EELI between optimized FCV and PCV.

SUPPLEMENTAL FIGURES

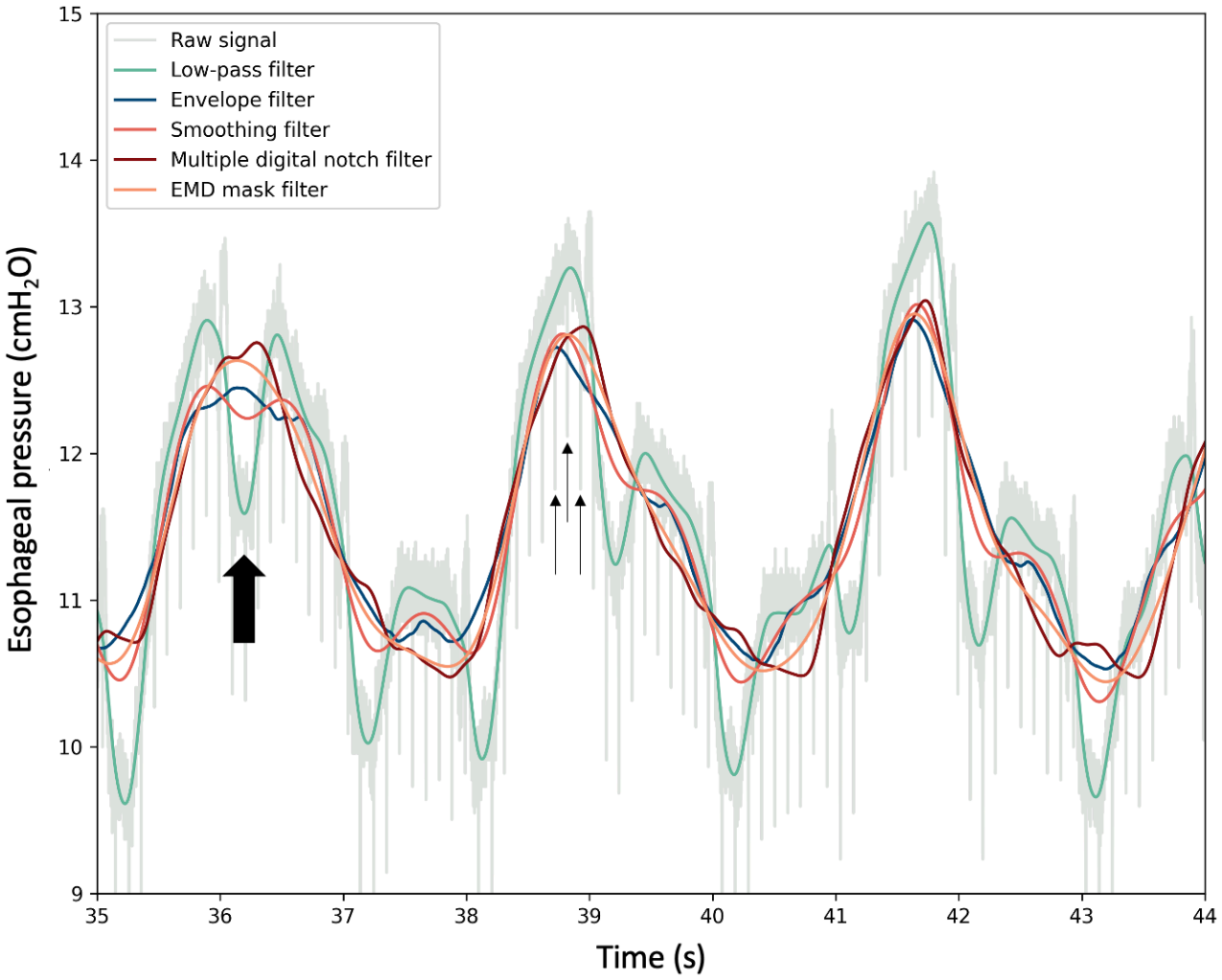

Supplemental Figure 1. The effects of different filtering techniques on a segment of the esophageal pressure (P_{es}) signal during pressure-controlled ventilation. The raw signal contains a high frequency artefact (spikes in signal indicated by small arrows) as well as large cardiac artefacts (large dips in signal indicated by large arrow). The low-pass filter is a simple second-order low-pass Butterworth filter with a cutoff frequency of 20 Hz. The envelope filter applies a Hilbert transform to the input signal. This transform creates an analytic signal from the real-valued input. The envelope of the analytic signal is extracted using the absolute value of the analytic signal. The final output is the smoothed envelope of the input signal. The smoothing filter slides a Gaussian window over the signal and computes the weighted average, resulting in a smoothed version of the signal. The multiple digital notch (MDN) filter uses multiple fifth-order Butterworth notch filters at the cardiac frequency ± 0.6 Hz and each harmonic frequency until a threshold of 3.5 Hz is exceeded. These notch filters are combined with a low-pass filter with a cutoff frequency of 3.5 Hz. The Empirical Mode Decomposition (EMD) filter decomposes a signal into its intrinsic mode functions (IMFs), which represent the oscillatory components of the signal. The EMD mask filter performs the EMD decomposition with masking. Masking is a technique used to influence the sifting process, highlighting or suppressing certain frequencies in the signal. In this case, the cardiac frequency divided by 0.67 and its harmonics are used as mask frequencies. The cardiac frequency is divided by 0.67 to compensate for mode-mixing of lower frequencies into the masked IMF and to obtain the most optimal mask frequency.[1] Since high-frequency noise is not removed by the cardiac masking frequencies, a second-order low-pass filter with a cutoff frequency of 3.5 Hz was applied before the EMD mask filter. The low-pass and smoothing filter are not successful at removing cardiac artefacts. MDN and EMD are more discriminatory and successfully remove the frequencies surrounding the heart rate and its harmonics. The envelope filter appears to remove the cardiac artefacts but more strongly modifies the shape of the signal compared to MDN and EMD filtering. MDN visually appears to preserve more information from the original signal than EMD and was therefore selected as the filtering method.

[1.] *Fosso O, Molinas M. EMD Mode Mixing Separation of Signals with Close Spectral Proximity in Smart Grids. 2018.*

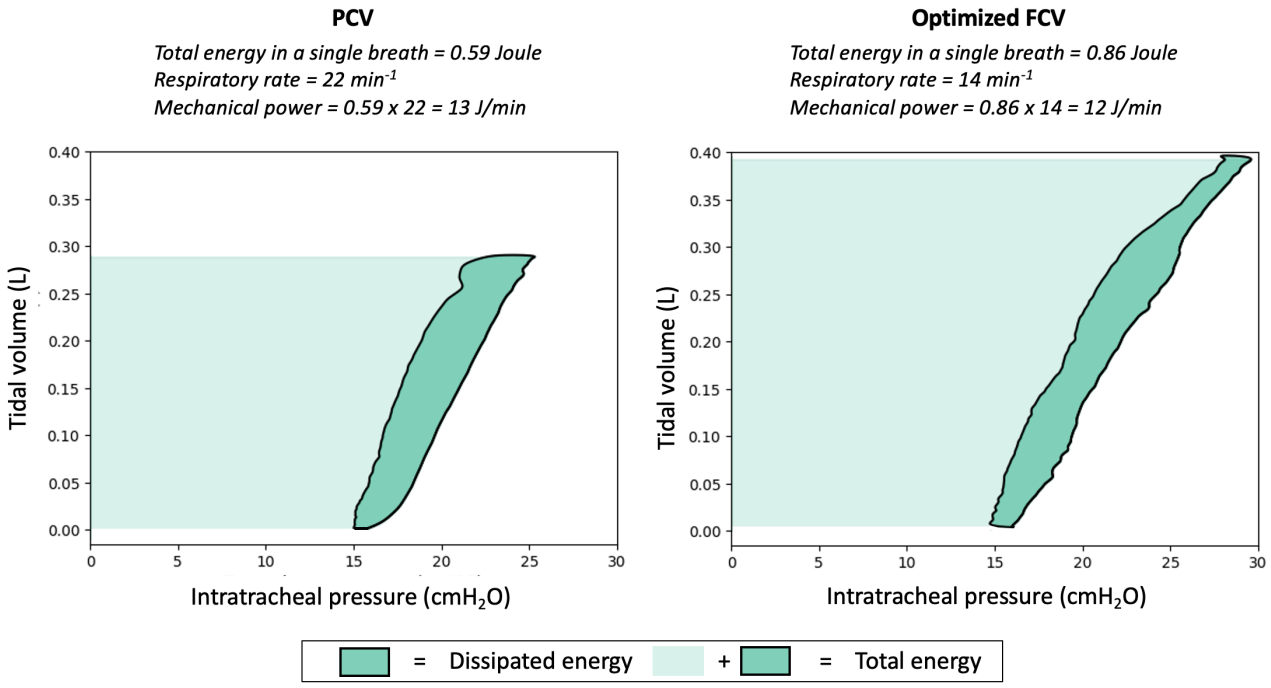

Supplemental Figure 2. Representative intratracheal pressure-volume loops (PV-loops) obtained in the same patient during pressure-controlled ventilation (PCV) and optimized flow-controlled ventilation (FCV), with corresponding calculations of mechanical power.

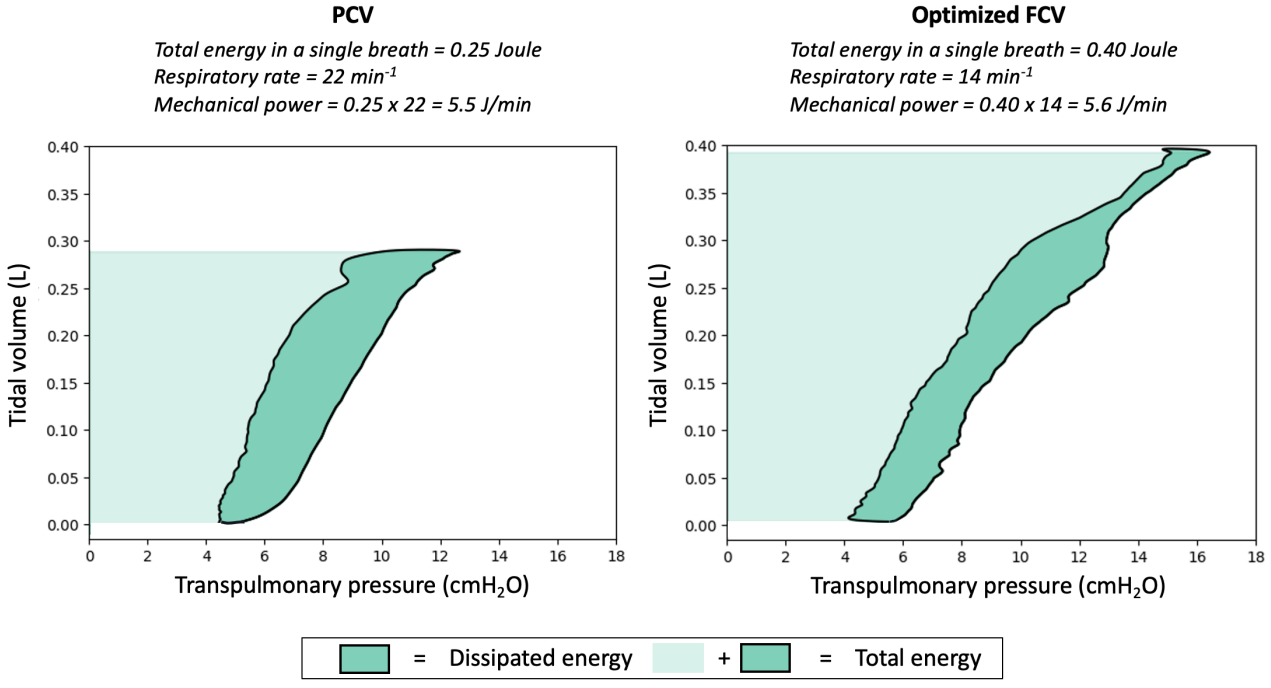

Supplemental Figure 3. Representative transpulmonary pressure-volume loops (PV-loops) obtained in the same patient (also the same patient as for the intratracheal PV-loops in Supplemental figure 2) during pressure-controlled ventilation (PCV) and optimized flow-controlled ventilation (FCV), with corresponding calculations of mechanical power.

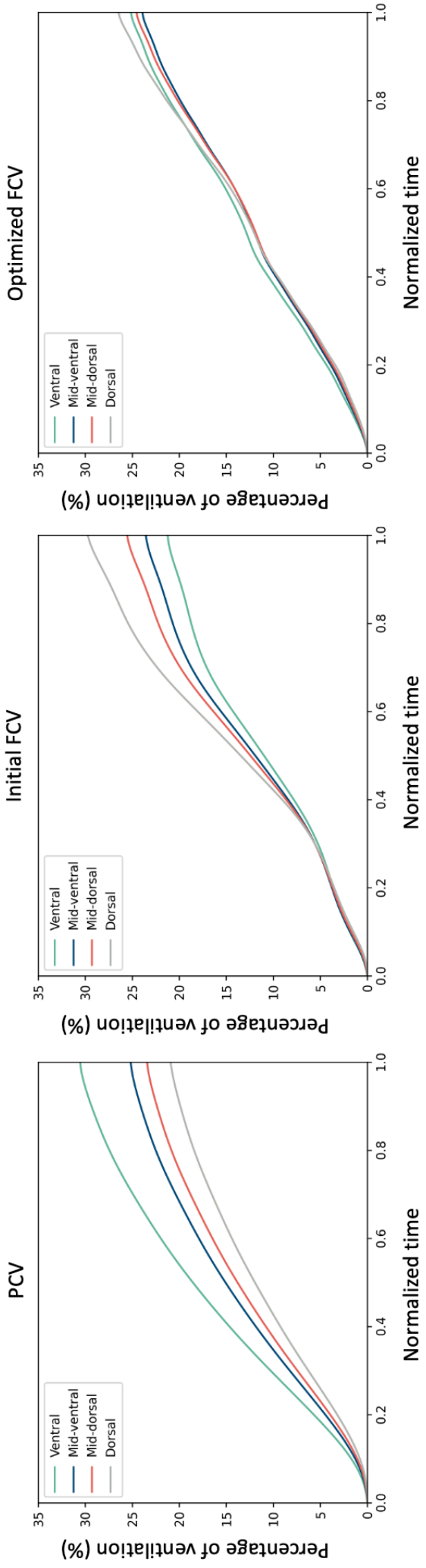

Supplemental Figure 4. Continuous regional impedance distribution of a single patient and per region of interest, in an average inspiration during PCV, initial FCV, and optimized FCV (left to right).

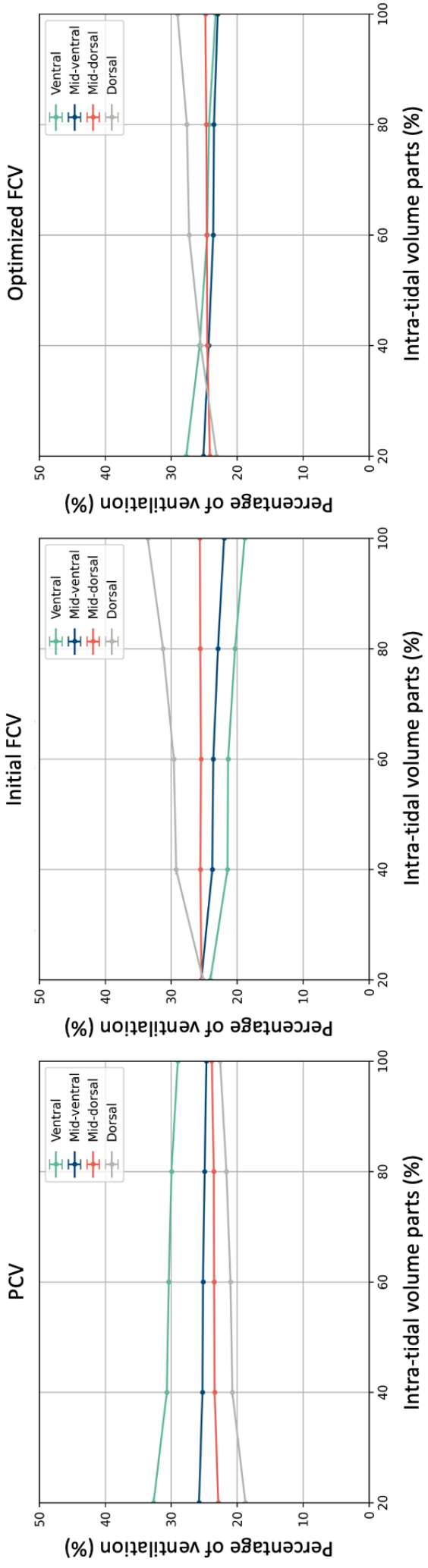

Supplemental Figure 5. Regional intra-tidal impedance distribution of a single patient per region of interest in an average inspiration during PCV, initial FCV, and optimized FCV (left to right). The inspiration was divided into five equal parts of ΔZ.

SUPPLEMENT CHAPTER 4

SUPPLEMENTAL FIGURES

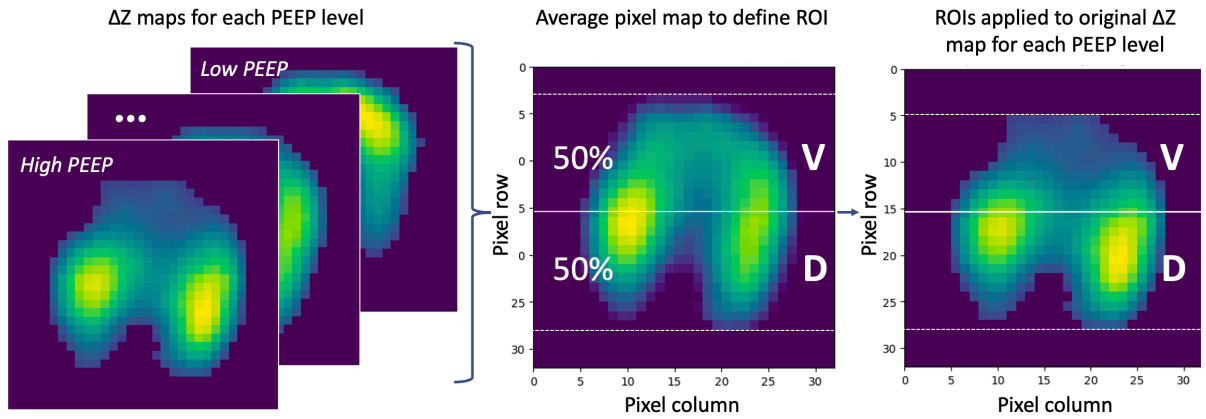

Supplemental Figure 1. Example of an average pixel impedance map created with the impedance maps from each PEEP step in the decremental PEEP trial. The regions of interest (ROI; ventral (V), and dorsal (D)) each represent exactly 50% of the total tidal impedance variation of this average pixel impedance map. Note that the division lines separating ROIs could lie within one pixel row (Supplemental Figure 2). This ROI division was then applied to the original impedance maps of each PEEP step for further computation of parameters. Dotted lines reflect the boundary of the functional lung space (i.e., ventilated pixels).

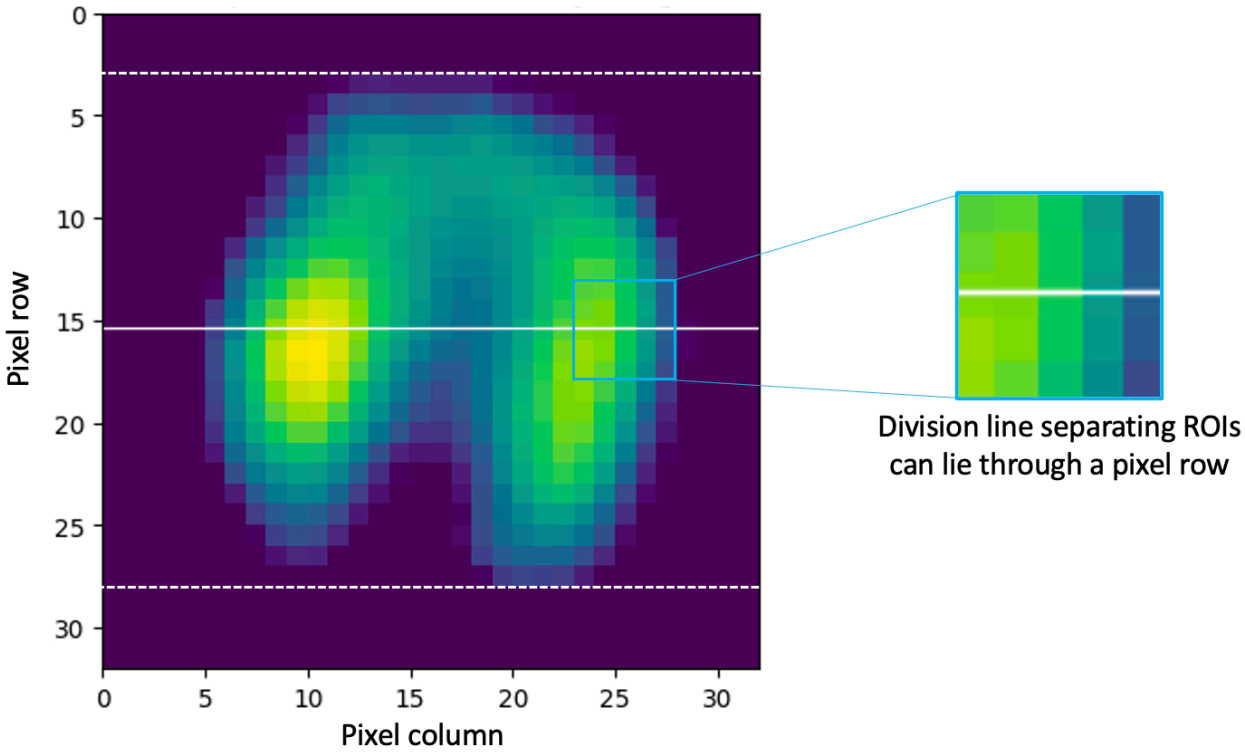

Supplemental Figure 2. Example to illustrate that the division line separating ROIs (ventral (V) and dorsal (D)) can lie in between a pixel row. Dotted lines reflect the boundary of the functional lung space (i.e., ventilated pixels).

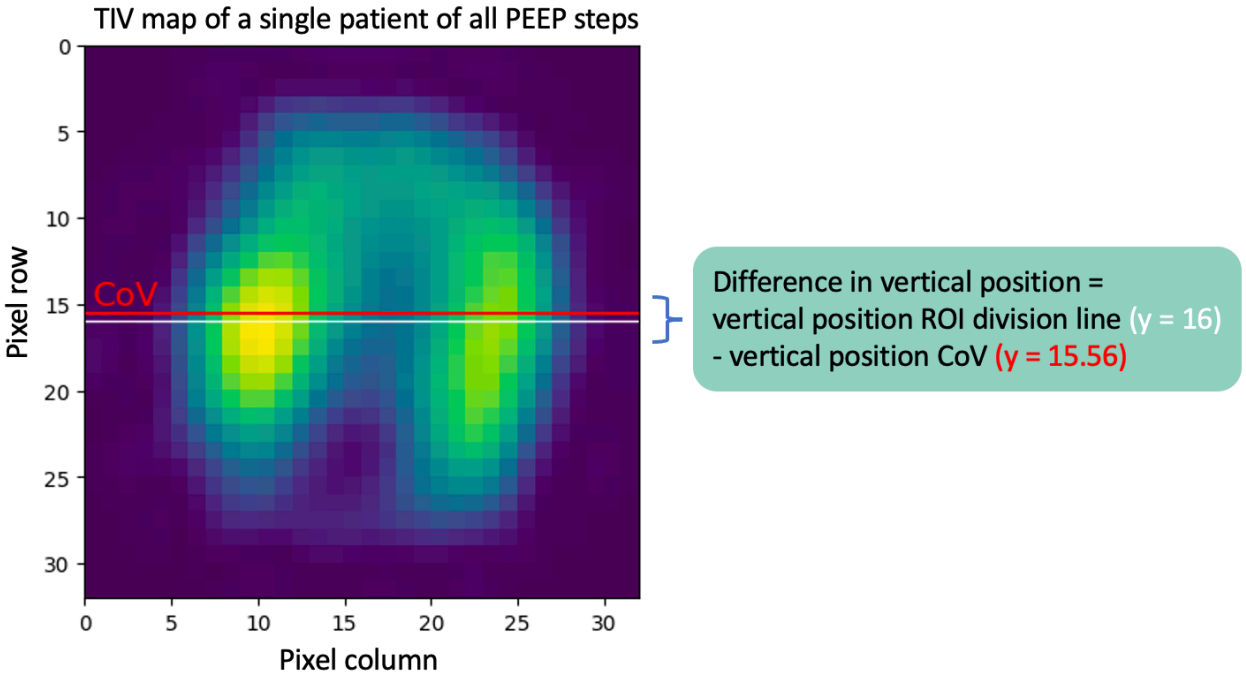

Supplemental Figure 3. Example of the computation of the difference in vertical position to compare the average vertical position of the CoV over all PEEP steps to the vertical position of the division line separating the ventral and dorsal region. The difference was computed for each patient with each ROI method. This figure shows an example for the global geometrical ROI.